HYDROGEOPHYSICS OF GRAVEL-DOMINATED ALLUVIAL FLOODPLAINS IN EASTERN OKLAHOMA

By

RONALD B. MILLER

B. A. Anthropology
University of California, Davis
Davis, California
1981

M. S. Geospatial Sciences
Missouri State University
Springfield, Missouri
2005

Submitted to the Faculty of the
Graduate College of the
Oklahoma State University
in partial fulfillment of
the requirements for
the Degree of
DOCTOR OF PHILOSOPHY
May, 2012

HYDROGEOPHYSICS OF GRAVEL-DOMINATED ALLUVIAL FLOODPLAINS IN EASTERN OKLAHOMA

Dissertation Approved:

Dr. Garey A. Fox

Dissertation Adviser

Dr. Daniel E. Storm

Dr. Todd Halihan

Dr. Chad J. Penn

Outside Committee Member

Dr. Sheryl A. Tucker

Dean of the Graduate College

ABSTRACT

Floodplains are important landscape features that are created over time by their resident streams. Contained within the floodplain, and unseen beneath the surface, are abandoned fluvial structures which remain in place as the stream migrates. Such structures include bars, bank deposits and old stream beds (paleochannels); these contribute to heterogeneity within the floodplain that can affect the flow of alluvial groundwater. Where there are coarse, high hydraulic conductivity sediments with a floodplain, the distribution can be either limited or broad-scale, and therefore can affect the movement of water either through "preferential flow paths" (PFPs) which may be limited spatially but are capable of conducting water at higher rates than surrounding material, or through "high-flow domains" which conduct water at high rates over broad areas. PFPs and high –flow domains may connect the stream directly to remote parts of the floodplain, or connect the floodplain surface to the alluvial aquifer and thus can affect the stream environment in significant ways, including transporting water and possibly water-borne constituents through the floodplain into or away from the stream. Additionally, floodplain heterogeneity can affect streambank stability by producing seeps that contribute to bank instability. The floodplains of the Ozark ecoregion of Oklahoma typically feature a silty topsoil layer (0.1 to 2 m) overlying a thick gravel subsoil. Previous work utilizing a network of monitoring wells at one Oklahoma site found that PFPs within the gravel vadose zone affect the lateral distribution of a tracer (Rhodamine WT).

While floodplain heterogeneity in general and PFPs in particular, have the potential to affect many aspects of stream water quality, the magnitude of that effect depends on their geometry and distribution across the environment. The purpose of this study is to attempt to map and quantify PFPs within the gravel floodplains of the Ozark ecoregion of eastern Oklahoma. Effective and efficient estimation of the presence of PFPs within floodplains depends on several factors: (1) a rapid method for determining the spatial distribution of heterogeneity within the floodplain subsurface and (2) determining how that heterogeneity affects the hydraulic characteristics of the subsurface. The gravel soil commonly present within the floodplains in the Oklahoma Ozarks present special problems, especially for the excavation required to conduct conventional soil sampling and hydraulic testing.

This study is divided into three sections that represent the process used to characterize the distribution of hydrologic characteristics in gravel-dominated floodplains.

1. The difficulties of hydraulic testing in gravel soil includes the toughness of the soil, the tendency for unsupported holes to collapse, and the large quantities of water required to establish and maintain hydraulic testing conditions in highly conductive soils. To overcome these difficulties, a steel permeameter was devised which would both support the hole and be driven into place with a direct-push drilling machine. A 3790 L (1000 gal) tank and an in-line pump system was used to supply water to the permeameter, and head elevation in the permeameter and the pump were monitored and recorded with pressure transducers. The permeameter measured hydraulic conductivities from 2 to 183 m d^{-1}, the latter value similar to the value (230 m d^{-1}) measured in an independent falling head trench test nearby.

2. Electrical resistivity imaging (ERI) is a non-invasive geophysical method for investigating subsurface features. A current of known voltage is passed through the subsurface between two current electrodes and the strength of the induced field is measured between two potential electrodes. The depth of investigation is related to the current electrode separation, and the strength of the induced field is related to the subsurface material. Two dimensional depth "profiles" were collected at three floodplain sites in the eastern Oklahoma Ozarks, including 14 at Barren Fork Creek (BFC), 5 at Flint Creek, and 5 at Honey Creek (HC). Permeameter tests were performed at selected depths and locations with known resistivity within the floodplains, and core samples of the gravel subsoil were retrieved from locations at two (BFC and HC) of the floodplains. Examination of the particle size distributions (PSDs) of the cores found that they generally consisted of particles either larger or smaller than 0.25 mm. Comparison of the % fine fraction (percentage less than 0.25 mm) for the cores showed significant ($\alpha = 0.05$) negative correlations between the measured ERI bulk resistivity ($P = 0.001$, $R^2 = 0.85$) and the saturated hydraulic conductivity, K_{sat}, ($P = 0.01$, $R^2 = 0.72$), suggesting that the fine fraction within the subsoil controlled both bulk resistivity and K_{sat}. Linear regression of hydraulic conductivity and resistivity was significant ($\alpha = 0.05$, $P = 0.00$, $R^2 = 0.57$), and allowed resistivity profiles to be interpreted as hydraulic conductivity profiles of the floodplain. Considering ERI profiles as vertically-oriented maps of hydraulic conductivity within the floodplain, the profiled area for hydraulic conductivity could be calculated. The median hydraulic conductivity for the profiles was 20 m d^{-1}, implying that half of the area of each profile had hydraulic conductivities within the

gravel range, indicating that the floodplain may behave as a high flow regime. Further, several ERI profiles from BFC were distinguished from the remaining profiles from all other sites by the presence of very high hydraulic conductivity/resistivity values at the 84^{th} percentile, a difference that was significant at $\alpha = 0.05$ ($P = 0.00$). The high hydraulic conductivity/resistivity areas of those ERI profiles occurred in a location noted by Heeren et al. (2010) that acted as a PFP in a tracer test.

3. To address the question of how the distribution of hydraulic conductivity affects the movement of water in the vadose zone of a gravel floodplain, the ERI profiles at BFC were interpolated to produce planar maps of hydraulic conductivity estimates for the entire 1.2 ha site. Those maps were compared to maps of the site water table during the flood event of May 1-5, 2009, in which the stream rose 2.2 meters (1.25 year return interval). The rapid response of the water table to the storm pulse was evident in a delay of only 1.5 hours and a reduction of peak elevation of only 0.25 m at 180 meters from the bank, which is consistent with the alluvial aquifer being a high-flow domain. The water table did respond to PFPs within the high flow domain as evidenced by the low slope of the rising water table within areas of very high hydraulic conductivity.

The correlation between resistivity, K_{sat}, and PFPs developed in this study is an important step in understanding PFPs and their distribution in Ozark floodplains. It can't be overlooked that the BFC site appears to be qualitatively and quantitatively different than the other study sites (HC and FC), and thus important follow-on research includes investigations into watershed processes that can influence the construction of PFPs in floodplains.

TABLE OF CONTENTS

LIST OF TABLES

LIST OF FIGURES

CHAPTER 1

Design and Application of a Direct-Push Vadose Zone Permeameter[1]

1.1 ABSTRACT

A borehole permeameter is well suited for testing saturated hydraulic conductivity (K_{sat}) at specific depths in the vadose zone. Most applications of the method involve fine grained soils that allow hand-auguring of test holes and which only require a small water reservoir to maintain a constant head. However, in non-cohesive gravels, hand-dug test holes are difficult to excavate, holes are prone to collapse, and large volumes of water are necessary to maintain a constant head for the duration of a hydraulic test. To overcome the difficulties presented by coarse alluvial gravels, a steel permeameter was designed that used direct-push to place a slotted-pipe at a sampling depth and a 3800 L trailer-mounted water tank to maintain constant head conditions. Head in the portable tank was measured with a pressure transducer and flow was calculated based on a volumetric rating curve. A U.S. Bureau of Reclamation analytical method was utilized to calculate K_{sat}. The calculated range of K_{sat} for the gravel permeameter was 2 to 275 m d^{-1} and measurements with the permeameter at a field site were similar to those reported in a test trench using falling-head data and the Hvorslev solution.

[1]Published in *Ground Water*, 2011

Miller, R.B., D.M. Heeren, G.A. Fox, D.E. Storm, and T. Halihan. 2011. Design and application of a direct-push in-situ gravel permeameter. Ground Water, doi: 10.1111/j.1745-6584.2010.00796.x.

1.2 INTRODUCTION

Alluvial floodplains commonly possess high conductivity gravel subsoils, which are complex depositional features that have an important role in the hydrological interaction between the stream and upland areas (Knighton, 1998; Bridge, 2003). Heterogeneity of soil texture derived from these complex origins may contribute to areas of preferential flow within the floodplain. Fuchs et al. (2009) and Heeren et al. (2010a, 2010b) studied preferential flow at an alluvial floodplain study site along the Barren Fork Creek in the Ozark ecoregion of Oklahoma with a gravel-dominated subsoil. Estimated saturated hydraulic conductivity (K_{sat}) of the preferential flow path at the site from falling-head tests ranged between 140 and 230 m d^{-1} (Fuchs et al., 2009). Subsequent geophysical surveys at the Barren Fork Creek and similar floodplain study areas on Flint Creek and Honey Creek indicated vertical heterogeneity at the sub-meter scale, which suggested that hydraulic conductivity at the sites may vary at the same scale (Heeren et al., 2010b). Experience with installing monitoring wells at these sites showed that the non-cohesive gravel subsoil was both prone to collapse and resistant to penetration. In response, a method for estimating K_{sat} at specific depths within the vadose zone of the site was designed to address the issues associated with the potentially high conductivity and resistance to penetration of the gravel.

Borehole permeameters are a commonly employed method for determining K_{sat} at specific depths in the vadose zone. Borehole permeameter tests were first described by Zangar (1953) and Glover (1953), and the tests were included in the U.S. Bureau of Reclamation (USBR) Ground Water Manual (1985). The original steady-state derivation by Glover (1953) assumed totally saturated flow within a region bounded by atmospheric pressure. This assumption was violated in practice especially in some fine-grained soils, and subsequent

modifications have focused on improving the models by including regions of partial saturation and matric suction (Stephens and Neuman, 1982; Stephens et al., 1983; Elrick and Reynolds, 1992; Cassiani, 1998). In coarse-grained and gravel-dominated soils the difference between the Glover (1953) free surface and the actual pressure distribution was not significant, and for these soils solutions based on Glover (1953), including the USBR methods, provide an adequate estimate of K_{sat} (Stephens and Neuman, 1982; Stephens et al., 1983; Stephens, 1995; Selker et al., 1999).

While traditional borehole permeameter tests are typically performed in fine-grained soils, the method becomes limited for use in gravel-dominated soils. Previous modifications of traditional borehole permeameter tests are inadequate for such conditions. For example, Bell and Schofield (1990) designed a permeameter for high conductivity soils with the primary criteria being portability and construction from easily available materials. The 40 L reservoir volume accommodated the amount of water that could be conveniently carried by a team of two, and although the reservoir size was larger than other commercially available units, the authors noted that in highly conductive soils steady-state could not be achieved before the water supply was exhausted.

This research presents a design for a borehole permeameter capable of performing adequately in gravel dominated soils. Design criteria included the following: (1) the ability to withstand the force needed to penetrate the gravel subsoil, (2) capable of providing support against collapse of the formation, (3) capable of providing a water supply sufficient to achieve steady state for a suitable test duration and maintain a constant head, and (4) capable of estimating K_{sat} for discrete depth intervals within the vadose zone of a heterogeneous gravel formation.

1.3 METHODS

The gravel borehole permeameter was constructed with a screened direct push pipe, a trailer-mounted reservoir system, and measurement instrumentation. The screened interval was constructed by cutting slots into a steel direct-push pipe section. The slotted casing was a 1.22 by 0.082 m (4 ft by 3.25 in) Geoprobe Systems (Kejr Inc., Salina, KS) pipe section with 27 vertical slots 0.002 m (0.07 in) wide by 0.203 m (8 in) long arranged in three groups around the pipe perimeter and separated by solid (unslotted) areas (Figure 1.1). The slots were located 0.97 m (3.2 ft) from the top of the pipe section. The pipe had a 79 mm wall thickness, and the slot arrangement was designed to conduct sufficient water for testing while providing the strength necessary to penetrate coarse gravels. The total screened area of the modified pipe (hereafter the permeameter) was 0.01 m2 with a ratio of open area to total area of 21%. After adding a solid drive shoe, the permeameter was lengthened to reach specified depths by threading on additional unmodified pipe sections. A Geoprobe 6200 TMP (Trailer-mounted Probe) with a direct-push force of 142 kN augmented with a 32 Hz pneumatic hammer was able to position the permeameter at selected depths in the coarse gravel. Although a drive shoe can cause "smearing" of borehole walls in fine-grained soils and artificially reduce the measured K_{sat}, this was not a problem in the coarse gravel subsoils of the study area.

The reservoir system was a 3.79 m^3 (103 gal) portable plastic water tank (Wako Inc., Enid OK) for which a stage/volume relationship was determined. The water tank was plumbed to the permeameter through a 5-cm diameter suction hose loosely inserted into the permeameter with an in-line 0.1 $m^3\ s^{-1}$ (152 gpm) gasoline-powered water pump (American Honda, Alpharetta, GA). Flow into the permeameter was controlled with a 5-cm brass gate valve. Head in the tank and permeameter were monitored at one second intervals with vented pressure

transducers (In-Situ Inc., Fort Collins, CO) (Figure 1.2). The in-line pump was able to produce a maximum discharge through the screen of 0.01 m^3 s^{-1} (152 gal min^{-1}).

Figure 1.1 Slotted section of gravel permeameter in driving position showing alignment of slot and slot-free areas.

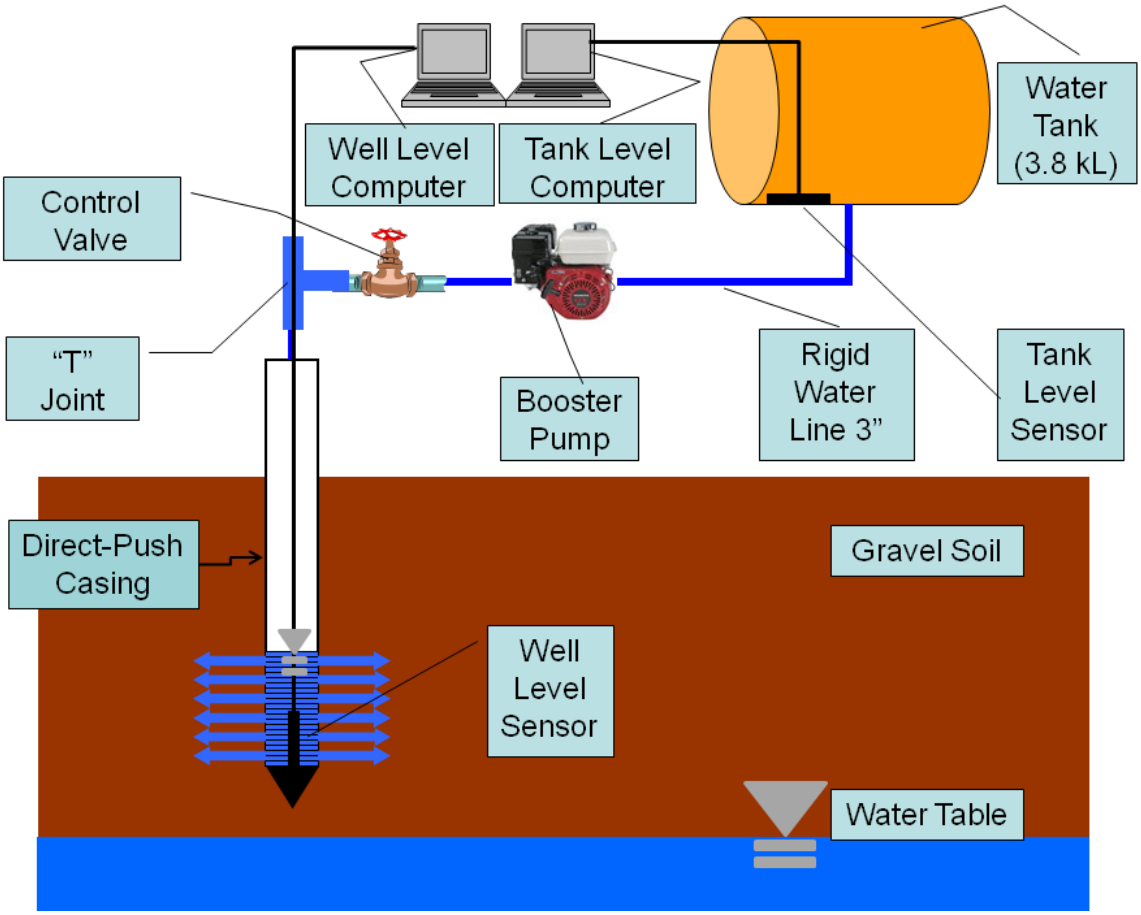

Figure 1.2. Schematic diagram of gravel permeameter showing general arrangement of water tank, pump, flow control valve and permeameter casing. Pressure transducers shown in the tank and well allowed real-time monitoring of water levels.

Test setup involved driving the permeameter to the selected depth in the gravel subsoil, connecting the water supply, and directing water into the permeameter. The permeameter screen was cleaned with a 7.5 cm nylon brush on an extendable handle and the debris removed with a peristaltic pump. When return water from the pump was clean, the transducer was placed in the permeameter and flow was adjusted to bring the head in the well to the desired elevation. Testing in the permeameter was initiated after the transducers registered a constant head with a constant

flow rate (pseudo steady-state), usually after 10 to 15 minutes. Test durations were approximately 15 minutes, consisting of transducer data recording the head in the permeameter, *H*, and the water level in the tank. The flow into the well (*Q*, $m^3 s^{-1}$) was calculated using the stage/volume relationship for the tank and the total elapsed time for the test.

The USBR (1985) method recommended a permeameter diameter of at least 15.25 cm to accommodate a float mechanism to maintain constant head in the permeameter for a sufficient time for the flow to achieve steady state. The 7.5-cm permeameter diameter was too narrow to fit a float, so steady state was maintained remotely by manually manipulating a gate valve while monitoring *H* with a pressure transducer. The USBR (1985) method defined steady state as "three or more measurements [at 5 minute intervals]…within plus or minus 6.1 cm (0.2 ft)" for a test section length of 1.52 m (5 ft) which created a ratio of 0.04 between the allowable deviation and *H*. The gravel permeameter was intended to determine K_{sat} of a much smaller thickness of vadose zone sediment, resulting in a smaller range of *H* than the example in USBR (1985). Therefore, constant *H* was evaluated with ±4% of the average *H* over the test interval instead of the recommended 6.1 cm and head depth varying within the ±4% range is considered to be within bounds of the test. For example a variation of 0.01 m for a head depth of 0.28 m within the permeameter would be considered steady-state.

The Glover (1953) derivation for computing K_{sat} in a borehole was adopted by the U.S. Bureau of Reclamation as a set of standard field methods termed "gravity permeability tests" (Ahrens and Barlow, 1951; Zangar, 1953; USBR, 1985) and were used for analysis of the test results. The USBR method includes two equations which are applied depending on the position of the test relative to the static water table. Equation (1.1) is for use in Zone 1, generally defined as situations where the water table is much deeper than the test depth (at least three times the

depth of the water in the borehole) (Stephens 1995), and equation (1.2) is used in Zone 2 when the test depth is close to the water table, the area between Zone 1 and the saturated water table:

$$K_{fs} = \frac{Q}{C_u r_e H} \tag{1.1}$$

$$K_{fs} = \frac{2Q}{\left[\left(C_s + 4\frac{r_1}{r_e}\right) r_e\right](T_u + H - A)} \tag{1.2}$$

where Q is discharge through the pipe, C_u and C_s are graphically-determined conductivity coefficients for positions far above or close to the water table, r_e is the effective radius (bore radius) of the well, r_1 is the outside radius of the casing, H is the steady-state depth in the well, A is the length of the screened interval, and T_u is the vertical distance from the steady-state water surface and the water table. The method is valid for test conditions where the saturated thickness (S) ≥ 5l (where l is the length of screened section), $l \geq 10\ r_1$, and $Q/a \leq 0.1$ ft s-1 (0.03 m s^{-1} where a is the perforated area of screen). The gravel subsoils of the study area had little fine material (Fuchs et al. 2009) and thus K_{fs} predicted by equations (1.1) and (1.2) was judged to be an adequate estimate of K_{sat} in these soils (Selker et al. 1999).

It should be noted that high K_{sat} conditions can lead to violations of the Q/a limitation of equations (1.1) and (1.2). The Q/a ratio is the velocity of water through the screen with 0.03 m s^{-1} as an estimate of the upper limit for the laminar flow for which Darcy's Law is valid (Ahrens and Barlow 1951). In these situations, H was reduced toward A (i.e., height of screen). Therefore, the measurement range of the gravel permeameter was between 2 and 275 m d^{-1} as determined

by the minimum detectable change in the water tank over a 30 minute interval to the maximum allowable Q when H equals A.

1.4 RESULTS AND DISCUSSION

The new gravel borehole permeameter was developed and tested at three alluvial sites in northeastern Oklahoma. Measured values for K_{sat} ranged from 2 to 183 m d^{-1} (Table 1.1), with the latter value an order of magnitude higher than the maximum K_{sat} value quantified by the high-conductivity permeameter designed by Bell and Schofield (1990). Glover (1953) noted that calculated results for K_{sat} were lower than electrical analog model results by 25% when the H/r was 6 and 6% to 8% when H/r was 20, and therefore concluded that the method has "reasonable validity" for $H/r \geq 10$. This constraint becomes an issue in highly conductive gravels where the flow necessary to maintain the H/r is high enough to violate the Q/a constraint. When $H = A$, the H/r ratio for the permeameter is 5 and therefore in highly conductive gravels valid estimates are likely to underestimate the actual K_{sat}.

Testing in the alluvial floodplains showed that the gravel subsoil could be extremely hydraulically conductive. In fact, one borehole permeameter test at the field site described by Fuchs et al. (2009) maintained a flow rate of approximately 0.004 m^3 s^{-1} (i.e., 60 gpm) for 12 minutes with a constant head of only 1.7 m. This test violated the Q/a limit and thus included non-laminar flow; therefore the calculated K_{sat} of 488 m d^{-1} was likely an underestimate, but served to demonstrate the requirement for a test method with very high volume capacity. Previous estimates of K_{sat} at the Barren Fork Creek site derived from measurements of falling head in a test trench based on the Hvorslev method (Fuchs et al., 2009) ranged from 140 to 230

m d^{-1} and were similar to the maximum K_{sat} values calculated with the gravel permeameter (Table 1.1).

Table 1.1. Gravel permeameter test results from three field sites in Eastern Oklahoma, including duration of test, flow volume, and mean head, *H*, in the permeameter. In order to evaluate the effectiveness of the manually controlled constant head, the percent of time within the bounds (±0.04% of mean *H*) is also reported. Q is the flow into the permeameter, *a* is the screened area of the permeameter and *Q/a* is a measure of the velocity of flow through the screen. In the USBR method, *Q/*a ratio values (in standard units) of 0.1 or less are assumed to indicate laminar flow. Saturated hydraulic conductivity, K_{sat}, was converted from conventional units utilized in the USBR (1985) method.

Site	Depth[1] (m)	Time[2] (m)in	Q[3] (m^3 min^{-1})	Q (ft sec^{-1})	H[4] (m)	H (ft)	Zone[5]	T_u[5]	C_u[5]	Cs[5]	K_{sat}[6] (10^{-3} ft s^{-1})	K_{sat} (m d^{-1})
BFC10[7]	2.01	33.17	0.016	0.009	0.3	0.98	1	3.6	60		5.6	146
BFC10[8]	2.46	24.05	0.01	0.006	0.29	0.94	2	2.1		43	3.7	96
BFC8[7]	1.27	24.67	0.006	0.004	0.26	0.85	1	5.7	55		2.8	73
BFC8[8]	1.72	21.58	0.019	0.011	0.26	0.86	1	4.3	67		6.8	180
BFC1	2.01	19.23	0.02	0.012	1.91	6.26	2	8.9		43	1.2	32
FC5	1.18	18	0.004	0.002	0.5	1.63	2	2.2		43	1.1	30
FC8	0.44	20.5	0.004	0.002	0.39	1.26	1	4.8	65		0.6	16
HC3	1.58	23.93	0.021	0.012	0.5	1.63	2	2.6		43	5.1	134
HC6	1.57	7	0.002	0.001	1.99	6.52	1	10.9	75		0.1	2

BFC = Barren Fork Creek; FC = Flint Creek; HC = Honey Creek

[1]Distance below ground surface to bottom of screen

[2]Duration of steady-state test

[3]Flow into permeameter at steady state

4Average height of water in permeameter above base of screen, corrected for free space below the base of the screen

[5]See Figure 1 for variable explanation (USBR, 1985)

[6]Estimated using USBR Method 3 (1985)

[7,8]Indicates single-hole depth sequence

The method depended on maintaining a constant *H* in the permeameter with a constant *Q*, and thus the gravel permeameter was evaluated on how well it achieved these two criteria. Manually manipulating the gate valve was able to maintain *H* in the permeameter within the ±4% range an average of 96% of the time for total test intervals that averaged 16 minutes (Table 1.1). Time plots for two typical tests show that the *H* measured within the permeameter can be considered at steady state for the given criterion (Figure 1.3).

The flow into the permeameter was gauged by the pressure transducer within the tank. In the first example (Figure 1.3a), the steady decline of the water level with time indicated that the constant *H* within the permeameter was produced by steady flow of water into the well. The relatively high *Q* from the tank resulted in an estimated K_{sat} of 183 m d^{-1}. The calculation for this test is shown in Figure 1.4. The second example (Figure 1.3b) shows the incremental drop in tank water level (2 cm over 30 min) produced by the minimum detectable flow rate; the K_{sat} of 16 m d^{-1} calculated for this test was close to the minimum for the method.

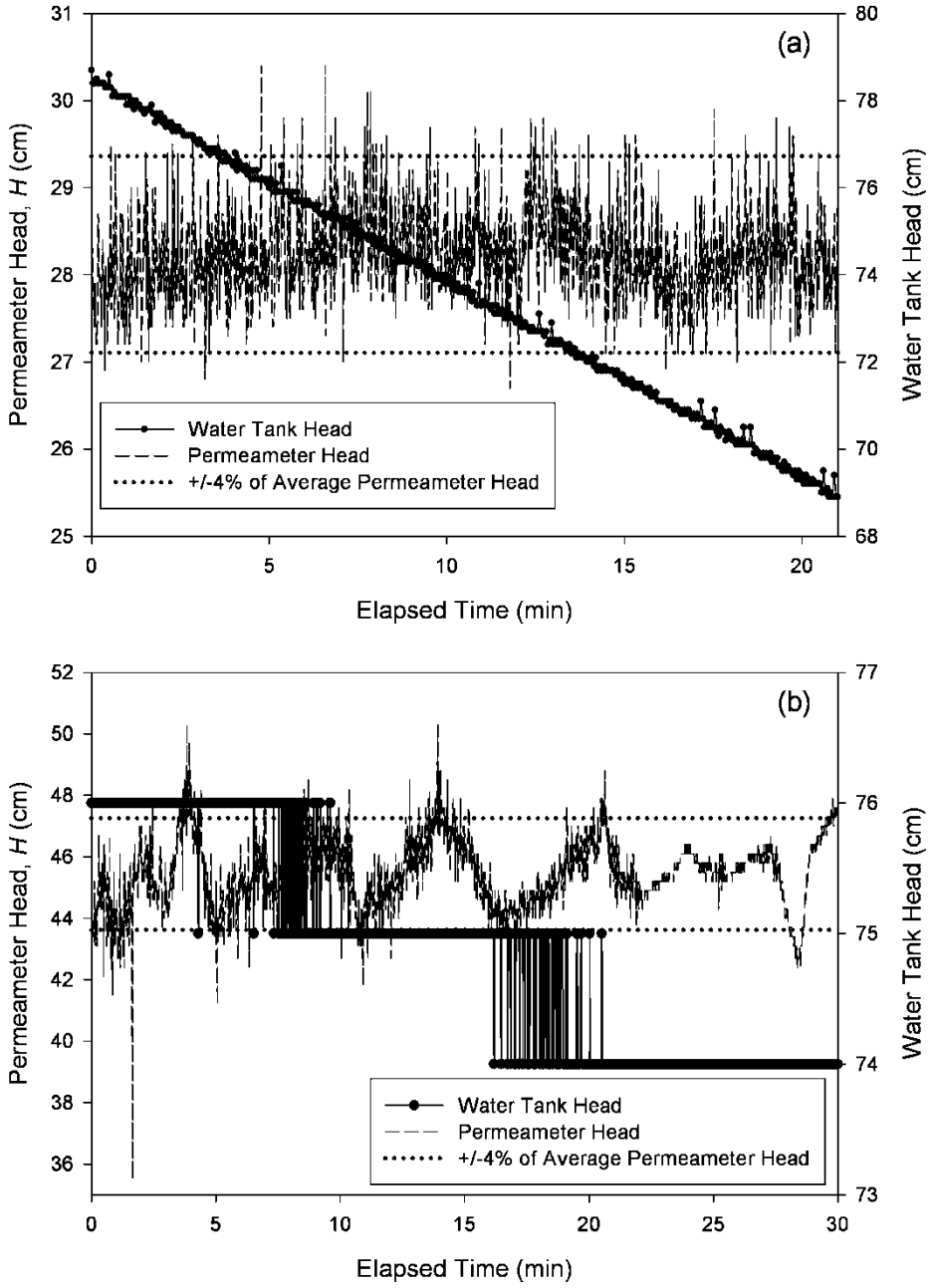

Figure 1.3. Constant head and tank drawdown time plots for tests (a) BFKsat8_T3, and (b) FLCR68_T1 described in Table 1.1. Solid line indicates average head (*H*) in the permeameter and dashed lines indicate 4% of *H*. During the steady-state period, *H* was within the bounds (a) 95% and (b) 88% of the time.

Field Data

H	Mean head (m)	0.28
t	Elapsed time (min)	21.6
d_{start}	Start tank depth (m)	0.787
d_{end}	End tank depth (m)	0.687
U	Depth to water table (m)	2.76
D	Depth to bottom of screen (m)	1.72

Constant values

A	Length of screen (m)	0.2
r_e	Effective radius of casing (m)	0.009

Flow Calculation

Flow (Q) is the difference in tank volume over the elapsed time of the test with the tank volume calculated using a tank volume rating curve, v_i

$$v_i(d_i) = -3.1818 d_i^{\,3} + 6.2808 d_i^{\,2} + 0.0663 d_i [L^3]$$

$$Q = \frac{v_{start} - v_{end}}{t}$$

$$= \frac{v(0.787) - v(0.687)}{21.6\,\text{min}} = 0.413\, {}^{m^3}\!/_{\text{min}} = 0.011\, {}^{ft^3}\!/_{\text{sec}}$$

Graphically-determined values from USBR (1985) Figures 10-7, and 10-6.

C_u	Unsaturated conductivity coeff [DIM]	67
Zone	Ratio of T_u/A and % saturated thickness	1

Field-saturated hydraulic conductivity (K_{fs})

$$K_{fs} = \frac{Q}{C_u r_e H}$$

$$= \frac{0.011}{67 \times 0.28 \times 0.86} = 0.0069\, {}^{ft}\!/_{\text{sec}}$$

$$\approx 183\, {}^{m}\!/_{d}$$

Figure 1.4. Example field-saturated hydraulic conductivity (K_{fs}) calculations for test BFKsat8-T3 (shown in Figure 1.3a). Note that measurements made in SI units were converted to standard units for calculation.

1.5 CONCLUSIONS

The standard borehole permeameter, which is a principal method for testing hydraulic conductivity at a specified depth in the vadose zone, is poorly suited for use in gravel-dominated soils. Non-cohesive and highly penetration-resistant soils present problems that were overcome by devising a permeameter that employed a slotted section of a Geoprobe push-probe pipe and a trailer-mounted tank as a water supply. The narrow diameter of the pipe prevented use of a float-style leveler to maintain a constant head, but real-time head readings from a pressure transducer and manual manipulation of a gate valve provided sufficient control to maintain constant head in the permeameter. Previous methods exhausted available water supplies before steady state was established and maintained for a test interval, but the large water supply from the portable tank allowed high-volume flow testing over sufficient time periods. The method was able to provide hydraulic conductivity estimates between 2 and 183 m d^{-1} for targeted depths in the vadose zone of the study areas using the USBR (1985) gravity permeability tests, with a theoretical maximum of 275 m d^{-1}. The method was capable of establishing and maintaining steady state in high conductivity gravels, including extreme flow conditions that exceeded the validity of the analytical tools.

CHAPTER 2

Geophysical and Hydraulic Characterization of Gravel-Dominated Alluvial Floodplains

2.1 ABSTRACT

The floodplains of many gravel-bed streams, including Ozark floodplains in northeastern Oklahoma, northwestern Arkansas, and southwestern Missouri, have a general stratigraphy that consists of a layer of topsoil covering gravel-dominated subsoil. This stratigraphy can create areas of rapid groundwater flow that may present environmental risk. Residual fluvial features in the subsoil, such as paleochannels, can act as preferential flow paths and extend the hyporheic zone across the floodplain. Broader regions of gravel can act as areas of rapid, broad-scale groundwater flow paths allowing rapid flow with low attenuation of potential contaminants. The objective of this research was to test whether electrical resistivity imaging (ERI) could be used to detect differences within the gravel subsoils and indicate the presence of high hydraulic conductivity domains. Multiple ERI profiles were collected at three floodplain sites in the Ozark region of northeastern Oklahoma along the Barren Fork Creek (BFC), Flint Creek (FC), and Honey Creek (HC). Soil cores were collected along ERI profiles at BFC and HC. The saturated hydraulic conductivity, K_{sat}, was estimated at several locations at all three sites with a borehole permeameter suitable for gravel soils. The fine fraction (< 0.25 mm) by mass of the cores was found to be correlated with resistivity ($R^2 = 0.84$) and hydraulic conductivity ($R^2 = 0.71$). Lower fine fractions were associated with higher hydraulic conductivity and resistivity.

Linear regression of the relationship between resistivity and hydraulic conductivity ($R^2 = 0.57$) allowed calibration of ERI profiles to identify high flow regions within the vadose zone of the alluvial floodplains. Large portions of the studied floodplains may be broad-scale high-conductivity features with potentially significant consequences for the movement of environmentally sensitive materials.

Keywords: Electrical resistivity imaging, Floodplain, Gravel, Preferential flow

2.2 INTRODUCTION

Floodplains, the complex and dynamic features created by rivers through erosion and re-deposition of bank materials, may contain paleochannels or linear deposits of coarse-grained sediments that form regions of high hydraulic conductivity. A complex pattern of paleochannels hidden under the floodplain surface has the potential to connect stream flows to distal floodplain areas (Stanford and Ward, 1992; Poole et al., 1997, 2002; Amoros and Bornette, 2002; Naiman et al., 2005), creating complex hydrologic pathways. Current hyporheic zone and bank storage concepts (Stofleth et al., 2008) rely on uniform flow and transport processes and do not account for the heterogeneity and preferential flow that may be present in these floodplains. Mastrocicco et al. (2009) found the potential for enhanced transport capacity into an alluvial aquifer for fertilizers in the relatively coarse sediments of floodplain paleochannels. Heeren et al. (2010, 2011) documented preferential flow through floodplain paleochannels at high-stream stage events which resulted in complex, large-scale flow patterns including preferential flow paths (PFPs). PFPs were defined as features within the gravel subsurface that have higher saturated hydraulic conductivity, K_{sat}, relative to the surrounding material and thus allow water to flow

more freely under saturated conditions. Proper understanding of the functional heterogeneity of floodplains is partly dependent on understanding the distribution of subsurface high conductivity features, such as paleochannels, that can influence flow and transport processes.

Electrical resistivity imaging (ERI) is a rapid and non-invasive geophysical method used to investigate a wide variety of environmental and geological issues in which a current of known amperage is passed between two current electrodes, and the potential of the induced field is measured as the difference in voltage between two "potential" electrodes placed between the current electrodes (Burger et al., 2006). The strength of the induced field is related to the electrical resistance of the earth material through which the current passes. In unconsolidated, near-surface materials the solid particles are generally insulators and the current is carried by ions adsorbed to the particle surface and dissolved in the pore fluid (Archie, 1942; McNeill, 1980; Rey et al., 2006). The depth of the ERI survey is related to the separation distance between the electrodes. A multiple electrode array allows configurations with varying separation distances, and produces a model of subsurface resistivity through mathematical inversion of the measured potential voltages into a two dimensional (distance and depth) arrangement of resistivity point estimates (Loke and Dahlin, 2002; Halihan et al., 2005). The resistivity of earth materials is non-unique, with many different materials having similar resistivities. Independent evidence, including well logs or core samples, is often used to interpret the geologic characteristics of resistivity patterns. The ERI method has been successfully utilized to determine preferential flow tendencies in complex vadose zone settings (Webb et al., 2008). Inverted resistivity models as a whole will be referred to hereafter as an "ERI profile", and single point resistivity estimates as "ERI resistivity" to distinguish those from the general concept of resistivity.

Baines et al. (2002), Bersezio et al. (2007), and Tye et al. (2011) are among those who have used ERI to map floodplain fluvial sediments, while Crook et al. (2008) used ERI to map the sedimentary structure of the active streambed itself. Investigations that have used ERI to detect gravel include Auton (1992) and Beresnev et al. (2002) for commercial gravel prospecting, Smith and Sjogren (2006) for geologic investigation of glacial deposits, and Gourry et al. (2003) and Green et al. (2005) for mapping buried paleochannels. Anterrieu et al. (2010) found that two-dimensional ERI profiles of a mining waste-rock pile correlated well with a model created from independently acquired data including cores, particle size distributions, and other geophysical surveys. These studies have shown that ERI can be used to detect gravel in contrast to other fine-grained sediment. What are lacking are studies to determine whether ERI can be used to detect differences within the gravel that can be used to calibrate hydraulic conductivity and the controls on these electrical signatures.

Gravel is a common component of both stream beds and floodplains in the Ozark ecoregion, which extends through parts of Oklahoma, Missouri and Arkansas (Figure 2.1), and is a soil component that can affect soil hydraulic properties in complex, potentially environmentally significant ways (Fuchs et al., 2009; Heeren et al., 2010; Miller et al., 2010). Gravels and gravel soils are complex assemblages whose hydraulic properties are affected by the distribution of particle sizes, the range of particle shapes, and packing arrangement. Recent work has conceptualized gravel soils as binary systems consisting of mixtures of coarse and fine elements (Koltermann and Gorelick, 1995; Zhang et al., 2011).

Binary soil models utilize soils consisting of two discrete size fractions. Consider a soil composed of fine and coarse elements, where the particle size of the fine fraction is smaller than the pore size of the coarse fraction, and the coarse particles have no secondary porosity.

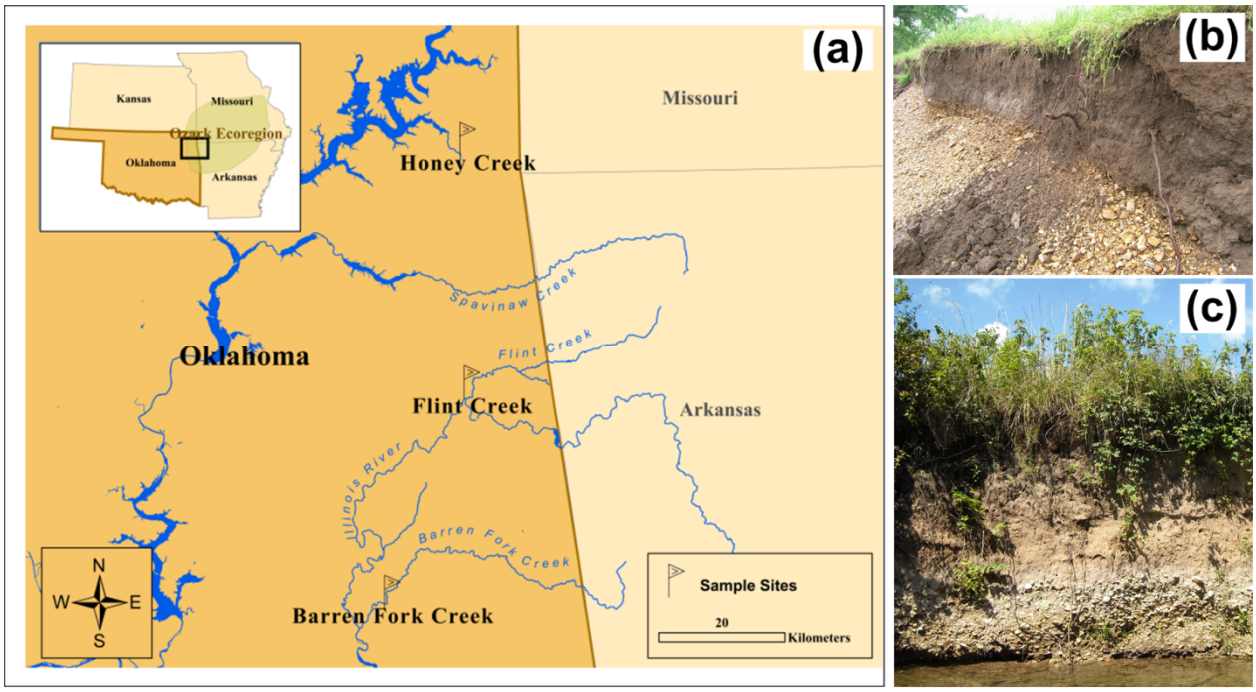

Figure 2.1. Map showing site locations (a) in Ozark region of eastern Oklahoma, and exposed streambanks showing gravel subsoils at two of the studied floodplain sites [(b) Barren Fork Creek and (c) Honey Creek].

A "coarse porosity" maximum (ϕ_c) exists when the fine fraction is zero and the entire soil consists of self-supporting coarse sediment with large, open pores (Figure 2.2). As the fine fraction increases, it initially occupies only the open pores created by the coarse fraction, and as it does so, it reduces the porosity of the mixture by replacing open space with the fine fraction. A porosity minimum (ϕ_{min}) is reached when all of the pore space within the coarse fraction is occupied by the fine fraction. In this condition, the only open pores exist within the fine fraction, and the coarse fraction behaves as pore-free inclusions, reducing the overall porosity.

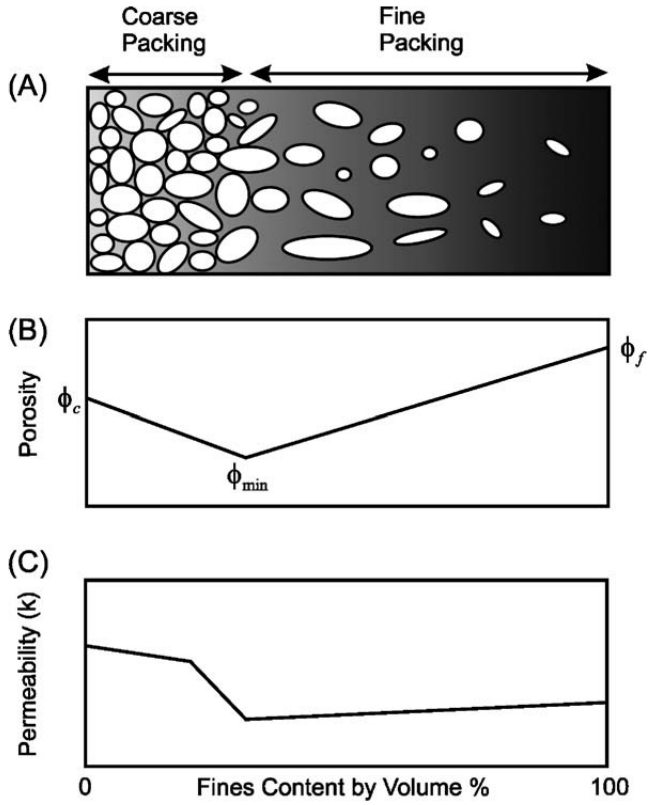

Figure 2.2. Ideal packing model for a volume of soil consisting of various coarse and fine phase fractions. The horizontal axis denotes the fraction fine material within the volume as a percent of total volume. The effect of changes in fines are illustrated with (a) a cartoon of the change in soil texture with the increase in fines; (b) the idealized change in porosity with the end members being the coarse (ϕ_c) and fine (ϕ_f) porosity maximums, and the porosity minimum (ϕ_{min}) occurring where the entire coarse pore space is filled with the fine phase; (c) variation in permeability with change in fine content. From Kamann et al. (2007) and used with permission by J. Wiley and Sons.

As the fine fraction continues to increase beyond ϕ_{min}, the coarse material is no longer self-supporting and the porosity increases because the amount of coarse material (as pore-free inclusions) decreases. The fine porosity maximum (ϕ_f) is reached when the soil contains only

the fine fraction. Kamann et al. (2007) and Zhang et al. (2011), among others, have conducted constant-head flow tests on coarse/fine mixtures, showing that K_{sat} increases rapidly when the fine content decreases past the porosity minimum. Thus the fines content of gravel-dominated soils have a controlling effect on its hydraulic behavior.

The objective of this research was to test whether ERI could be used to detect differences within gravel-dominated vadose zones of alluvial floodplains that may indicate the presence of high hydraulic conductivity zones. A critical component for this effort was to determine if a relationship existed between the measured ERI resistivity and both the physical and the hydraulic properties of the gravel subsoil. And if that relationship existed, determine the controls on that relationship so that it can be applied in other gravel-dominated settings. The approach was to collect soil cores and conduct hydraulic testing coincident with locations on ERI profiles, and then perform soil analysis to determine the sediment controls on the ERI resistivity and hydraulic conductivity values. The results were used to calibrate the ERI resistivity datasets to hydraulic parameters.

2.3 METHODS

2.3.1 Study Sites

Three alluvial floodplain sites in the Ozark ecoregion of northeastern Oklahoma were investigated with ERI, soil coring and hydraulic testing. The sites were named after the resident stream and included Barren Fork Creek (BFC, hay field), Flint Creek (FC, riparian forest), and Honey Creek (HC, riparian forest and hay-field). Although the sites were from different watersheds and varied in stream order, land cover, land use and watershed size, they had similar silt loam soils (dominantly Razort gravelly loam and Elsah very gravelly loam) and dominant

bedrock types (cherty limestone, mainly Keokuk/Reeds Spring formation) (Tables 2.1 and 2.2). The BFC site (latitude 35.90°, longitude -94.85°) was an open pasture located on the outside of a bend on Barren Fork Creek. The HC site (latitude 36.54°, longitude -94.70°) was located on the inside of a horseshoe bend in Honey Creek and contained both pasture and riparian forest. The FC site (latitude 36.20°, longitude -94.71°) occupied a narrow, forested floodplain adjacent to a relatively straight stretch of Flint Creek.

Table 2.1. Watershed characteristics and geology of the study sites located in the Ozarks of northeast Oklahoma: Barren Fork Creek (BFC), Flint Creek (FC), and Honey Creek (HC).

Site	Watershed†			Geology§		
	USGS Gage†	Watershed Area‡ (km^2)	Median Daily Discharge¶ ($m^3 s^{-1}$)	Formation	General Rock Type	Percent of watershed area (%)
BFC	7197000	845	3.6	Keokuk/Reeds Spring	Cherty limestone	70
				Ada	Sandstone and shale	20
				Bloyd and Hale	limestone and shale	10
FC	7196000	300	1.6	Keokuk/Reeds Spring	Cherty limestone	85
				Pitkin, Fayetteville, Bat	Sandstone and shale	15
HC	7189542	150	0.54	Keokuk/Reeds Spring	Cherty limestone	100

†US Geological Survey National Water Information System (USGS NWIS)

‡Based on 1-arcsecond National Elevation Dataset (US Geological Survey National Map, http://seamless.usgs.gov)

§From Stoeser et al. (2005)

¶Calculated from USGS NWIS mean daily flow records for each gage

Erosion of the carbonate bedrock by slightly acidic waters has left a large residuum of chert gravel in Ozark soils, with floodplains generally consisting of coarse chert gravel overlain by a mantle (1 to 300 cm) of gravelly loam or silt loam. The similarity of source materials for stream sediment within the different watersheds, including similar bedrock and floodplain soils, allowed the assumption that the composition of the floodplain materials for the study sites would also be similar.

Table 2.2. Land use and soil types for the Barren Fork Creek (BFC), Flint Creek (FC), and Honey Creek (HC). Razort soil series is an alluvial soil occurring in the Ozark region (Oklahoma, Arkansas and Missouri) consisting of silt loam A and B horizons overlying a very gravelly silt loam C horizon. The Elsah soil series similarly occurs on floodplains and consists of a silt loam A horizon containing chert gravel overlying a C horizon with 35 to 75 percent gravel content.

Site	Site Area (ha)	Primary Land Use	Soil Series†	Percent of Site Area (%)
BFC	1.4	Hay Field	Razort	97
			Elsah	3
FC	0.6	Riparian Forest	Elsah	62
			Healing	38
HC	0.7	Riparian Forest & Hay Field	Razort	100

† SSURGO Soils Database for Oklahoma (NRCS, 2011)

The cause of any variation within the ERI profiles from the floodplain sites was an unknown in the study and, since the electrical resistivity of earth materials can vary widely and may overlap with other materials, independent evidence was required to interpret the geologic and hydrologic characteristics of resistivity patterns (Zohdy et al., 1974; Burger et al., 2006).

2.3.2 Electrical Resistivity Imaging (ERI)

Resistivity surveys were conducted at the floodplain sites for the purpose of characterizing the heterogeneity of the unconsolidated floodplain sediments, especially in the vadose zone between the ground surface and the alluvial water table. ERI data were collected using a SuperSting R8/IP Earth Resistivity Meter (Advanced GeoSciences Inc., Austin, TX) with a 56-electrode array. The resistivity sampling with the SuperSting R8/IP, and subsequent inversion utilized a proprietary routine devised by Halihan et al. (2005), which produced higher

resolution images than conventional techniques. The ERI surveys at the sites occurred between June 2008 and March 2009. Fourteen lines were collected at the BFC site, five at FC, and five at the HC site. Some of the lines were "roll-along" lines that consisted of sequential ERI profiles with at least one-quarter overlap of electrodes to produce long, continuous vadose zone profiles without reducing spatial resolution. The profiles at the BFC site employed electrode spacings of 0.5, 1.0, 1.5, 2.0 and 2.5 m with associated depths of investigation of approximately 7.5, 15.0, 17.0, 22.5 and 25.0 m, respectively. The FC and HC sites utilized 1-m electrode spacing exclusively. The zone of interest was the vadose zone, the soil above the baseflow water table, which was within 3 m of the ground surface at each site and thus well within the ERI depth of investigation.

The ERI survey electrode locations were located spatially with a TopCon Hyper Lite Plus differential GPS (TopCon Positioning Systems, Inc. Livermore, CA) capable of 1.0 cm horizontal and 1.5 cm vertical precision. The raw GPS points were corrected using the National Geodetic Survey Online Positioning User Service (OPUS) Rapid Static correction, which can place points accurately within 3 cm horizontally and 5 cm vertically depending on the quality of the GPS data. The ERI resistivity data were interpolated into grids and contoured using Surfer 8 (Golden Software, Inc., Golden, CO). Inverted and interpolated resistivity data were termed "ERI profiles" as opposed to "ERI pseudosections", which were the "raw" resistivity measurements as collected in the field.

2.3.3 Soil Cores and Particle Size Analysis

Soil samples from locations on ERI profiles collected at two of the floodplain sites (BFC and HC) provided independent means for interpreting the profiles. Core sample locations on the ERI profiles were spatially located within 10 cm using the TopCon Hyper Lite Plus. The large

particles that make up gravel-dominated soils make them problematic for soil sampling. Difficulties occur with all sampling methods and include large particles blocking tube sampler openings and the collapse of pits excavated in unconsolidated gravel. Furthermore, gravel soils are resistant to penetration and thus core sampling often requires mechanical assistance that may cause breakage of large particles. If the largest particle sizes present in the soil exceed the sampler diameter, the collected sample may not truly represent the actual size distribution.

With a realization of these limitations, seven direct push cores and one bucket sample from the surface were recovered from locations on ERI profiles representing a range of ERI resistivity values. Core samples were collected at known depths with a Geoprobe Systems (Salina, KS) 6200 TMP (Trailer-mounted Probe) direct-push drilling machine using a dual-tube core sampler with a 4.45 cm opening. The sampler opening (size) limited the particle size that could be sampled and large cobbles occasionally clogged the sampler resulting in incomplete cores for that depth interval. In addition to samples recovered with the core sampler, one sample was collected from bank sediments at BFC with a shovel and bucket after an extreme erosion event exposed the bank profile (Fox et al., 2011) that had been previously surveyed with ERI. Efforts were made for these samples to be representative and to include the complete sediment size range, and for simplicity all samples are referred to as “cores” or “core samples”. The samples were weighed, dried in an oven at 70°C then re-weighed. The dried samples were then disaggregated with a mortar and rubber pestle.

Cores were dry-sieved using a series of sieves from 16 to 0.25 mm, and the mass retained on each sieve was weighed. Large particles, especially those gravel-sized and above, were difficult to sieve and commonly hand measurement of the “b” axis (longest intermediate axis perpendicular to the long “a” axis) of the particle was utilized as a rough sieve approximation

because that dimension largely controls whether a particle will pass a particular sieve (Bunte and Abt, 2001). The size distribution of the particles retained on a 16 mm sieve was determined by measuring the "b"-axis of the largest particle with a digital caliper and assuming that 100% of the sample would pass this size sieve. Three or four size "bins" for each core were calculated to encompass the size range between this maximum and 16 mm and the total coarse fraction was assigned to those bins by caliper measurement of the "b" axis. The mass of each bin was then measured.

The particle size distribution (PSD) of the mass retained on the finest sieve (< 0.25 mm) was determined using a Cilas 1180 Particle Size Analyzer (Cilas USA, Madison, WI), which calculated the ratio of particle sizes based on the obscurance of a laser beam. The Cilas 1180 measured the relative volume for particle size ranges of a representative sample. The PSD of the mass passing 0.25 mm was calculated by multiplying the percent distribution from the sample by the total volume of the fine dry-sieved fraction.

The PSD by mass for each core was prepared by calculating the proportion of mass passing each sieve of decreasing size to 0.25 mm. However, the PSD of the mass passing 0.25 mm was reported in terms of volume. In order to report a complete PSD, the mass retained on each sieve was converted to a volume by dividing by an assumed density of quartz, 2.65 g cm^{-3}, and combining with the PSA-derived volume distribution.

X-ray diffraction (XRD) was used to determine the presence of clay minerals in each sample. Minerals have unique and regular crystal structures consisting of layers of atoms. The unique pattern produced by the diffraction of a beam of X-rays through a mineral's crystal structure is described mathematically by Bragg's law that defines the relationship between the X-ray wavelength, the X-ray angle of incidence, and the separation distance between crystal layers

(Moore and Reynolds, 1997; Poppe et al., 2001). A randomly-oriented mount was prepared with a representative sub-sample of the fine fraction (<0.25 mm) from each core, which was ground to a fine powder with a ball mill, suspended in tap water and centrifuged at 1500 rpm for two minutes to isolate clay minerals in the water column. A slide containing sufficient material for XRD analysis was prepared by repeatedly applying water bearing the suspended clay to the surface of a slide and allowing the water to evaporate and then tested with a Phillips PW3020 computer-automated X-ray diffractometer (Kittrick and Hope, 1963). Statistical analyses were conducted using Minitab 15 (Build 15.1.30.0, Minitab, Inc., State College, PA).

2.3.4 Hydraulic Testing

Field measurements of K_{sat} were collected at successive depths in the vadose zone of all three floodplain sites using a slotted section of the direct push pipe as a permeameter. The permeameter method consisted of a screened direct push pipe, a trailer-mounted water reservoir, and measurement instrumentation, and provided K_{sat} estimates ranging between 2 and 180 m d^{-1} for targeted depths in the vadose zone, including successive depth measurements within the same borehole. The testing results were analyzed using the US Bureau of Reclamation Gravity Permeability Test Method 3 (USBR, 1985), which was suitable for non-cohesive soils. A detailed description of the method can be found in Miller et al. (2011).

2.4 RESULTS AND DISCUSSION

2.4.1 Resistivity Surveys

ERI resistivity values at the sites ranged over several orders of magnitude with the lowest and the highest values found at BFC (Table 2.3). The ERI resistivity data were positively skewed, indicating a large number of low values and a small number of extreme high values. ERI profiles from the sites suggested complex patterns within the vadose zone (Figure 2.3), with

regions of high ERI resistivity (800 Ω-m or greater) within a general region of lower resistivity that was approximately 300 Ω-m or less. The high ERI resistivity values on the BFC profiles (~2000 Ω-m) were similar to those observed at the surface of an ERI profile from a gravel bar located near the BFC floodplain site (2000 – 5000 Ω-m, Figure 2.4), providing corroborating evidence that the high resistivity features within the floodplain may be clean, open-framework gravel similar to that found on the bar surface. Similarly, the resistivity values of 100-300 Ω-m close to the surface of the profiles corresponds to the surface Razort or Elsah soil layer, which was observed at all three sites (Figure 2.3). These associations can help to interpret the profiles in a general way, but more direct information was needed to interpret the complexity evident in the profiles and especially to determine the presence of high hydraulic conductivity domains in the vadose zone.

Table 2.3. Descriptive statistics for the vadose zone ERI resistivity data at Barren Fork Creek, Honey Creek, and Flint Creek. All values except sample number (n) and skewness are reported as Ω-m, or as $\log_{10}$ Ω-m.

	Barren Fork Creek		Honey Creek		Flint Creek	
	ERI Resistivity	$\log_{10}$ ERI Resistivity	ERI Resistivity	$\log_{10}$ ERI Resistivity	ERI Resistivity	$\log_{10}$ ERI Resistivity
n	12,799	12,799	3,823	3,823	1,297	1,297
Mean	494	2.48	281	2.39	271	2.37
Standard Deviation	611	0.42	152	0.24	156	0.24
Minimum	11	1.04	30	1.48	33	1.52
Median	266	2.43	247	2.39	235	2.37
Maximum	11,830	4.07	1,190	3.08	1,220	3.09
Skewness	5.06	0.27	1.23	-0.19	1.65	-0.15

2.4.2 Soil Samples

The PSDs of the core samples from BFC and HC showed a wide range of textures (Figure 2.5). Those cores with the coarsest textures were predominantly gravel-sized (> 2 mm), with BFC1 and HC5 having 93 and 89% larger by mass, respectively. The finest textures were predominantly silt (0.002 – 0.05 mm), with HC2 and HC3 having 65 and 46% in this size range, respectively. The coarse (sand-sized and larger) particles were identified as chert fragments.

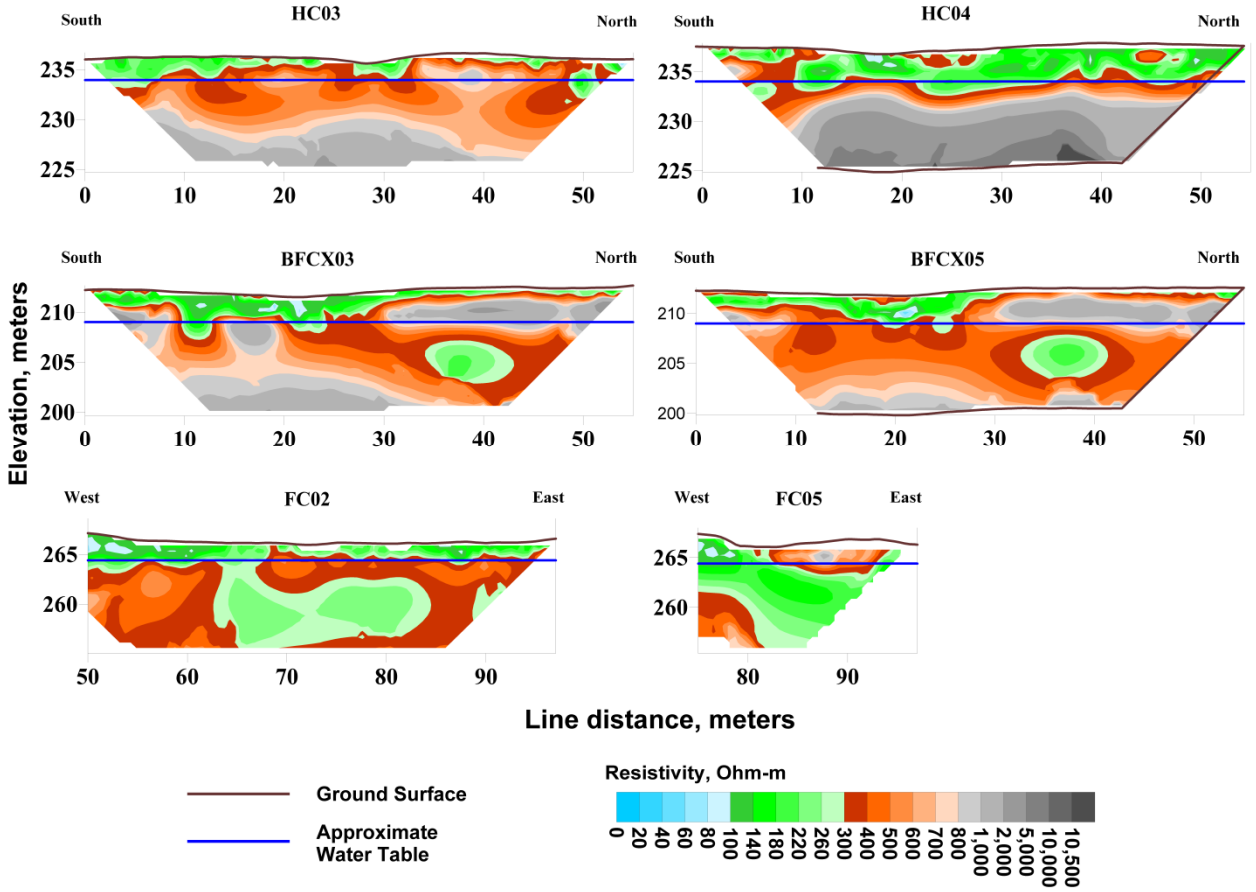

Figure 2.3. Example Electrical Resistivity Imaging (ERI) profiles from floodplain sites at Honey Creek (HC03 and -04), Barren Fork Creek (BFCX03 and -05), and Flint Creek (FC02 and -05). The Flint Creek profiles extend onto the stream terrace, but only the floodplain segment is shown. The study depth is between the blue and brown lines.

X-ray diffraction was used to identify the mineralogy of the finest particles (< 0.25 mm). Random slide mounts showed no peak at 8.8 2° theta indicating an absence of illite, a residual component of bedded limestone and thus the most likely clay mineral (Figure 2.6). Considering the chert source material in the watershed, the quartz in the fine material was likely to be fine chert fragments.

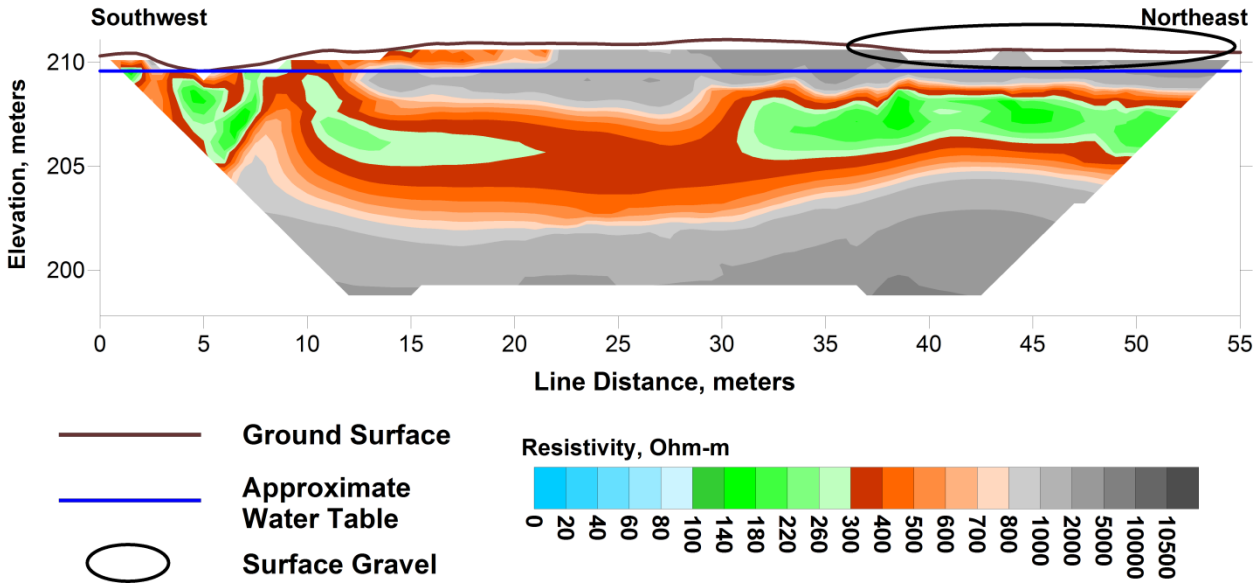

Figure 2.4. Electrical Resistivity Imaging (ERI) profile of gravel bar located approximately 100 m upstream of the Barren Fork Creek (BFC) study site. The profile is oriented across the gravel bar and perpendicular to Barren Fork Creek in a southwest to northeast direction, terminating at the stream edge. Clean gravel is exposed at the surface of the gravel bar along the stream (circled area at the northeast end of the profile). Similarity between the resistivity of this material and the resistivity near a known preferential flow path (PFP) at BFC provides corroborating evidence that the PFP consists of clean gravel.

Many of the PSDs exhibited a flat trend near the particle size of 0.25 mm, implying that many of the cores consisted of particle sizes that were either much larger or smaller than 0.25 mm, and further indicating that the soils resembled the artificial binary models of coarse and fine

phases that have been designed to better understand gravel soils (Koltermann and Gorelick, 1995; Kamann et al., 2007; Zhang et al., 2011). The binary gravel studies showed that, within a system of fixed coarse and fine elements, the fines content of a coarse gravel soil controlled its hydraulic behavior, and therefore the proportion of fines in a binary soil could be used to describe the soil. For this study the soils were assumed to be similar enough that they could be treated as members of a continuum of mixtures of coarse and fine elements with the division placed at 0.25 mm, with the proportion of the PSD < 0.25 mm (hereafter fine fraction) used to describe each soil.

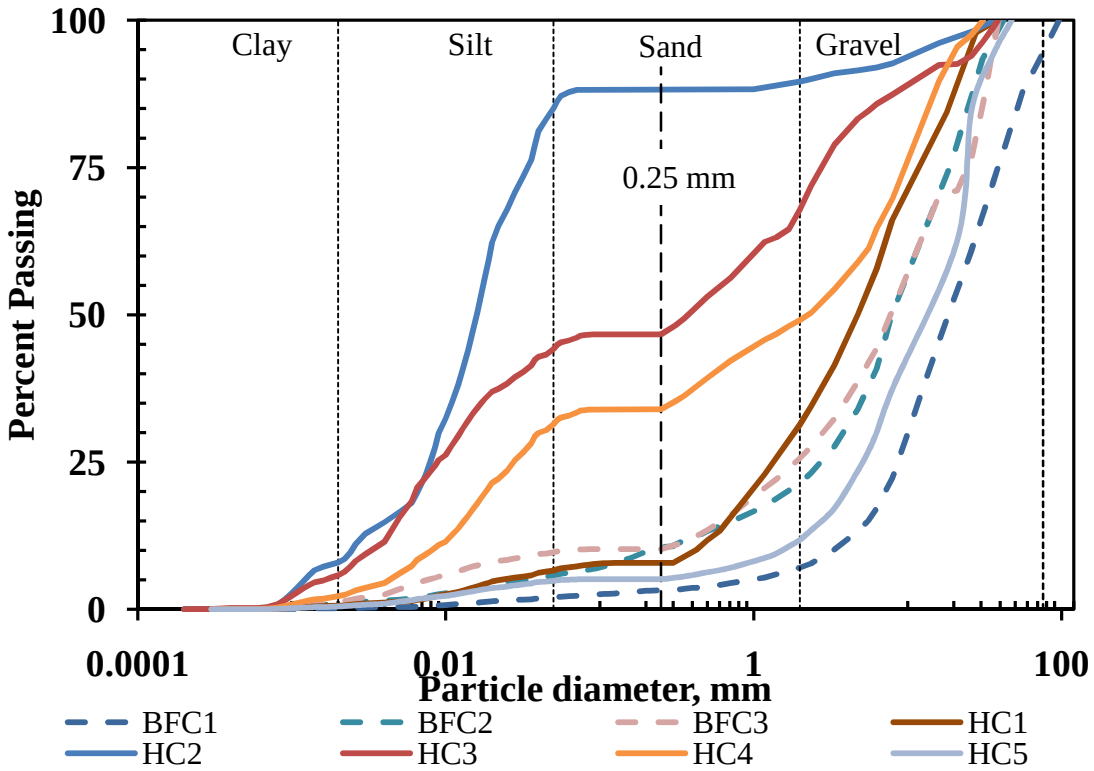

Figure 2.5. Particle size distributions for floodplain subsoil samples. Samples from Barren Fork Creek are labeled BFC (shown with dashed lines), and samples from Honey Creek as HC (shown with solid lines).

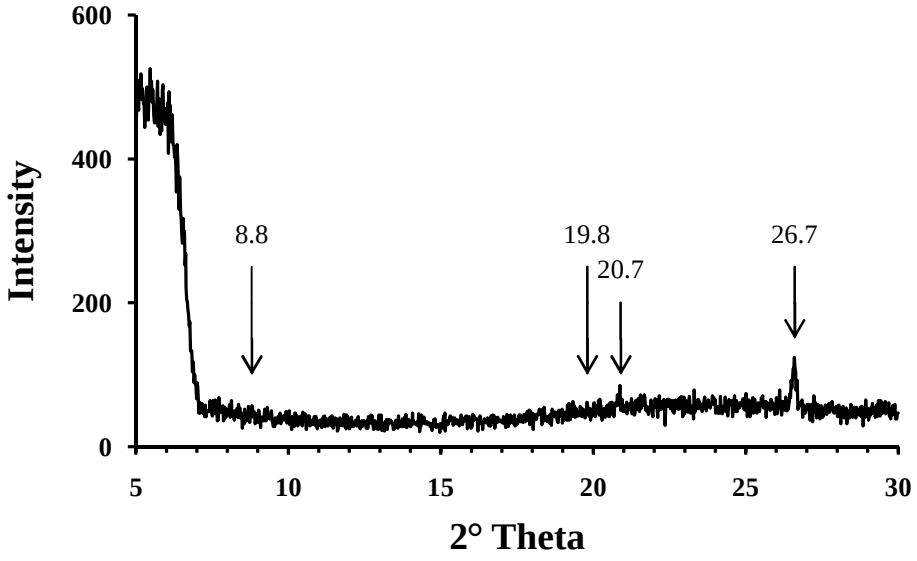

Figure 2.6. Random mount diffractogram for clay-sized fraction from Barren Fork Creek showing little response at 8.8 and 19.8 2θ, indicating limited presence of illite, and slightly larger response at 20.7 and 26.7 2θ indicating quartz. *2θ* is the measured angle between the X-ray beam transmitted and the beam diffracted through the crystal structure, and is dependent upon the distance of separation between layers of atoms; intensity "spikes" in the diffractogram (labeled values with arrows) indicate constructive interference. The pattern of intensity spikes is diagnostic of minerals, and is described mathematically by Braggs Law, which defines the relationship between X-ray wavelength, layer separation distance, and angle of incidence (Poppe et al. 2001).

2.4.3 Resistivity and Fine Fraction

Core samples were collected at locations along ERI profiles corresponding to ERI resistivity data locations. A plot of the measured ERI resistivity versus the fine fraction showed a negative relationship in which ERI resistivity decreased as the fine fraction increased (Figure 2.7). A power function best fit the relationship. Linear regression of the log-transformed

variables was significant at $\alpha = 0.05$ ($P = 0.001$) with an R^2 of 0.85. In unconsolidated materials the particles themselves are commonly insulators, and electrical current is carried by pore fluid and by surface conduction in the electrical double-layer present on clay minerals (if present); therefore, areas with high clay mineral content or with high soil moisture (or both) will have lower resistance to electrical current (Archie 1942; McNeill, 1980). Since the XRD results showed negligible clay within the fine fraction, it was assumed that soil moisture primarily affected the resistance of the subsurface.

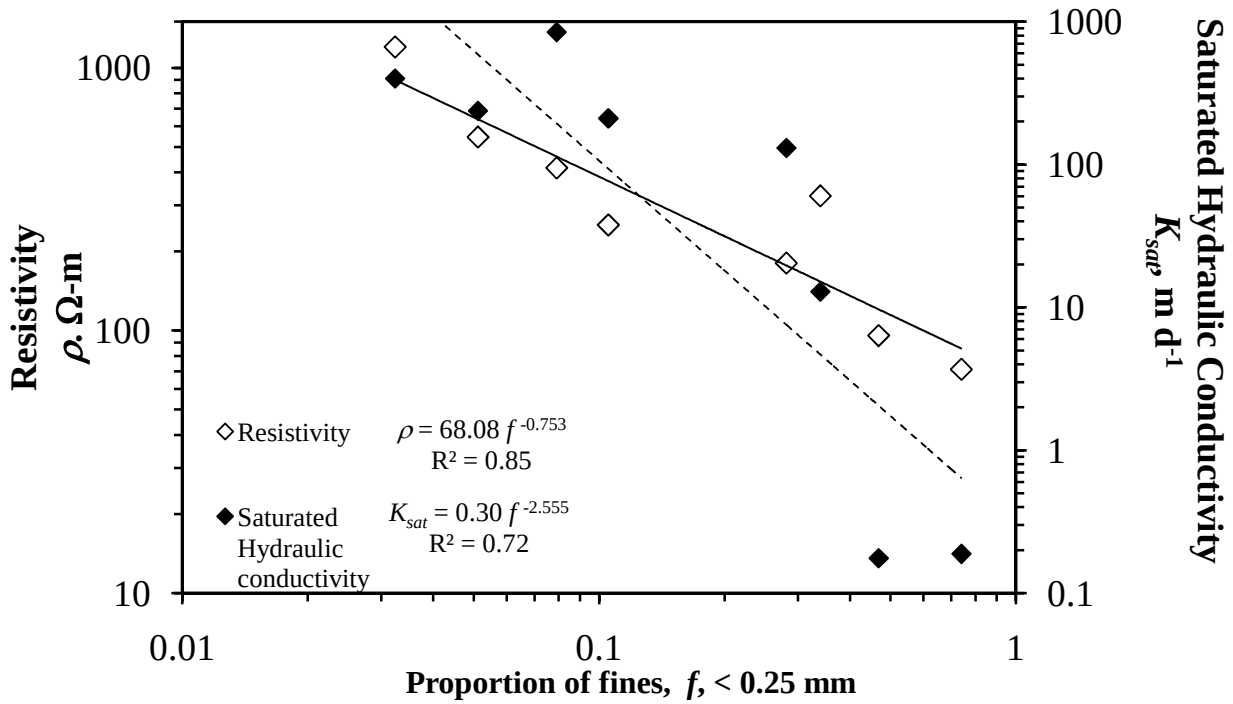

Figure 2.7. Relationship between fine fraction (f, <0.25 mm) and ERI resistivity (ρ, Ω-m, open symbols, solid line) and field-measured saturated hydraulic conductivity (K_{sat}, m d^{-1}, filled symbols, dashed line) from subsoil samples taken from locations on Barren Fork Creek and Honey Creek floodplains.

The negative power relationship between ERI resistivity and fine fraction was similar to the volumetric water content/ERI resistivity relationship shown in Samouelian et al. (2005), suggesting that the ERI resistivity/fine fraction relationship was similarly responding to the moisture within the fine fraction. Fine-textured soils have much greater moisture-holding capacity compared to coarser ones (Fetter, 2001), so it was possible that the variation in ERI resistivity of the soils was due to the variation of the fine fraction within the subsurface gravel soils. The actual moisture content/ERI resistivity relationship was unknown, since those measurements were not taken at the time of the survey, and similarly, the soil moisture profile could not be obtained at the time the cores were collected since concurrent hydraulic testing required saturating the soil.

2.4.4 Fine Fraction and Hydraulic Conductivity

Field hydraulic testing was conducted at locations on ERI profiles and some were conducted at locations from which the cores were obtained. Thus each hydraulic test was associated with an ERI resistivity value and some with both an ERI resistivity and a particle size distribution. A plot of the fine fraction and hydraulic conductivity showed a negative power relationship similar to that between the fine fraction and measured ERI resistivity (Figure 2.7) in which low fractions of fine material corresponded to high hydraulic conductivity. Linear regression of the log-transformed variables shows that the regression was significant at $\alpha = 0.05$ ($P = 0.008$) with an R^2 of 0.72. Existing work on artificial binary soil mixtures of coarse and fine elements found that the hydraulic conductivity of the mixtures was highest when the fine fraction approached zero and the material consisted of coarse material with interconnected, open pores (Koltermann and Gorelick, 1995; Kamann et al., 2007; Zhang et al., 2011) (Figure 2.2). The hydraulic behavior of the naturally-occurring gravel soils present in the floodplain was

similar to that of artificially-constructed coarse soils, suggesting that the fraction of fine material within the gravel subsoil was an important factor in describing the hydraulic behavior of those coarse soils. In short, ERI resistivity was a measure of the fines fraction of the gravel subsoil at the sites, which in turn were correlated to hydraulic conductivity.

2.4.5 Resistivity and Hydraulic Conductivity

The similarity of the power relationships between the fine fraction and both ERI resistivity and K_{sat} implied that there may be a direct relationship between ERI resistivity and K_{sat}. In addition to the hydraulic conductivity tests performed in conjunction with core samples, some tests were conducted without core sampling. As before, the ERI resistivity of those hydraulic conductivity tests were known because the tests were conducted along existing ERI profiles. Simple linear regression of the test results and the ERI resistivity was significant at $\alpha = 0.05$ ($P = 0.004$, $R^2 = 0.57$) and showed a positive relationship between resistivity and hydraulic conductivity (Figure 2.8). An intercept (0.06 m d^{-1}) was calculated as part of the regression, but was not significant ($P = 0.99$) and was therefore dropped from the final relationship:

$$K_{sat} = 0.11\ \rho \quad (1)$$

where ρ (Ω-m) is ERI resistivity, and K_{sat} (m d^{-1}) is hydraulic conductivity. Equation (1) allows resistivity profiles to be interpreted as maps of hydraulic conductivity, although it can only be applied to unconsolidated sediments that are compositionally similar to the core samples.

2.4.6 Resistivity and High Flow Zones

The ERI profiles provide a two-dimensional vertical view into the floodplain subsurface showing heterogeneities within that subsurface. Hydraulic testing and core sampling have shown that the heterogeneity of resistivity corresponds to heterogeneity of hydraulic conductivity, opening the possibility of determining the magnitude of the high-flow zones within

each profile. The "Grid Volume" function in Surfer 8 was used to calculate the area within the vadose zone of each profile greater than a given resistivity.

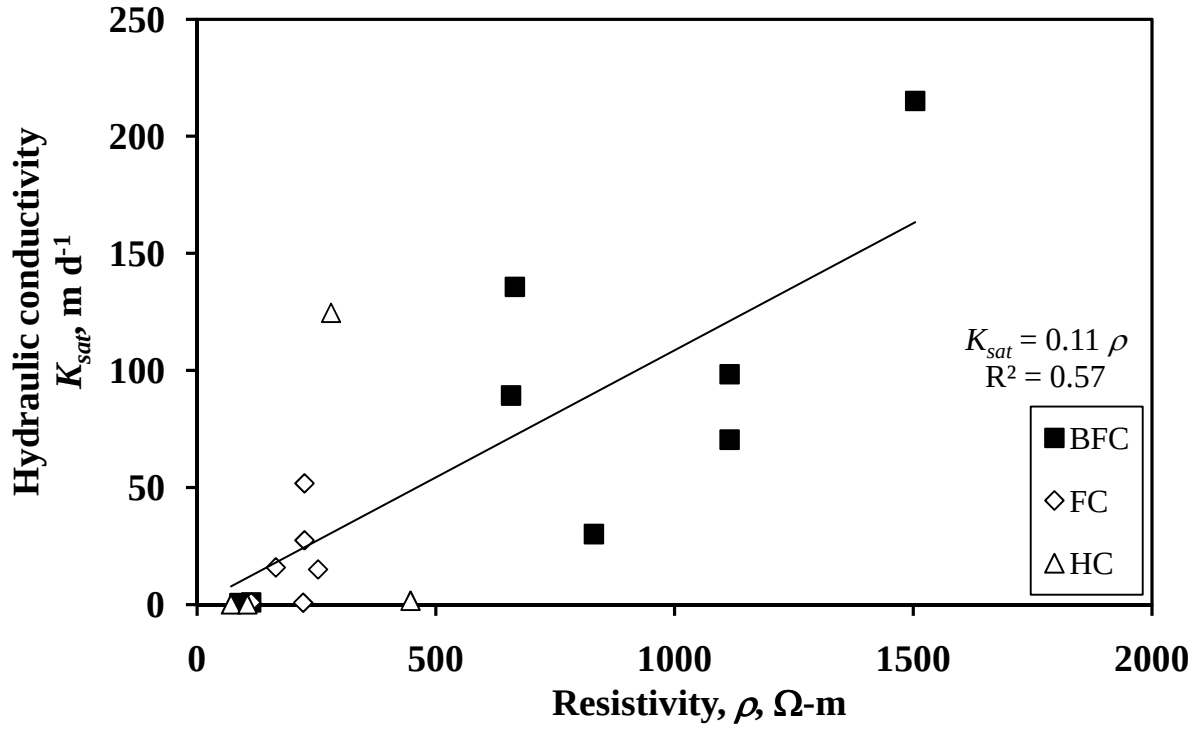

Figure 2.8. Linear regression between ERI resistivity (ρ, Ω-m) and field hydraulic conductivity (Ksat, m d^{-1}). Samples from Barren Fork Creek (BFC), Flint Creek (FC), and Honey Creek (HC) are indicated by separate symbols. The regression includes all samples, and is significant at α = 0.05 (P = 0.004).

A series of those area calculations with increasing resistivities produced a cumulative distribution of resistivity by area which was converted to hydraulic conductivity using equation (1). A normalized area was calculated by dividing each area by the total area for that line (Figure 2.9). The area (m^2) of resistivity/hydraulic conductivity for BFC, HC and FC given in Figures 2.9a, 2.9c, and 2.9e, respectively, show the range of areas for each ERI profile. This area was a function of the length of the line and the vertical distance between the ground surface and the

water table at the line location. BFC_RA, the BFC line with the greatest area, was a "roll-along", consisting of multiple co-linear ERI profiles (180 m in total) collected separately and

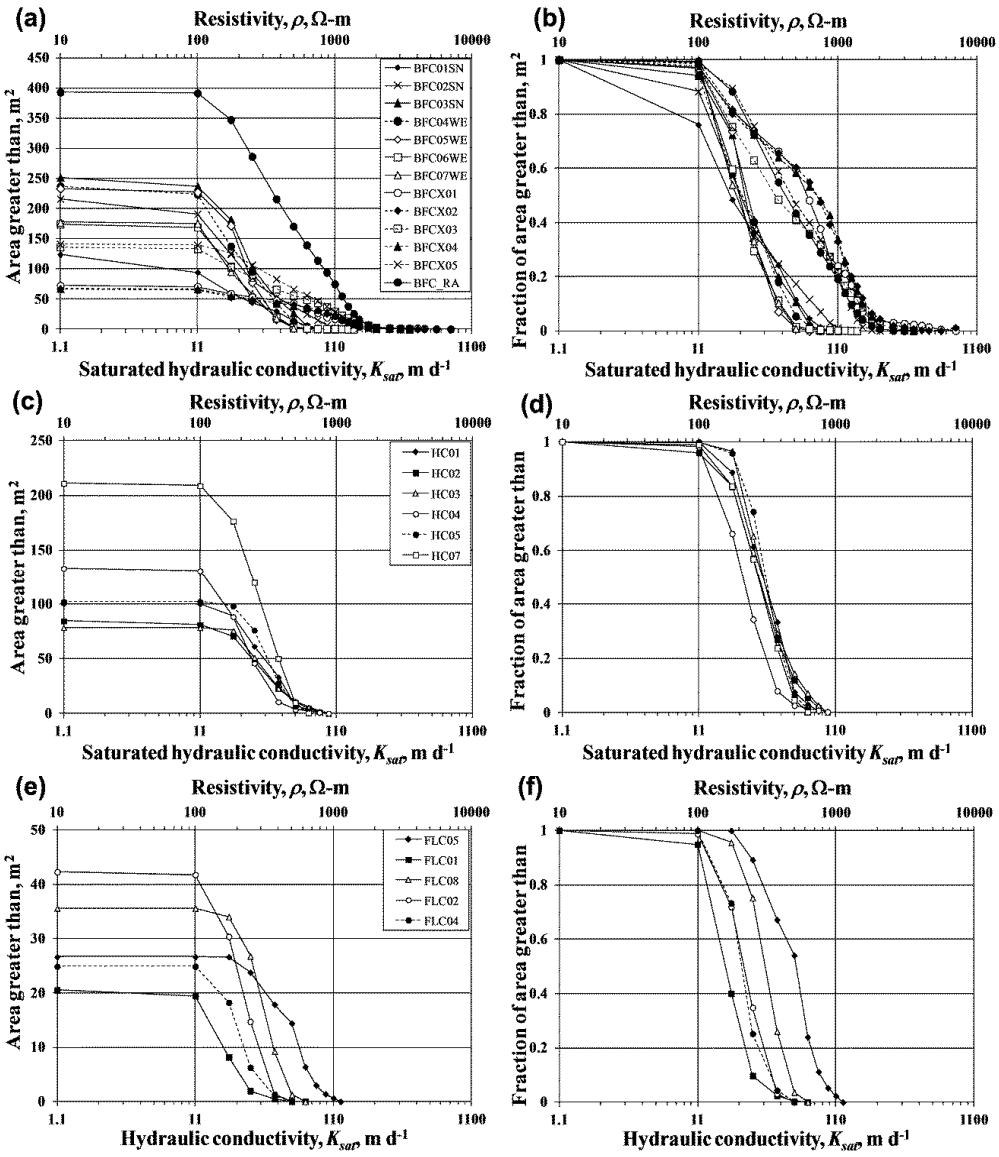

Figure 2.9. Area of resistivity and estimated hydraulic conductivity for ERI profiles from Barren Fork Creek (a and b), Honey Creek (c and d), and Flint Creek (e and f). The top axis of each plot shows the ERI resistivity (Ω-m) and the bottom axis the hydraulic conductivity (m d^{-1}). The vertical axis of plots "a", "c" and "e" is total area of the vadose zone portion of the ERI profile, and for plots "b", "d" and "f" the vertical axis is the relative fraction of area.

then processed as a single unit. Other BFC lines with larger areas (BUT02SN, BUT03SN, and BUT06WE) have relatively large electrode separations and therefore larger total line distances (1.5, 82.5; 2, 110; 2.5, 137 m, respectively). Similarly BFCX01, the BFC ERI profile with the smallest total area, had the smallest electrode spacing (0.5 m) and hence total length (27.5 m). The HC ERI profiles all had one m spacing. The relatively large area for HC07 was due to it being 84 m long, a result of its configuration as a "roll-along" rather than a single line. The FC ERI profiles had the smallest total area because of the narrow width of the forested floodplain. The one m electrode spacing for the ERI profiles at the FC site caused the profiles to extend across the narrow floodplain and onto the adjoining terrace, and only the portion of the FC ERI profiles that fell within the floodplain was included in the figures and calculations.

The range of ERI resistivity spanned nearly four orders of magnitude at BFC, and about three orders of magnitude at HC and FC, with BFC having relatively large fractions greater than 1000 Ω-m (Figures 2.9b, 2.9d, and 2.9f). The fractional area of the BFC ERI profiles fell into two distinct configurations: one featuring a higher proportion of low resistivity and fewer high resistivity resulting in a steeper curve (BUT01SN, BUT02SN, BUT03SN, BUT04WE, BUT05WE, BUT06WE and BUT07WE), and the other featuring a relatively large number of high resistivity values resulting in a shallower curve (BFCX01, BFCX02, BFCX03, BFCX04, BFCX05 and BFC_RA) (Figure 2.9b). The HC fractional area plot showed ERI profiles with very similar patterns, all of which had resistivity that fell into a range similar to that of the low-resistivity BFC profiles (100 – 1000 Ω-m) (Figure 2.9d). The FC fractional area plot showed that most of the ERI profiles fell within the range of 100 – 1000 Ω-m, but the patterns of the ERI profiles were not consistently similar (Figure 2.9f).

The "high-resistivity" BFC fractional area curves appeared unique among all ERI profiles in having a large area of high resistivity (Figure 2.10). The presence of large areas of high resistivity within those ERI profiles would correspond to areas of very high hydraulic conductivity in the subsurface and could indicate the presence of a high flow area. The 84^{th} percentile denotes one standard deviation above the mean (in a normal distribution) and is a standard representative of large values in a distribution in disciplines such as fluvial sedimentology (Bunte and Abt, 2001). The 84^{th} percentile values calculated from the ERI profile data were chosen to be representative of the high resistivity for each profile (Figure 2.10). To test whether the high-resistivity BFC ERI profiles were significantly different than the other ERI profiles, a two-sample t-test was performed on the 84^{th} percentile values. The mean of the 84^{th} percentile of the high-resistivity BFC ERI profiles was significantly different when compared to the mean of all other 84^{th} percentiles ($P = 0.000$, $\alpha = 0.05$). ANOVA and Tukey's pairwise comparison of the differences between the individual sites (high-resistivity BFC, low-resistivity BFC, HC and FC) showed that the high-resistivity BFC ERI profiles were significantly different than all other sites (95% family confidence level) but that the remaining sites were not statistically different.

The magnitude of the high resistivity relative area within the ERI profiles caused a significant difference between the high-resistivity profiles at BFC and the remaining lines from all sites. The high-resistivity BFC ERI profiles had 16% of the area with resistivity greater than 1000 Ω-m, equivalent to a hydraulic conductivity of 110 m d^{-1} or greater, while the remaining profiles had an equivalent area with resistivity above only 300 Ω-m and equivalent hydraulic conductivity of 33 m d^{-1}. This established the existence of small areas within those high

resistivity profiles with very high hydraulic conductivity, which could form preferential flow paths within the gravel floodplain as observed by Heeren et al. (2011).

The median ERI resistivity was at least 185 Ω-m (hydraulic conductivity 20 m d^{-1}) for the low-conductivity ERI profiles. This means that, while the maximum hydraulic conductivity for those lines was much less than the high-resistivity ERI profiles, at least half of the each of the remaining ERI profiles had hydraulic conductivity of 20 m d^{-1}, which was within the range of well-sorted gravel (Fetter, 2001). The vadose zone of the BFC, HC and FC floodplains were

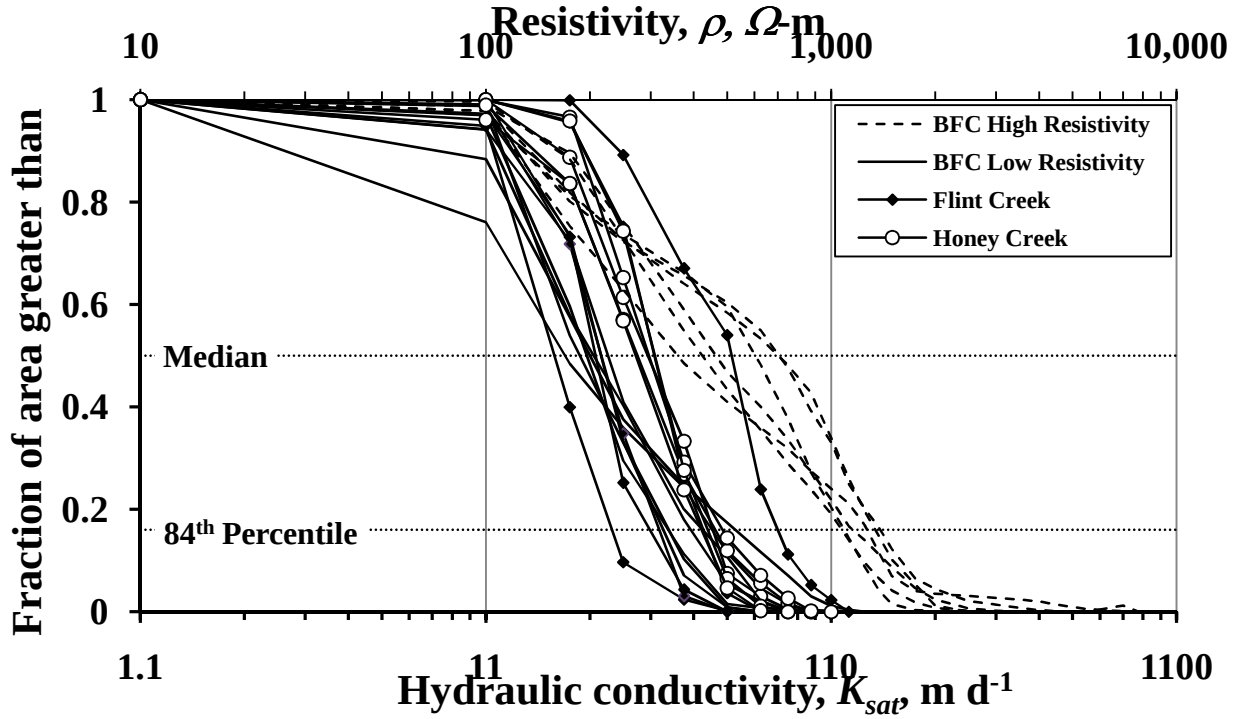

Figure 2.10. Area fraction plot for all ERI profiles. ERI profiles from Barren Fork Creek (BFC) are divided into "High resistivity" and "Low resistivity" based on significant differences between 84^{th} percentile values ($\alpha = 0.05$).

thus likely to behave as broad-scale zones of high hydraulic conductivity and form an active connection between the floodplain and the stream under the appropriate, saturated conditions.

The three study sites represent part of the range of gravel floodplains within the Ozark ecoregion. The similarity of the low-resistivity ERI profiles from those sites encouraged the conjecture that all gravel floodplains with similar soil and bedrock characteristics within the Ozarks share at least these basic characteristics: resistivities that occupy the range from 10 to 1000 Ω-m, and large areas within the floodplain at with hydraulic conductivities of 20 m d^{-1} or above. Consequently large areas within Ozark gravel floodplains may be broad-scale high-conductivity features with potentially significant consequences for the movement of environmentally sensitive materials. Furthermore, the "high-resistivity" ERI profiles from BFC included limited areas that featured very high resistivity and hydraulic conductivity. Such areas, if they are directly connected to the stream, have the potential to transport environmentally sensitive materials to a stream without attenuation (Fuchs et al., 2009). The high-resistivity features were only detected at BFC, but it seems unlikely that the BFC site is unique within the Ozarks.

2.5 SUMMARY AND CONCLUSIONS

The geophysical technique ERI was used in three floodplain sites and detected differences within the gravel subsoil that was based on an analysis of core samples that showed differences in fines content within the gravel. Additionally, in-situ tests with a gravel permeameter showed that the fines content was correlated to the hydraulic conductivity of the subsoil. Linear regression of the ERI resistivity to the hydraulic conductivity was significant ($\alpha = 0.05$), and allowed the resistivity profiles to be interpreted as hydraulic conductivity maps. The area distribution for resistivity and hydraulic conductivity was calculated for the ERI

profiles using Surfer 8. The fractional area plots followed two distributions: “low resistivity” ERI profiles shown at all three sites and “high resistivity” shown for some of the BFC ERI profiles. The 84^{th} percentile values for the two distributions, chosen to represent the area of high resistivity within the ERI profiles, were statistically different ($P = 0.000$, $\alpha = 0.05$), while the “low resistivity” ERI profiles from all sites were not statistically different at $\alpha = 0.05$. The “low resistivity” ERI profiles corresponded to hydraulic conductivities of 20 m d^{-1} or more extending over least half of the area, indicating that large portions of the studied floodplains may be broad-scale high-conductivity features with potentially significant consequences for the movement of environmentally sensitive materials. Those “low resistivity” ERI profiles appeared at all three study sites and may be typical for all Ozark gravel floodplains. The “high resistivity” ERI profiles contained small areas with extremely high hydraulic conductivity (110 m d^{-1}), a configuration which could constitute a preferential flow pathway and transport environmentally sensitive materials without attenuation under the appropriate conditions. The “high resistivity” ERI profiles were unique to BFC for this study, but it seems unlikely that the BFC site was unique within the Ozarks, and further work is required to determine the fluvial, geologic and geomorphic factors that contribute to creating similar high resistivity and hydraulic conductivity features.

CHAPTER 3

Influence of Variability in Hydraulic Conductivity on Surface Water/Groundwater Interactions in an Alluvial Floodplain

3.1 ABSTRACT

Floodplains are environmentally sensitive features composed of complex depositional patterns of ancient and recent stream sediments that are often distinct from surrounding non-fluvial rocks and soils, and are important factors controlling the interaction between surface and groundwater, including the movement, fate and transport of environmental contaminants including nutrients. Where coarse sediments occur in floodplains those interactions may be rapid, and occur tens or hundreds of meters from the stream. Research is needed to address the manner in which coarse floodplain materials with high hydraulic conductivity affect the movement patterns of alluvial groundwater. This study will examine groundwater patterns during a flood event at a study site on Barren Fork Creek, which is in the Ozark region of Oklahoma, a region where chert gravel is common as stream-bed material and within the alluvial floodplains. Estimates of hydraulic conductivity within the floodplain vadose zone were prepared by interpolating selected elevations of vertical ERI profiles and then transforming those values with a linear function relating resistivity and hydraulic conductivity. Event peak elevations from the monitoring wells showed an elevation attenuation of only 0.25 m, and a time

delay of 1.5 hours at a distance of 180 m from the stream, indicating that the vadose zone aquifer was a “high-flow domain” that responded quickly to changes in stream elevation. Water table elevations from a flood event May 1-5, 2009 were compared to maps of hydraulic conductivity from the corresponding elevation. Areas with high hydraulic conductivity matched areas with lower water table slope at the same elevation, indicating that extreme high hydraulic conductivity affects the water table even in a matrix with high hydraulic conductivity characterized as a high flow domain. This implies that the most important hydraulic characteristic of the study floodplain is the bulk hydraulic conductivity; the hydraulic conductivity of the median and above.

3.2 INTRODUCTION

Floodplains are generally planar landscape features that are composed of ancient and current stream sediments, which are typically higher in hydraulic conductivity than the adjacent hillslope sediments (Woessner, 2000). Groundwater within the floodplain will flow generally down-plain, in a direction generally parallel to the surface water flow. As the surface stream meanders across the floodplain, the groundwater flow lines may converge on or cross the stream channel, creating “gaining”, “losing”, or “flow-through” reaches, and promoting different qualities of interchange between surface water and groundwater. The magnitude of the exchange at the floodplain scale will be affected by factors such as topography, river geometry and depositional structure (Woessner, 2000). Surface water-groundwater interaction is important as a habitat gradient in which organisms utilize and influence the movement of nutrients and energy (Findlay et al., 1993; Stanford and Ward, 1993; Battin, 1999; Hancock et al., 2005; Boulton et al., 2008). Surface water-groundwater interaction is also an important factor in the movement,

fate and transport of environmental contaminants including nutrients (Kazezyilmaz-Alhan and Medina, 2006; Landmeyer et al., 2010; Heeren et al., 2011).

The presence of coarse sediments with relatively high hydraulic conductivity can link surface flows to distal floodplain areas beyond the range of anticipated interaction (Sophocleous, 1991; Stanford and Ward, 1992; Poole et al., 1997; Amoros and Bornette, 2002; Naiman et al., 2005). If these structures are limited in extent, for example a linear feature such as a paleochannel, these surface water-groundwater interactions may be termed a "preferential flow path" (PFP). Additionally, a floodplain consisting mainly of high hydraulic conductivity sediments may exhibit high levels of interaction between the stream and the groundwater throughout the floodplain; such a system may be termed a "high-flow domain".

The Ozark ecoregion of Missouri, Arkansas, and Oklahoma is an area of approximately 62000 km^2, characterized by carbonate rock or sandstone plateaus dissected by steep-sided stream valleys. Erosion of the carbonate bedrock (primarily limestone) by slightly acidic water has left a large residuum of chert gravel in Ozark soils, and produced gravel bed streams with floodplains generally consisting of coarse chert gravel overlain by a mantle (1–300 cm) of gravelly loam or silt loam (Figure 3.1). Evidence of rapid and preferential flow within gravelly Ozark aquifers was found by Fuchs et al. (2009) at a floodplain site on Barren Fork Creek (BFC) in the Oklahoma Ozarks, who found that conservative tracers and dissolved phosphorus moved in preferential pathways significant distances within the gravel zone under an injection trench dug through the cohesive topsoil. Also, Heeren et al. (2010), working under natural flow conditions independently at the same site, found that phosphorus at concentrations similar to the stream could be found in alluvial groundwater samples taken simultaneously from monitoring wells placed more than 100 meters from the stream.

Figure 3.1. Gravel and gravel-dominated soils in alluvial floodplains at various sites in the Ozark ecoregion of eastern Oklahoma. Locations shown are: (a) and (d) Barren Fork Creek near Eldon, OK (latitude 35.90°, longitude -94.85°), (b) Honey Creek near Grove, OK (latitude 36.54°, longitude -94 .7), (c) Flint Creek near Kansas, OK (latitude 36.20°, longitude -94.71°).

In Chapter 2, the study used Electrical Resistivity Imaging (ERI), along with limited core sampling, and hydraulic testing to survey the subsurface at the BFC site and found that the resistivity within the gravel subsoil was correlated to the fraction of fine material (< 0.2 mm diameter), with higher resistivities correlated to lower fractions of fine material. Furthermore, there was a positive linear relationship between the resistivity of the subsoil and hydraulic

conductivity at tested locations. The ERI survey showed that gravel with low fines content and high hydraulic conductivity existed within the vadose zone of the floodplain at BFC, representing a potential high hydraulic conductivity pathway between the floodplain surface and the alluvial groundwater.

It is important to understand the role of high hydraulic conductivity sediments, and how they affect the movement of groundwater within a floodplain. Connection between a stream and alluvial groundwater that occur over large distances, or that create a vertical connection between the floodplain surface and groundwater both could have important ramifications for stream water quality. Such connections might be most evident under rising stream stage conditions, when the groundwater gradient is forcing water into coarse sediments normally within the vadose zone.

The purpose of this research was to (1) extrapolate an existing ERI survey of the BFC site in order to create an estimate of the distribution of resistivity throughout the site, (2) to utilize the relationship between resistivity and hydraulic conductivity to create a site map of hydraulic conductivity for selected depths within the vadose zone of the floodplain, and (3) to compare these maps to water table elevations to understand how variations in hydraulic conductivity influence surface water/groundwater interactions. The general assumption would be that limited preferential flow could occur and influence this interaction in gravel floodplains containing such high hydraulic conductivity soils.

3.3 METHODS

3.3.1 Study Area

The Ozark ecoregion consists of broad, uplifted plateaus of carbonate sedimentary rocks dissected by deep river canyons occupied by clear, high-gradient streams. Residual chert gravel derived from weathering of the bedrock is common in the stream beds, the banks, and in the

alluvial floodplains. The study site consists of level pastureland on Barren Fork Creek (latitude 35.90°, longitude -94.85°), and is located within the Ozark ecoregion of Oklahoma. The study site was named after the creek, and will be referenced henceforth as the Barren Fork Creek site (BFC). Alternate spellings of the stream name include Baron and Barron Fork; our chosen variant seemed most compliant with local usage. Bedrock within the watershed is primarily cherty limestone (Keokuk/Reeds Spring formation), and soils at the BFC site are silt and silt/gravel (Razort and Elsah series) of fluvial origin. The 1.2 ha site occupies the south bank of a northward bend in Barren Fork Creek (Figure 3.2), and is approximately 2.5 km downstream from a USGS stream gage (Baron Fork at Eldon, 7197000), hereafter termed "USGS gage". The median daily discharge at the USGS gage from 61 years of records is 3.6 m^3s^{-1}.

The study site is located near the south wall of an alluvial valley, trending generally east to west and consisting of limestone valley walls (Figure 3.3). Caves, sinkholes, springs and other karst features associated with carbonate rocks have the potential to affect the local hydrology, are not known exist within the study area; however their presence cannot be ruled out. The alluvial floodplain itself consists of a mantle of silt and silt-gravel soils (1-3 m, Razort and Elsah soil series) overlying a deep, gravelly subsoil. Groundwater within the alluvial floodplain is assumed to flow down-valley (with the stream direction), with the local configuration of the stream within the valley.

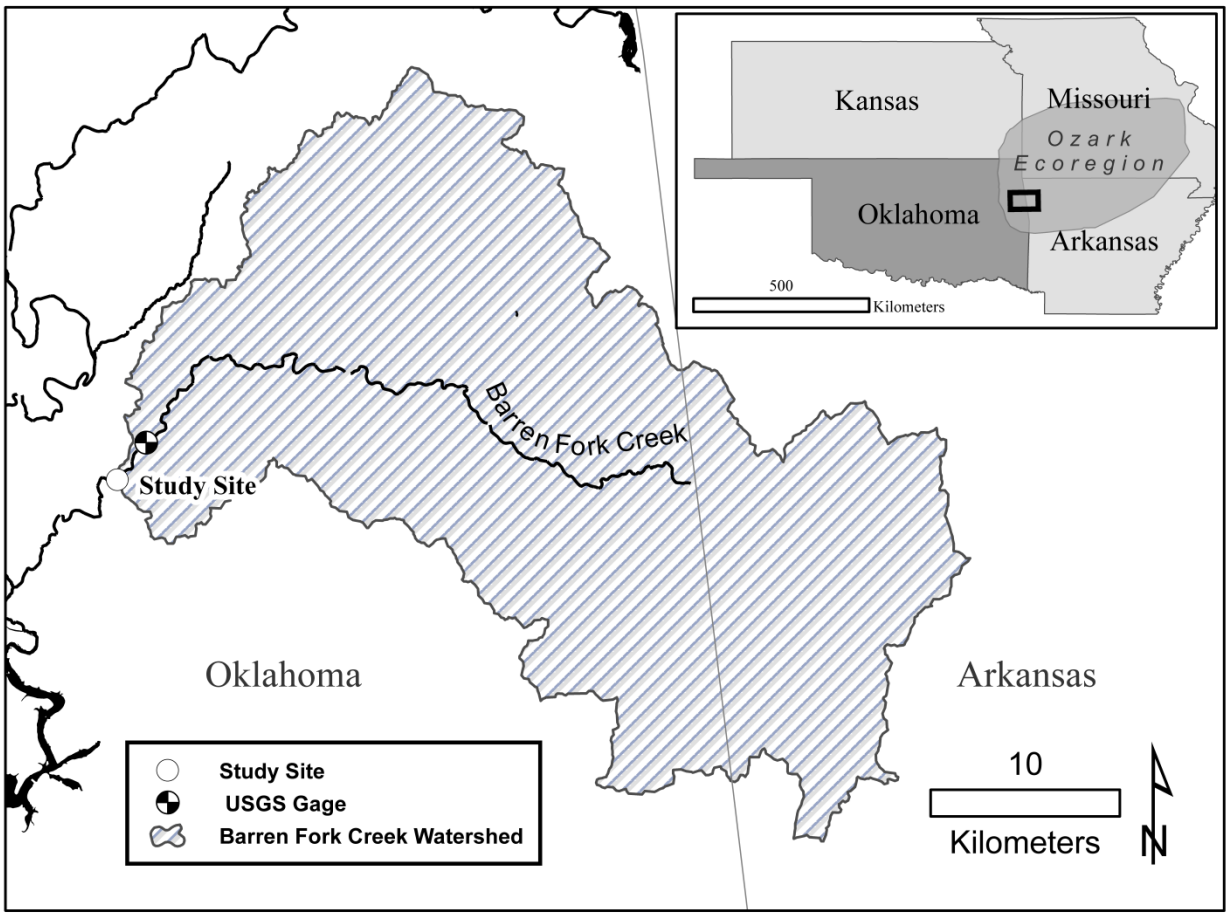

Figure 3.2. Location of Barren Fork Creek (BFC) study site and it's watershed within the Ozark Ecoregion of Oklahoma.

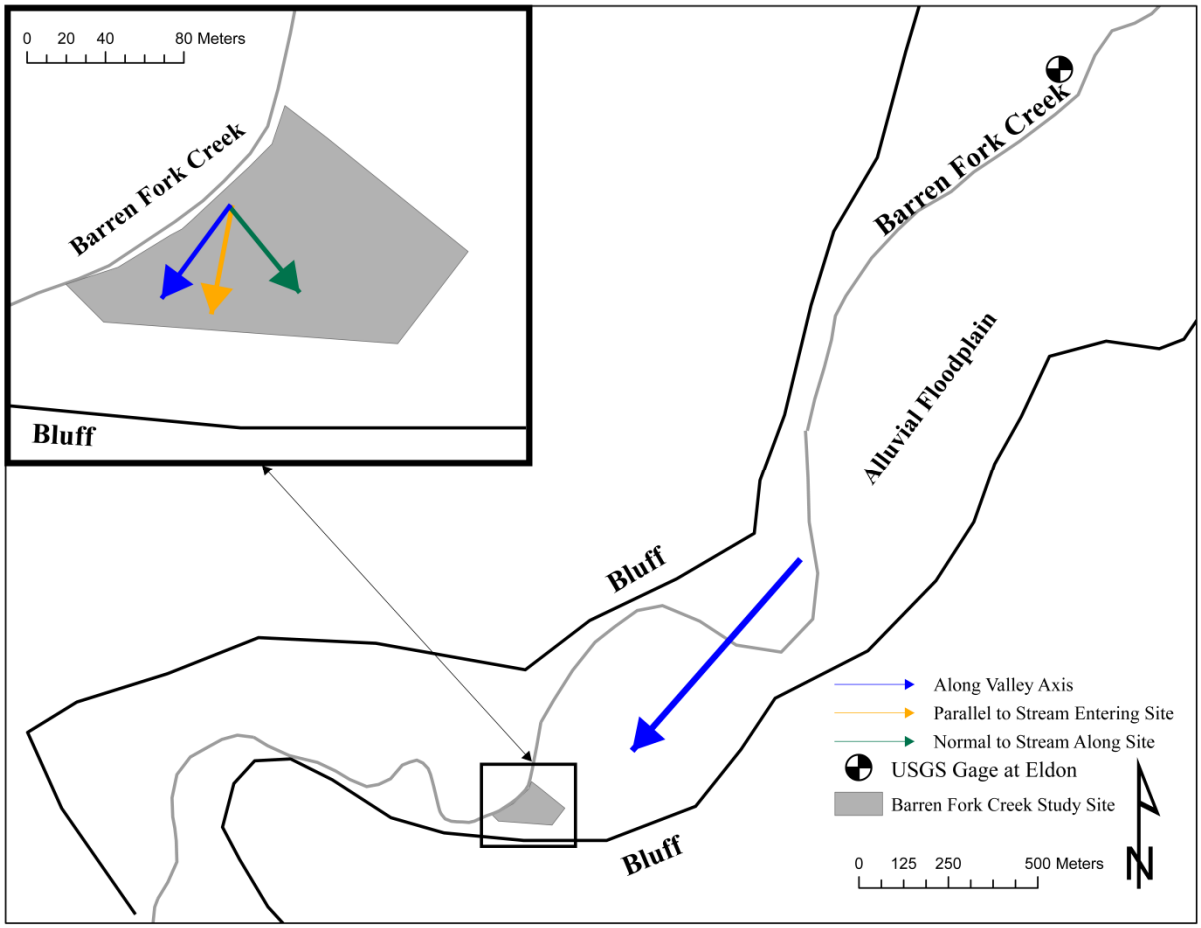

Figure 3.3. Map of the Barren Fork Creek floodplain in the vicinity of the study site. The terrain includes a flat floodplain surface bounded by steep limestone bluffs. Barren Fork Creek flows northeast to southwest. The angle of the bank at the study site relative to the stream is 228°. Colored arrows indicate the general direction (degrees, clockwise from north) of the valley axis (blue arrow, 215-225°), of Barren Fork Creek where it enters the study site (yellow arrow, 190°), and of the direction normal to the bank where it is adjacent to the study site (green arrow, 138°).

3.3.2 Groundwater Monitoring

Observation wells were installed in the alluvial floodplain with a Geoprobe Systems direct-push drilling machine (6200 TMP, Kejr, Inc., Salina, KS). The wells were driven to refusal, a depth of 4 to greater than 5 m, and included a 2 to 3 m screened section at the base with the remainder solid PVC. Bentonite clay was placed around the top of the well casing to prevent surface runoff from entering the borehole. The wells were instrumented with automated water level loggers (HoboWare, Onset Computer Corp., Cape Cod, MA, water level accuracy of 0.5 cm) to monitor water pressure and temperature at 5-min intervals from April 2009 to April 2010, with one logger placed above the water table to account for changes in atmospheric pressure. The logger data were processed with HoboWare Pro software, which accounted for changes in atmospheric pressure as well as changes in water density due to temperature and produced water table elevation data (1 cm accuracy). Reference water table elevations were obtained with a water level indicator, and laser level. Well locations were surveyed using a TOPCON HiperLite Plus Real-time Kinematic (RTK) global positioning system configured with a base station and rover unit (4 cm accuracy). These data were corrected for positional errors using the National Geodetic Survey Online Positioning User Service (OPUS). A set of 33 observation wells were originally installed and 23 were instrumented; however, active erosion of the streambank at the study site carried away some wells and loggers. The position of the bank was surveyed with GPS on April 18, 2009, and 20 loggers were utilized in the current study for the storm pulse examined in this paper.

3.3.4 Electrical Resistivity Imaging

Electrical Resistivity Imaging (ERI) surveys were conducted at the floodplain sites for the purpose of characterizing the heterogeneity of the unconsolidated floodplain sediments,

especially in the vadose zone between the ground surface and the alluvial water table. The ERI data were collected using a SuperSting R8/IP Earth Resistivity Meter (Advanced GeoSciences Inc., Austin, TX) with a 56-electrode array. Fourteen lines were collected at the BFC site between June 2008 and March 2009, each of which produced a two-dimensional vertical profile of the aquifer along the length of the electrode array. The surveys variously employed electrode spacings of 0.5, 1.0, 1.5, 2.0 and 2.5 m with associated profile lengths of 28, 56, 84, 112, and 140 meters, and depths of investigation of 7.5, 15.0, 17.0, 22.5 and 25.0 m, respectively. The zone of interest was the vadose zone, the soil above the baseflow water table, which was within 3 m of the ground surface at the site and thus well within the ERI depth of investigation. The resistivity sampling with the SuperSting R8/IP, and subsequent inversion utilized a proprietary routine devised by Halihan et al. (2005), which produced higher resolution images than conventional techniques. The ERI survey electrode locations were spatially georeferenced with the same GPS equipment and methods utilized for the monitoring wells.

3.3.5 Interpolations

Interpolation techniques were used to create site-wide estimates of both water table elevation and resistivity from the point values produced by the recording instruments. Interpolations of water table elevations were made using Surfer 8 (Golden Software, Inc., Golden, CO). Estimates of the water table surface were produced with the "Minimum Curvature" method in Surfer, which approximates the surface by iteratively fitting a continuous curve (often visualized as a flexible sheet), under tension from the edges, to the data. In the study, the minimum tension was utilized, which allowed the surface to best conform to the data. The minimum curvature method produces a smooth surface that has been used in many earth science applications (Smith and Wessel, 1990). Estimates of the general directional trend of the

water table surface were derived by fitting a first-order polynomial to the water table elevations using the "Polynomial Regression" method in Surfer to create a best-fitting "plane", and then calculating the aspect (direction) of that planar surface (in degrees clockwise from north). These planar estimates were used to compare the changes in water table direction as stream stage changed over time.

Interpolations of resistivity data were created using the Conditional Simulation interpolation method, which preserved the distribution of sampled characteristics across the site (Journel and Huijbregts, 1978), using the geostatistical program GS+ (Gamma Design Software, LLC, Plainwell MI). The ERI data (resistivity, ρ, Ω-m) were log-transformed to better approximate a normal distribution, then anisotropic variograms were prepared and used in the conditional simulation. The resulting grid of interpolated values was back-transformed to the original resistivity units. The final grid of values was imported into Surfer 8 for display.

3.3.6 Analysis

The factors controlling the movement of alluvial groundwater include (1) the local geometry and position of the stream channel within the floodplain, (2) the relation of stream stage to the water table, and (3) the distribution of hydraulic conductivities within the floodplain (Woessner, 2000). The first two factors can be addressed with watershed maps, Barren Fork Creek hydrographs, and the water table directions derived from planar interpolations. The third factor was addressed by comparing water table interpolations with hydraulic conductivity maps based on interpolating resistivity measurements that exploited a relationship between resistivity and hydraulic conductivity applicable to Ozark gravel subsoils. To address the question of whether the spatial variation in hydraulic conductivity can affect the flow of groundwater at the study site, water table maps were overlaid on resistivity maps. Water table interpolations were

derived at multiple times from a runoff event with a peak flow of 204.5 $m^3 s^{-1}$ and a return interval of approximately 1.25 years recorded at the USGS gage. The event began at 10:00 AM on 5/1/2009, peaked at 6:00 PM on May 3, 2009, and the recession continued until 10:00 PM on 5/5/2009, when a subsequent runoff event was recorded on the hydrograph (Figure 3.4).

3.4 RESULTS AND DISCUSSION

The main down-valley trend in the vicinity of the study site was difficult to determine, as the site was located in a bendway of the valley, but the range of down-valley directions for the straight section of the valley upstream of the site was approximately 215 to 225° (clockwise from north, Figure 3.3), therefore it is likely that groundwater flowing with a down-valley trend will exhibit a gradient direction that is close to or greater than this range. Barren Fork Creek approached the site at the northeast corner of the site at an angle of about 190°, and then passed along the northwest border of the site at an angle of about 228°, which is close to the down-valley trend direction. A water table gradient direction close to 190° would imply that the groundwater flow was influenced by the stream as it approached the site. Because the angle between the bank and the site is 228°, only gradient directions greater than this are likely to produce “gaining stream” conditions in which water from the alluvial aquifer re-enters the stream. Note that interestingly a specific direction does not occur at a specific stream stage but rather as a function of the change in stream stage (Figure 3.4).

During the runoff event the stream stage increased 2.2 m (211.9 to 214.1m, Figure 3.4), and the water table gradient ranged over a 104° span (138° to 242°). The initial period shown on the event hydrograph was a period of recession after the previous event peak 12 days earlier, in which the stream stage was decreasing slowly (Figure 3.4).

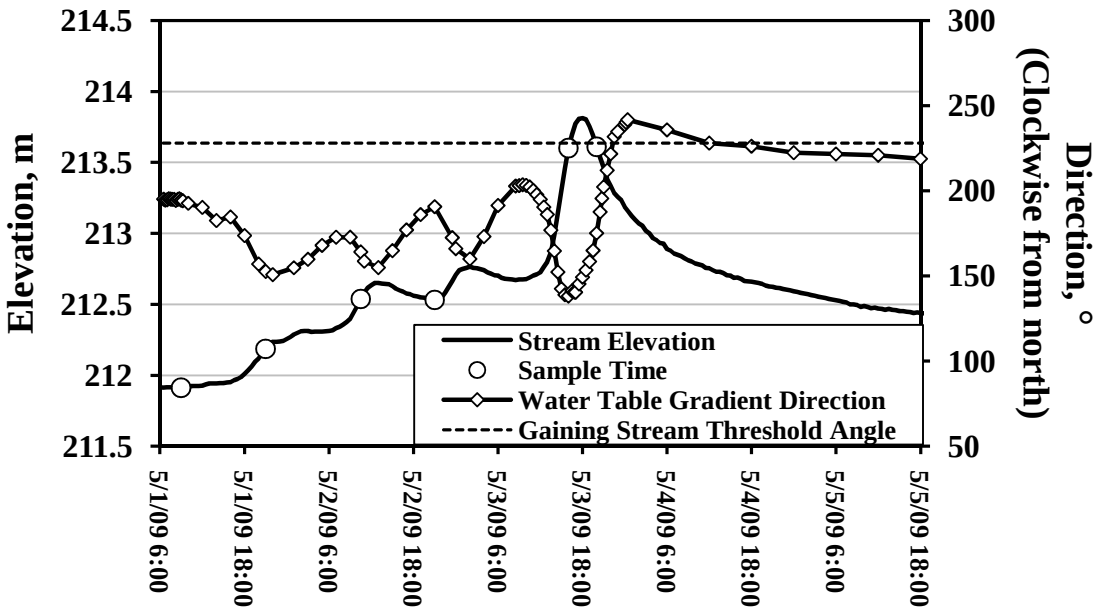

Figure 3.4. Stream hydrograph and change in water table gradient direction with change in storm hydrograph for storm runoff event May 1-5, 2009 on Barren Fork Creek, OK (30 minute stage record, USGS gage 7197000). Open circles indicate times for water table/resistivity comparisons. Actual values are shown in Table 3.1. "Stream Stage" is the hydrograph derived from USGS gage at Barren Fork records, "Water Table Gradient Direction" is the angle of aspect derived from planar interpolations of water table elevations from the Barren Fork Creek study site, and the "Gaining Stream Threshold Angle" was calculated from the angle (clockwise from north) of the stream bank at the study site. Water table (WT) gradient angles greater than this angle are estimated to produce discharge from the alluvial aquifer to the stream.

The peak water table elevation, and the time of delay after the first recorded peak for each monitoring well were plotted against the well distance from the stream (Figure 3.5). The peak elevation in the wells farthest from the stream (180 m) was only about 0.25 m reduced from

the peak recorded at the wells within 1 m of the stream; a condition that indicates that little energy was lost to the intervening aquifer material. The peak traveled rapidly as well, with the peak in the wells most distant from the stream occurring about 1.5 hours after the peak near the stream. Rapid water movement with little energy loss as water moved through the aquifer was a condition expected of a "high-flow domain".

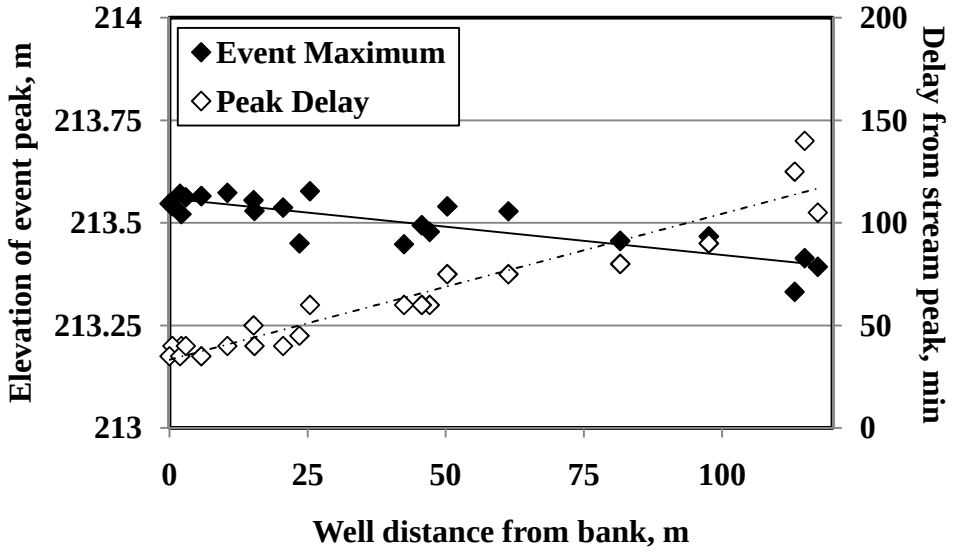

Figure 3.5. Elevation of maximum flood peak (m) measured in monitoring wells, and delay in time (min) between event peak in the stream and the monitoring well versus distance (m) from the stream. The regressions are significant ($\alpha = 0.05$), and R^2 for Event Maximum is 0.68 and Peak Delay is 0.91

The water table gradient direction at this time was 195°, a direction slightly greater than the angle at which the Barren Fork Creek approaches the site. The gradient direction decreased (i.e. shifted counter-clockwise) as the stream stage increased, and increased (i.e. shifted clockwise) as the stream stage fell over the three peaks of the event. The minimum gradient direction (138°) occurred at the event peak, and the maximum gradient direction (242°) occurred at 12:30 AM May 4, 2009, during the initial hours of the hydrograph recession following the event peak.

The minimum gradient direction (138°) corresponds approximately to the direction normal to the angle of the bank along the northwest site boundary (Figure 3.3), and indicates that the water table was primarily responding to water entering the aquifer from the stream during the high stage of the event peak. The maximum gradient direction (242°) occurred during the recession limb of the hydrograph, a period in which water flowed from the aquifer into the stream. Water table gradient directions that were greater than the angle of the bank at the study site (228°) indicated that water was flowing from the aquifer to the stream. This "gaining stream" condition persisted for 13 hours, between 10:30 PM 5/3/2009 and 12:00 PM 5/4/2009 (Figure 3.4), before shifting to a gradient direction (~220°) that may be considered to constitute a down-valley trend. The study alluvial aquifer thus appeared to respond primarily to local stream conditions except at very high stream stages, when down-valley flow prevailed.

An important element for understanding the hydraulic behavior of the alluvial aquifer was how the spatial variation of hydraulic conductivity affected the shape of the water table and thus the flow of groundwater. A geophysical study of the study floodplain using Electrical Resistivity Imaging (ERI) was undertaken to gain understanding of the subsurface variation. One important finding of Chapter 2 was that that the aquifer consisted of gravel with varying

proportions of fine material, and that high resistivity within the floodplain corresponded to a lower proportion of fines. A linear relationship ($R^2 = 0.57$) was established between resistivity and hydraulic conductivity in gravel floodplains, including the Barren Fork Creek study site, which allowed the resistivity survey to be used to estimate hydraulic conductivity using the equation

$$K_{sat} = 0.11\ \rho \qquad (3.1)$$

where K_{sat} is hydraulic conductivity (m/d), and ρ is resistivity (Ω-m).

Comparisons between the configuration of the water table and the hydraulic conductivity of the aquifer were made by (1) selecting a point in time from the event hydrograph, (2) interpolating a planar "slice" of the aquifer by selecting ERI data at that elevation, (3) interpolating the water table from the well logger records at that time, and (4) overlaying the two interpolated maps. Several stream stages were chosen from the runoff hydrograph as marker elevations for comparison, including baseflow, rising limb, falling limb, and a transition between falling and rising limbs (Table 3.1, Figure 3.4). Several of the elevations (212.5 and 213.8 m) included comparisons with two water table interpolations in order to assess whether the distribution of hydraulic conductivity affected those water table gradient directions differently. The aquifer characteristics will be discussed primarily in terms of resistivity, since that was the directly measured parameter, when appropriate the resistivity will be transformed to hydraulic conductivity using equation (3.1).

The means and medians for the distributions of interpolated resistivity for each elevation "slice" increased with elevation, indicating that the presence of low-fines gravel deeper within the floodplain vadose zone. The distributions were also positively skewed and kurtotic; indicating that the aquifer was dominated by the lower resistivity values (Table 3.2).

Table 3.1. Date and time, stream stage and hydrograph slope for water table interpolations. Stream stage was taken from USGS gage Barren Fork at Eldon (7197000) 30-minute stage record. Hydrograph slope was calculated using a 7-record moving window centered each time increment. Positions on event hydrograph are shown in Figure 3.4.

Sample Time	Stream Stage (m)	Slope
5/1/2009 9:00	211.9	0.07
5/1/2009 21:00	212.2	1.23
5/2/2009 10:30	212.5	1.98
5/2/2009 21:00	212.5	0.22
5/3/2009 16:00	213.8	5.44
5/3/2009 20:00	213.8	-3.41

Importantly, when the resistivity values were converted to hydraulic conductivity, all values at each elevation slice are within the range for gravel (~2.5 to 250 m/d, Schwartz and Zhang, 2003), and most were >25 m/d. This implied that the vadose zone of the aquifer was highly hydraulically conductive and likely to respond quickly to stage changes in the stream. The lowest aggregate resistivity and hydraulic conductivity exists in the highest "slice" (213.8 m) close to the floodplain surface, a zone known from experience at the site to consist primarily of silt-dominated floodplain soil (Razort and Elsah) rather than gravel.

Table 3.2. Resistivity statistics for interpolated elevation "slices" of the Barren Fork Creek study site alluvial aquifer. "Elevation" is of the interpolated plane within the alluvial floodplain in meters above MSL, and corresponds to the stream stage elevation in Table 3.1.

Elevation (m)	Mean (Ω-m)	Standard Deviation (Ω-m)	Minimum (Ω-m)	Median (Ω-m)	Maximum (Ω-m)	Skewness	Kurtosis
211.9	391.1	340.2	48.0	257.0	2652.1	2.4	5.8
212.2	356.0	257.4	29.5	252.8	2467.1	1.9	3.6
212.5	346.4	340.5	33.3	227.4	2587.2	2.6	6.7
213.8	187.7	75.3	27.1	165.1	906.1	1.8	6.3

The spatial variation in resistivity, and hence hydraulic conductivity, was not distributed randomly at the different elevations, but rather was clustered which created distinct regions of high and low resistivity/hydraulic conductivity within the aquifer (Figure 3.6). The primary feature was a zone of high resistivity/hydraulic conductivity that appeared along the northwest edge of the site parallel to the stream in the lower three elevation interpolations (211.9, 212.2, and 212.5 m; Figure 3.6 (a), Figure 3.6 (b), and Figure 3.6 (c) and 3.6 (d) respectively). The sediments from this high resistivity feature were coarse, and the similarity of the particle size distribution of samples from this location to samples taken the surface of from a nearby gravel bar supported the hypothesis that the feature was a buried gravel bar. There was also a high resistivity/hydraulic conductivity feature that appeared close to the center of the site that was most obvious at 212.2 m (Figure 3.6 (b)), but can be seen at the lowest elevation (211.9 m, Figure 3.6 (a)) and also at the higher elevation (212.5 m, Figure 3.6 (c) and 3.6 (d)). Between

the two high resistivity/hydraulic conductivity features was a zone of very low resistivity/hydraulic conductivity, shown in blue and dark green tones, that was most obvious in Figures 3.6 (b), 3.6 (c) and 3.6 (d). A possible interpretation of this feature was as a paleo-channel/depression between the two gravel bars which was filled after abandonment, primarily with finer sediments.

In general, the water table maps associated with rising-limb conditions (Figures 3.6 (b), 3.6 (c), and 3.6 (e)) had steeper gradients, as represented by more closely spaced contours, than the baseflow water table (Figure 3.6 (a)), and the transitional and falling limb water tables (Figure 3.6 (d) and 3.6 (f), respectively). As noted earlier, the primary driver for the configuration of the water table appeared to be the change in the stream stage, and the water table maps showed that type of change in direction. However some of the features within that contours appeared to be related to the differences in hydraulic conductivity; principally, the high resistivity/hydraulic conductivity zones bordering the creek and in the center of the site appeared to correspond to areas of low water table slope, recorded as wider space between the contours. Similarly, the low resistivity/hydraulic conductivity zone between the two high zones appeared to correspond to a steeper slope characterized by more closely-spaced contours (Figure 3.6 (a)-3.6 (d)). At stream stages near the event peak the water table is at an elevation within the aquifer that lacks the zones of very high resistivity/hydraulic conductivity seen in the lower elevations (Figures 3.6 (e) and (f)). The rising limb at this elevation showed consistent slope, implying that the variation in hydraulic conductivity was insufficient to affect the movement of water (Figure 3.6 (e)), however the falling limb showed that the higher resistivity/hydraulic conductivity along the northern and southeastern edges affected the water table in the characteristic way by reducing the slope (Figure 6(f)).

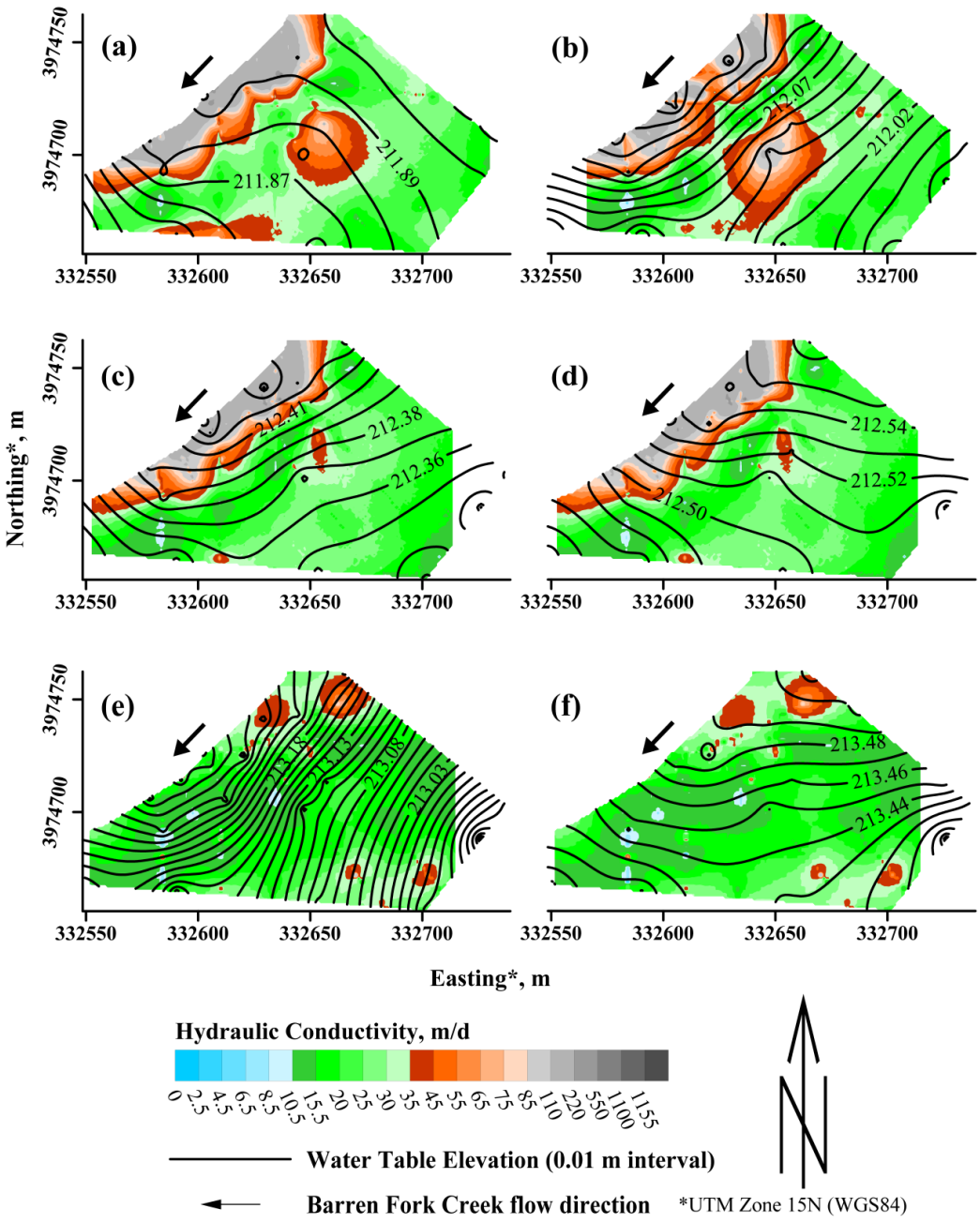

Figure 3.6. Comparison of interpolated hydraulic conductivity and water table maps for selected times and stream stages during runoff event May 1-5, 2009 at Barren Fork Creek study site. Map comparisons shown are (a) baseflow (5/1/2009 09:00, 211.9 m), (b) rising limb (5/1/2009 21:00, 212.2 m), (c) rising limb (5/2/2009 10:30, 212.5 m), (d) transition (5/2/2009 21:00, 212.5 m), (e) rising limb (5/3/2009 16:00, 213.8 m), and (f) falling limb (5/3/2009 20:00, 213.8 m).

3.5 CONCLUSIONS

This study was an effort to look for evidence for the existence of high-flow domains and PFPs within the gravel-dominated floodplain of the Barren Fork Creek study site, and to test the resistivity/hydraulic conductivity relationship within the floodplain. The method used was to compare study area-wide estimates of hydraulic conductivity to the changing water table as the alluvial groundwater responded to a flood event in Barren Fork Creek. Hydraulic conductivity estimates were created by interpolating selected elevations (i.e. depths from within the floodplain) from the ERI profiles into a map of the estimated hydraulic conductivity by applying the linear model. A storm runoff pulse passed the site over May 1-5, 2009 featuring 2.2 m of stage increase, which caused the water table to rise into the gravel-dominated vadose zone at the site. Water table maps, corresponding to the times when stream elevation matched the selected hydraulic conductivity elevations, were prepared from groundwater elevation data obtained from pressure transducers placed in monitoring wells at the site. When the flood peaks from each monitoring well were compared, it appeared that there was little attenuation of the energy of the storm pulse even at the furthest point in the study site; at 180m the flood peak had only dropped 0.25 m and was delayed by 1.5 hours. This lends credence to the idea that the floodplain was a "high-flow domain". Further evidence for a high-flow domain is provided by the direction of the water table as estimated by a fitted plane. The direction of the water table shifted over time as the storm pulse travelled through the floodplain; beginning in a direction similar to the stream as it approached the site, changing until it was normal to the stream during the rising limb and, shifting to a direction that was nearly parallel to the valley axis during the recession limb. This indicates both that the water table responds on a time scale of hours, similar to that of the storm pulse itself, and that the groundwater responds primarily to regional factors.

The comparisons between the hydraulic conductivity and water tables maps showed that areas of highest resistivity coincided with areas of relatively low water table slope and vice versa. Limited areas of preferential flow exist within the floodplain, characterized by extremes in hydraulic conductivity/resistivity and, since high hydraulic conductivity implies less resistance to flow and therefore less loss of energy over distance, this is the response one would expect to see in the water table. However the floodplain as a whole constituted a high-flow domain with rapid responses to the flood wave seen within the groundwater at extreme distances (up to 180 m) from the stream bank, and therefore the most important hydraulic characteristic of the study floodplain is the bulk hydraulic conductivity, consisting of the values above and including the median.

CHAPTER 4

Dissertation Summary and Conclusions

The objectives of this research were to better understand the hydrogeologic role of gravel within the subsoil of floodplains in the Ozark region of eastern Oklahoma. Gravel is a common component of the floodplains and is derived from the weathering and fluvial deposition of chert from the limestone bedrock in the region. The coarse gravel was thought to contribute to the rapid movement of water either as preferential flow paths (PFP), which were defined as small scale features capable of conducting water at higher rates than the surrounding material, or as high-flow domains which are broad-scale features with high hydraulic conductivity. Both features were hypothesized to consist of paleochannels and other remnant fluvial features within the floodplain. Where they exist, PFPs and high-flow domains have the potential to affect the interaction of streams and alluvial groundwater by extending the hyporheic zone laterally deep into the floodplain, or to affect recharge rates by connecting the floodplain surface to the alluvial groundwater. These interactions can affect the flow of water, the movement of water-borne contaminants, or both. An estimate of the spatial distribution of high flow features can help in developing stream flow and runoff models specific to areas with gravel-dominated floodplains, and may ultimately influence landuse planning.

The study used non-invasive electrical resistivity imaging (ERI) surveys of floodplains, and found heterogeneity in the electrical properties of the gravel subsurface. Further work with

core samples and hydraulic testing established that the heterogeneity was due to differences in the proportion of coarse and fine material that affected both the resistivity of the material and its ability to conduct fluids. Resistivity (the material property measured in the field) was found to be related to hydraulic conductivity (K_{sat}, the functional property of a PFP) with a positive, linear relationship, and that the highest resistivity and hydraulic conductivity appeared to coincide with floodplain water movements that indicated PFPs at study sites with networks of monitoring wells. Floodplain maps interpolated from the resistivity showed some degree of overlap between high resistivity values and the high water surface indicating the presence of a PFP connected to the stream under rising limb conditions.

4.1 SPECIFIC CONCLUSIONS IN REGARD TO EACH DISSERTATION CHAPTER

The study was divided into three sections, each building on the work of the previous ones. The first section was a method development in response to the difficulty of hydraulic testing in gravel soils, which include the toughness of the soil, the tendency for unsupported holes to collapse, and the large quantities of water required to establish and maintain steady-state conditions necessary for testing. The method developed was able to:

- Drive a steel permeameter to a desired depth in order to hydraulically test a specific section of the floodplain formation.
- Establish and maintain steady state conditions with high flows of water (e.g. 21 l/min) for long test periods (> 30 min).
- Conduct tests at successive depths within the same borehole.
- Test *hydraulic conductivity* within the vadose zone within the range 2 – 180 m/d using USBR (1985) Method 3 that is accurate to an order of magnitude in gravel soils.

The purpose of the second part of the study was to survey the hydraulic behavior of the gravel subsoil in the vadose zone of several floodplains within the Ozark ecoregion of eastern Oklahoma. The sites included floodplains on Barren Fork Creek (BFC), Flint Creek (FC), and Hone Creek (HC). The rapid and non-destructive geophysical method electrical resistivity imaging (ERI), that detects differences in materials through their resistance to an electric current, was used to map two-dimensional vertical sections (ERI profiles) at the study sites. In addition, hydraulic testing was performed with the gravel permeameter and core samples were also obtained from locations and depths of known resistivity on the study floodplains.

- Analysis of the particle size distribution (PSD) of the cores found that the subsoil was mixture of coarse and fine elements, with the coarse particles generally larger, and the fine particles smaller than 0.25 mm.
- When the cores samples were normalized and the fine fraction calculated, a statistically significant negative power relationship was found between fine fraction and the hydraulic conductivity ($R^2 = 0.72$, $P = 0.008$) and resistivity ($R^2 = 0.85$, $P = 0.001$). This implied that the fine fraction of the subsoil controlled much of both the hydraulic and electrical behavior of the subsoil.
- Linear regression of resistivity and hydraulic conductivity was significant ($R^2 = 0.57$, $P = 0.004$), and allowed the ERI profiles to be interpreted as maps of hydraulic conductivity by applying the formula $K_{sat} = 0.11\rho$, where K_{sat} is saturated hydraulic conductivity, and ρ is resistivity.
- The median hydraulic conductivity on all profiles from all sites was at least 20 m d^{-1}, which is within the range for gravel soils. This high hydraulic conductivity suggests that

at least half of the subsurface at each floodplain is likely to behave as a "high-flow domain" with the ability to conduct water at rates of 20 m d^{-1} or greater.

- Several ERI profiles at BFC had high resistivity values that were significantly higher (P = 0.00) than the remaining ERI profiles at BFC and the other sites measured at the 84th percentile. Those ERI profiles were obtained from an area within the BFC study site where a trench injection test found a tracer (Rhodamine WT) to move in a manner that suggests preferential flow.

The previous work had shown that Barren Fork Creek had the widest range of hydraulic conductivity in the floodplain and was thus most likely to contain a PFP. Therefore, the third part of the study was an effort to look for evidence of enhanced flow and PFPs and to test the resistivity/hydraulic conductivity relationship within the floodplain. The method was to compare study area-wide estimates of hydraulic conductivity to the changing water table as the alluvial groundwater responds to a flood event in Barren Fork Creek. Hydraulic conductivity estimates were created by interpolating selected elevations (i.e. depths from within the floodplain) from the ERI profiles into a map of the estimated hydraulic conductivity by applying the linear model derived in the previous analysis. A storm runoff pulse passed the site over May 1-5, 2009 featuring 2.2 m of stage increase, which caused the water table to rise into the gravel-dominated vadose zone at the site. Water table maps, corresponding to the times when stream elevation matched the selected hydraulic conductivity elevations, were prepared from groundwater elevation data obtained from pressure transducers placed in monitoring wells at the site.

- When the flood peaks from each monitoring well were compared, it appeared that there was little attenuation of the energy of the storm pulse even at the furthest point in the

study site; at 180m the flood peak had only dropped 0.25 m and was delayed by 1.5 hours. This lends credence to the idea that the floodplain was a "high-flow domain"

- Further evidence for a high-flow domain is provided by the direction of the water table as estimated by a fitted plane. The direction of the water table shifted over time as the storm pulse travelled through the floodplain; beginning in a direction similar to the stream as it approached the site, changing until it was normal to the stream during the rising limb and, shifting to a direction that was nearly parallel to the valley axis during the recession limb. This indicates both that the water table responds on a time scale of hours, similar to that of the storm pulse itself, and that the groundwater responds primarily to regional factors.
- The comparisons between the hydraulic conductivity and water tables maps showed that areas of highest resistivity coincided with areas of relatively low water table slope and vice versa. Since high hydraulic conductivity implies less resistance to flow and therefore less loss of energy over distance, this is the response one would expect to see in the water table. Therefore, despite the floodplain as a whole constituting a high-flow domain, areas of preferential flow exist within the floodplain, characterized by very high hydraulic conductivity/resistivity.

4.2 FUTURE RESEARCH

The issue of floodplain heterogeneity in general and PFPs in particular is complex and, as seen in this research, site-specific. This research was able to assess floodplain heterogeneity using a general ERI survey, but more a detailed survey would yield much better estimates of the connectivity of subsurface features. In addition, given that floodplains are dynamic landscape features that are constantly created and destroyed by their resident streams, it is important to investigate the geomorphic links to the creation of PFPs. In particular, research is needed into

geospatial connections that can affect the spatial distribution of PFPs such as the interplay of stream characteristics (i.e. median and peak flow, reach slope), gravel source areas (i.e. tributaries), and watershed characteristics (i.e. landuse/land cover, underlying geology, history of landscape disturbance). The most valuable tool would be an economical method to estimate the presence and distribution of PFPs and high-flow domains so that they can be effectively included in regional watershed or groundwater models.

CHAPTER 5

References

Ahrens, T.P., and A.C. Barlow. 1951. Permeability tests using drill holes and wells. U. S. Bureau of Reclamation Geology Report No. G-97.

Amoros, C., and G. Bornette. 2002. Connectivity and biocomplexity in waterbodies of riverine floodplains. Freshwater Biol. 47: 761-776.

Anterrieu, O., M. Choteau, and M. Aubertin. 2010. Geophysical characterization of the large-scale internal structure of a waste rock pile from a hard rock mine. Bulletin Eng. Geol. Environ. 69: 533-548.

Archie, G. 1942. The electrical resistivity log as an aid in determining some reservoir characteristics. Petroleum Technology Technical Paper 1422.

Auton, C. 1992. The utility of conductivity surveying and resistivity sounding in evaluating sand and gravel deposits and mapping drift sequences in northeast Scotland. Eng. Geol. 32: 11-28.

Baines, D., D. Smith, D. Froese, and P. Bauman. 2002. Electrical resistivity ground imaging (ERGI): A new tool for mapping the lithology and geometry of channel-belts and valley-fills. Sedimentology 49: 441-449.

Battin, T. J. 1999. Hydrologic flow paths control dissolved organic carbon fluxes and metabolism in an alpine stream hyporheic zone. Water Resources Research. 35(10):3159-3169.

Bell, R.W., and N.J. Schofield. 1990. Design and application of a constant head well permeameter for shallow high Ksat soils. Hydrological Processes 4, no. 4: 327–342.

Beresnev, I. A., C. E. Hruby, and C. A. Davis. 2002. The use of multi-electrode resistivity imaging in gravel prospecting. Journal of Applied Geophysics 49: 245-254.

Bersezio R., M. Giudici, and M. Mele. 2007. Combining sedimentological and geophysical data for high-resolution 3-D mapping of fluvial architectural elements in the Quaternary Po Plain (Italy). Sedimentary Geology 202(1-2): 230-248.

Boulton, A. J., G. D. Fenwick, P. J. Hancock and M. S. Harvey. 2008. Biodiversity, functional roles, and ecosystem services of groundwater invertebrates. Invertebrate Systematics. 22:103-116.

Bridge, J.S. 2003. Rivers and Floodplains: Forms, Processes, and Sedimentary Record. Oxford, UK: Blackwell Publishing.

Bunte, K., and S. Abt. 2001. Sampling Surface and Subsurface Particle-Size Distributions in Wadable Gravel- and Cobble-Bed Streams for Analyses in Sediment Transport, Hydraulics, and Streambed Monitoring. USFS General Technical Report 74, USDA. Rocky Mtn. Res. Sta. Fort Collins, CO.

Burger, H., A. Sheehan, and C. Jones. 2006. Introduction to Applied Geophysics: Exploring the Shallow Subsurface. W. W. Norton and Co., New York, NY.

Cassiani, G. 1998. A new method for the interpretation of the constant-head well permeameter. Journal of Hydrology 210(1-4): 11–20.

Crook, N., A. Binley, R. Knight, D. Robinson, J. Zarnetsky, and R. Haggerty. 2008. Electrical resistivity imaging of the architecture of substream sediments. Water Resour. Res. 44, doi:10.1029/2008WR006968.

Elrick, D. E. and W. D. Reynolds. 1992. Methods for analyzing constant-head well permeameter data. Soil Science Society of America Journal 56: 320–323.

Fetter, C. W. 2001. Applied Hydrogeology, 4th Ed. Prentice Hall. Upper Saddle River, NJ.

Findlay, S., S. Strayer, C. Goumbala and K. Gould. 1993. Metabolism of steamwater dissolved organic carbon in the shallow hyporheic zone. limnology and Oceanography. 38(7): 1793-1499.

Fox, G. A., D. M. Heeren, R. B. Miller, A. R. Mittelstet, and D. E. Storm. 2011. Flow and transport experiments for a streambank seep originating from a preferential flow pathway. J. Hydrol. 403(3-4): 360-366.

Fuchs, J. W., G. A. Fox, D. E. Storm, C. Penn, and G. O. Brown. 2009. Subsurface transport of phosphorus in riparian floodplains: Influence of preferential flow paths. Journal of Environmental Quality 38(2): 473–484.

Fuchs, J.W., G.A. Fox, D.E. Storm, C. Penn, and G.O. Brown. 2009. Subsurface transport of phosphorus in riparian floodplains: Influence of preferential flow paths. Journal of Environmental Quality 38(2): 473–484.

Glover, R. E. 1953. Flow from a test hole located above groundwater level. In Theory and Problems of Water Percolation, ed. Zanger, C. N., App. B. Engineering Monograph 8. US Bureau of Reclamation.

Gourry, J-C., F. Vermeersch, M. Garcin, and D. Girot. 2003. Contribution of geophysics to the study of alluvial deposits: a case study in the Val d'Avaray area of the River Loire, France. Journal of Applied Geosciences 54: 35-49.

Green, R., R. Klar, and J. Prikryl. 2005. Use of integrated geophysics to characterize paleo-fluvial environments, Geotechnical Special Publication 138: Site Characterization and Modeling, ASCE, New York, NY.

Halihan, T., S. Paxton, I. Graham, T. Fenstemaker, and M. Riley. 2005. Post-remediation evaluation of a LNAPL site using electrical resistivity imaging. Journal of Environmental Modeling 7: 283-287

Hancock, P. J., A. J. Boulton and W. F. Humphreys. 2005. Aquifers and hyporheic zones; Towards an ecological understanding of groundwater. Hydrogeology Journal. 13: 98-111.

Heeren, D. M., G. A. Fox, R. B. Miller, D. E. Storm, A. K. Fox, C. J. Penn, T. Halihan, and A. R. Mittelstet. 2011. Stage-dependent transient storage of phosphorus in alluvial floodplains. Hydrologic Processes 25(20): 3230-3243, doi: 10.1002/hyp.8054.

Heeren, D.M., R.B. Miller, G.A. Fox, D.E. Storm, A.K. Fox, and A.R. Mittelstet. 2010a. Impact of preferential flow paths on stream and alluvial groundwater interaction. In Proc. ASCE EWRI World Environmental and Water Resources Congress. Reston, Va.: American Society of Civil Engineers.

Heeren, D.M., R.B. Miller, G.A. Fox, D.E. Storm, C.J. Penn, and T. Halihan. 2010b. Preferential flow path effects on subsurface contaminant transport in alluvial floodplains. Transactions of the ASABE 53(1): 127–136.

Kamann, P., R. Ritzi, D. Dominic, and C. Conrad. 2007. Porosity and permeability in sediment mixtures. Ground Water 45: 429-438.

Kazezyilmaz-Alhan, C. M. and M. A. Medina. 2006. Stream solute transport incorporating hyporheic zone processes. Journal of Hydrology. 329:26-38.

Kibichii, S,, J.R. Baars and M. Kelly-Quinn. 2009. Optimising sample volume and replicates using the Bou-Rouch method for the rapid assessment of hyporheic fauna. Marine and Freshwater Research. 60:83-96.

Kittrick, J., and E. Hope. 1963. A procedure for the particle-size separation of soils for X-ray diffraction analysis. Soil Science 96: 319-325.

Knighton, D. 1998. Fluvial Forms and Processes: A New Perspective. London: Arnold.

Koltermann, C., and S. Gorelick. 1995. Fractional packing model for hydraulic conductivity derived from sediment mixtures. Water Resources Research 13: 3283-3297.

Landmeyer, J. E., P. M. Bradley, D. A. trego, K. G. Hale and J. E. Haas. 2010. MTBE, TBA, and TAME attenuation in diverse hyporheic zones. Ground Water. 48(1):30-41.

Loke, M. H., and T. Dahlin. 2002. A comparison of the Gauss–Newton and quasi-Newton methods in resistivity imaging inversion. Journal of Applied Geophysics 49:149–162.

Mastrocicco, M., N. Colombani, and S. Palpacelli. 2009. Fertilizers mobilization in alluvial aquifer: laboratory experiments. Environmental Geology 56:1371-1381.

McNeill, J. D. 1980. Electrical Conductivity of Soils and Rocks. Technical Note TN-5, Geonics Limited, Ontario, Canada.

Miller, R. B., D. M. Heeren, G. A. Fox, D. E. Storm, and T. Halihan. 2011. Design and application of a direct-push in-situ gravel permeameter. Ground Water 49(6): 920-925, doi: 10.1111/j.1745-6584.2010.00796.x.

Miller, R. B., D. M. Heeren, G. A. Fox, T. Halihan, D. E. Storm, and A. R. Mittelstet. 2010. Use of multi-electrode resistivity profiling to estimate vadose-zone hydraulic properties of

preferential flow paths in alluvial floodplains. In Proceedings ASCE EWRI World Environmental and Water Resources Congress. Reston, Va.: American Society of Civil Engineers.

Moore, D., and R. Reynolds. 1997. X-Ray diffraction and the Identification and Analysis of Clay Minerals: Second Edition. Oxford University Press. New York, NY.

Naiman, R., H. Descamps, and M. McClain. 2005. Catchments and the physical template. In: Naiman, R. J. (Ed.), Riparia: Ecology, Conservation, and Management of Streamside Communities. Elsevier Academic Press, Boston, MA.

NRCS. 2011. United States Department of Agriculture. Soil Survey Geographic (SSURGO) Database for Cherokee and Delaware Counties, OK. Available online at http://soildatamart.nrcs.usda.gov. Accessed 4/02/2011.

Poole, G., J. Stanford, C. Frissell, and S. Running. 2002. Three-dimensional mapping of geomorphic controls on flood-plain hydrology and connectivity from aerial photos. Geomorphology 48: 329-347.

Poole, G., R. Naiman, J. Pastor, and J. Stanford. 1997. Uses and limitations of ground penetrating RADAR in two riparian systems. In: Gibert J., J. Mathieu and F. Fournier (Eds.), Groundwater/Surface Water Ecotones: Biological and Hydrological Interaction and Management Options. Cambridge University Press, Cambridge.

Poppe, L. J., V. F. Paskevich, J. C. Hathaway and D. S. Blackwood. 2001. A Laboratory Manual for X-Ray Diffraction. USGS OFR 01-041. http://pubs.usgs.gov/openfile/of01-041/index.htm.

Rey, E., D. Jongmans, P. Gotteland, and S. Garambois. 2006. Characterization of soils with stony inclusions using geoelectrical measurements. J. Appl. Geophysics 58: 188-201.

Samouelian, A., I. Cousin, A Tabbagh, A. Bruand, and G. Richard. 2005. Electrical resistivity in soil science: A review. Soil and Tillage Research 83: 173-193.

Scarsbrook, M. R., and J. R. Halliday. 2002. Detecting patterns in the hyporheic community structure: Does sampling method alter the story? New Zealand Journal of Marine and Freshwater Research. 36:443-453

Selker, J. S., C. K. Keller and J. T. McCord. 1999. Vadose Zone Processes. Boca Raton, FL: CRC Lewis Publishers.

Smith, R., and D. Sjogren. 2006. An evaluation of electrical resistivity imaging (ERI) in Quaternary sediments, southern Alberta, Canada. Geosphere 2(6): 287-298

Smith, W. H. F., and Wessel, P. 1990, Gridding with Continuous Curvature Splines in Tension, Geophysics, 55(3): 293-305.

Sophocleous, M. A. 1991. Stream-floodwave propagation through the Great Bend alluvial aquifer, Kansas: Field measurements and numerical simulations. Journal of Hydrology. 124: 207-228.

Stanford, J. A. and J. V. Ward. 1993. An ecosystem perspective of alluvial rivers: Connectivity and the hyporheic corridor. Journal of the North American Benthological Society. 12(1):48-60.

Stanford, J., and J. Ward. 1992. Management of aquatic resources in large catchments: Recognizing interactions between ecosystem connectivity and environmental disturbance. In: Naiman R. J. (Ed.), Watershed Management. New York. Springer-Verlag.

Stephens, D. B. 1995. Vadose Zone Hydrology. Boca Raton, FL: CRC Lewis Publishers.

Stephens, D. B. and S. P. Neuman. 1982. Vadose zone permeability tests: steady state results. Journal of the Hydraulics Division, ASCE 108, no. HY5, 640–658.

Stephens, D. B., S. Tyler, K. Lambert, D. Watson, R. Rabold, R. Knowlton, E. Byers, S. Yates and S. P. Neuman. 1983. In situ determination of hydraulic conductivity in the vadose zone using borehole infiltration tests. Technical Completion Report 1423648. New Mexico Water Resources Research Institute.

Stoeser, D., G. Green, L. Morath, W. Heran, A. Wilson, D. Moore, and B. Van Gosen. 2005. Preliminary integrated geologic map databases for the United States: Central States: Montana, Wyoming, Colorado, New Mexico, North Dakota, South Dakota, Nebraska, Kansas, Oklahoma, Texas, Iowa, Missouri, Arkansas, and Louisiana. USGS Open File Report 2005-1351. Available online at http://pubs.usgs.gov/of/2005/1351/. .Accessed [4/02/2011].

Stofleth, J., F. D. Shields and G. A. Fox. 2008. Hyporheic and total transient storage in small, sand-bed streams. Hydrologic Processes 22: 1885-1894.

Tye, A., H. Hessler, K. Ambrose, J. Williams, D. Tragheim, A. Scheib, M. Raines, and O. Kuras. 2011. Using integrated near-surface geophysical surveys to aid mapping and interpretation of geology in an alluvial landscape within a 3-D soil-geology framework. Near Surface Geophysics 9: 15-31.

U.S. Bureau of Reclamation (USBR). 1985. Ground Water Manual: A Water Resources Technical Manual Revised Reprint. Denver, CO. U.S. Department of the Interior, Bureau of Reclamation.

Webb, G., S. W. Tyler, J. Collord, D. Van Zyl, T. Halihan, J. Turrentine, and T. Fenstemaker. 2008. Field Scale Analysis of Flow Mechanisms in Highly Heterogeneous Mining Media. Vadose Zone Journal 7(2): 899-908. doi:10.2136/vzj2007.0130.

Woessner, W. W. 2000. Stream and fluvial plain ground water interactions: Rescaling hydrogeologic thought. Ground Water. 38(3): 423-429.

Zangar, C. N. 1953. Theory and Problems of Water Percolation, Engineering Monograph 8. US Bureau of Reclamation.

Zhang, Z., A. Ward, and J. Keller. 2011. Determining the porosity and saturated hydraulic conductivity of binary mixtures. Vadose Zone Journal 10: 313-321.

Zohdy, A. A. R., G. P. Eaton, and D. R. Mabey. 1974. Application of surface geophysics to ground-water investigations. Application of Surface Geophysics to Ground-water Investigations of the United State Geological Survey. Book 2, chapter D-1.

APPENDIX A

Locator Map and ERI Profiles for the Barren Fork Creek Study Site in Eastern Oklahoma

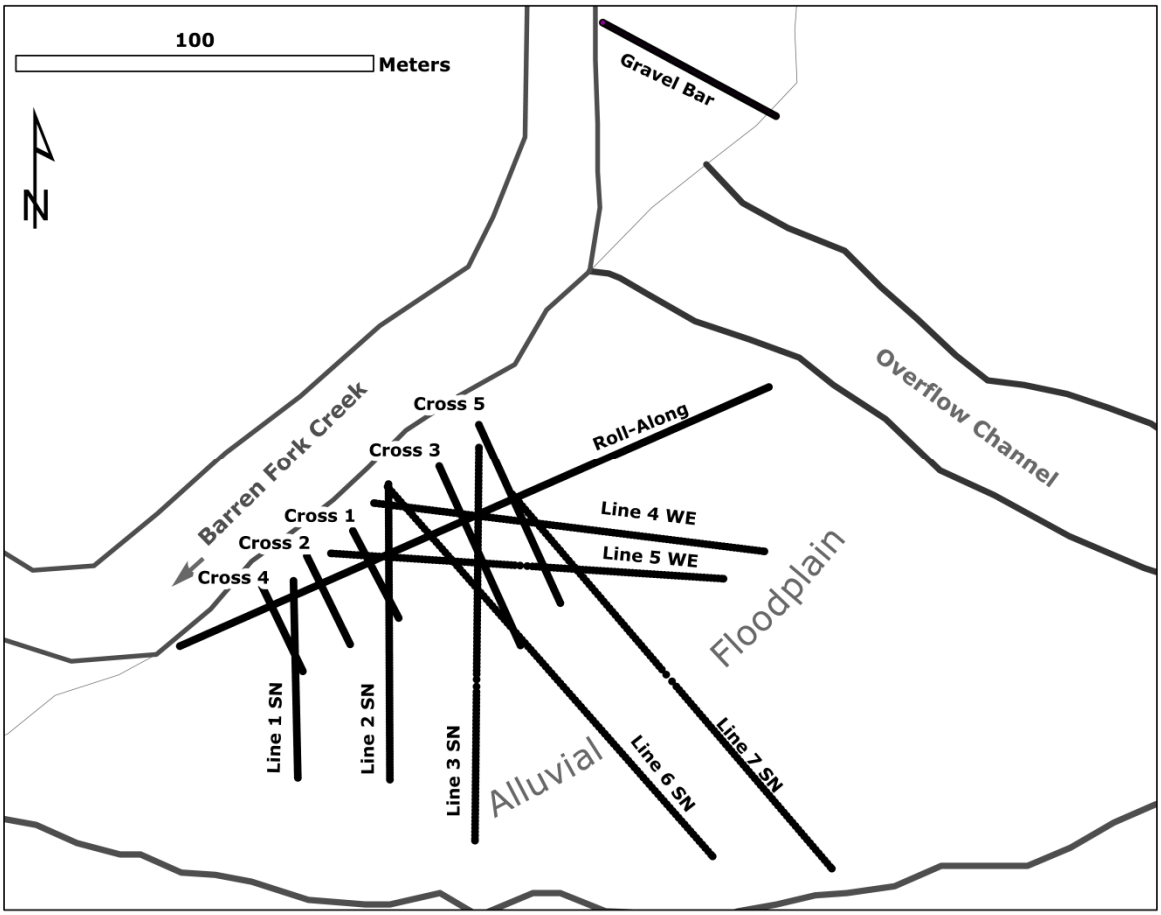

The Barren Fork Creek study site is located east of Tahlequah, Oklahoma (latitude 35.90°, longitude -94.85°). Map units are meters (UTM Zone 15 N, WGS 84). Solid black lines indicate locations of ERI profiles.

Barren Fork Cross Line #1 (Nov 8, 2008)
SE to NW Orientation 0.5 m Electrode Spacing

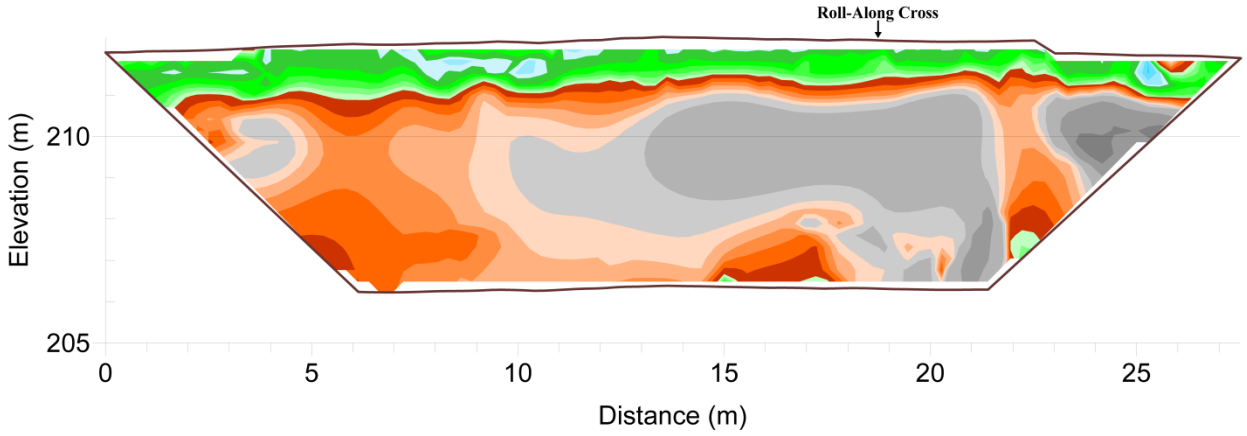

Barren Fork Cross #2 (Nov. 8, 2008)
SE to NW Orientation 0.5 m Electrode Spacing

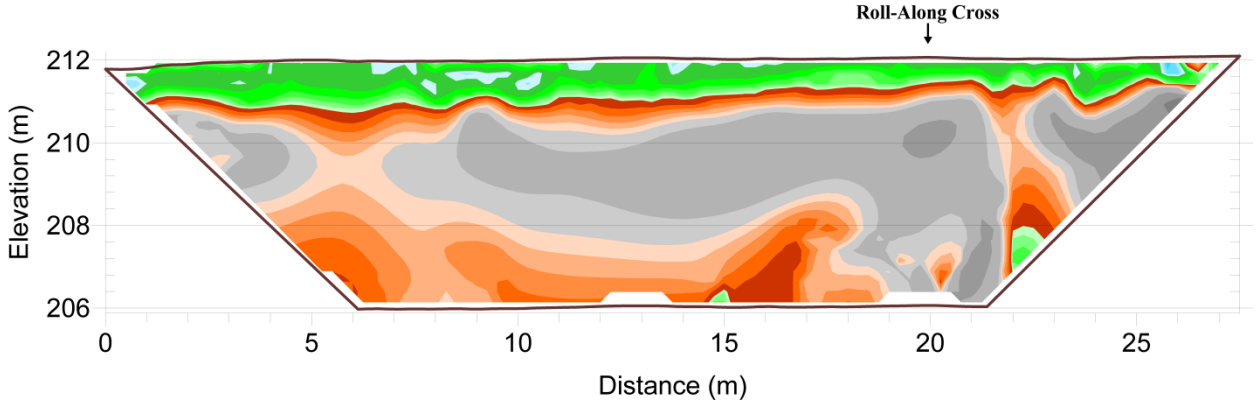

Barren Fork Cross #3 (Nov. 8, 2008)
SE to NW Orientation 1 m Electrode Spacing

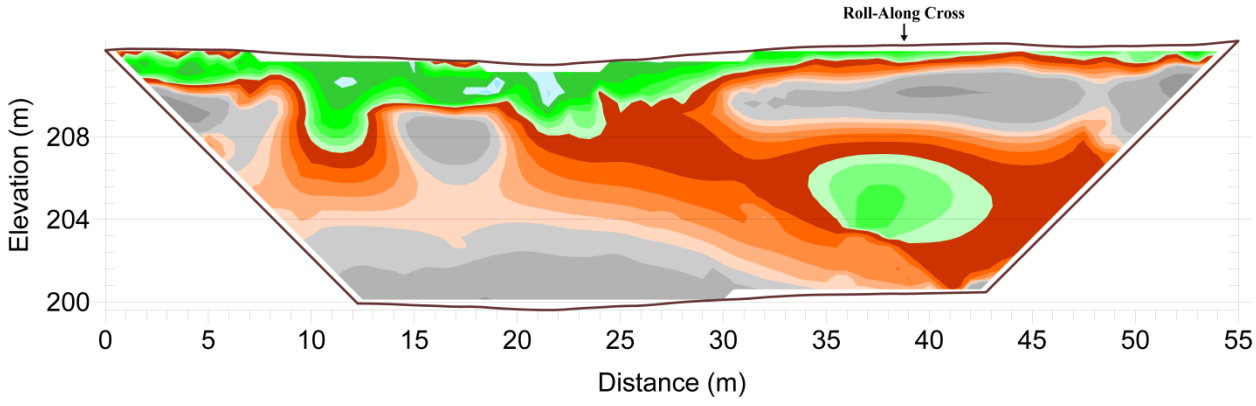

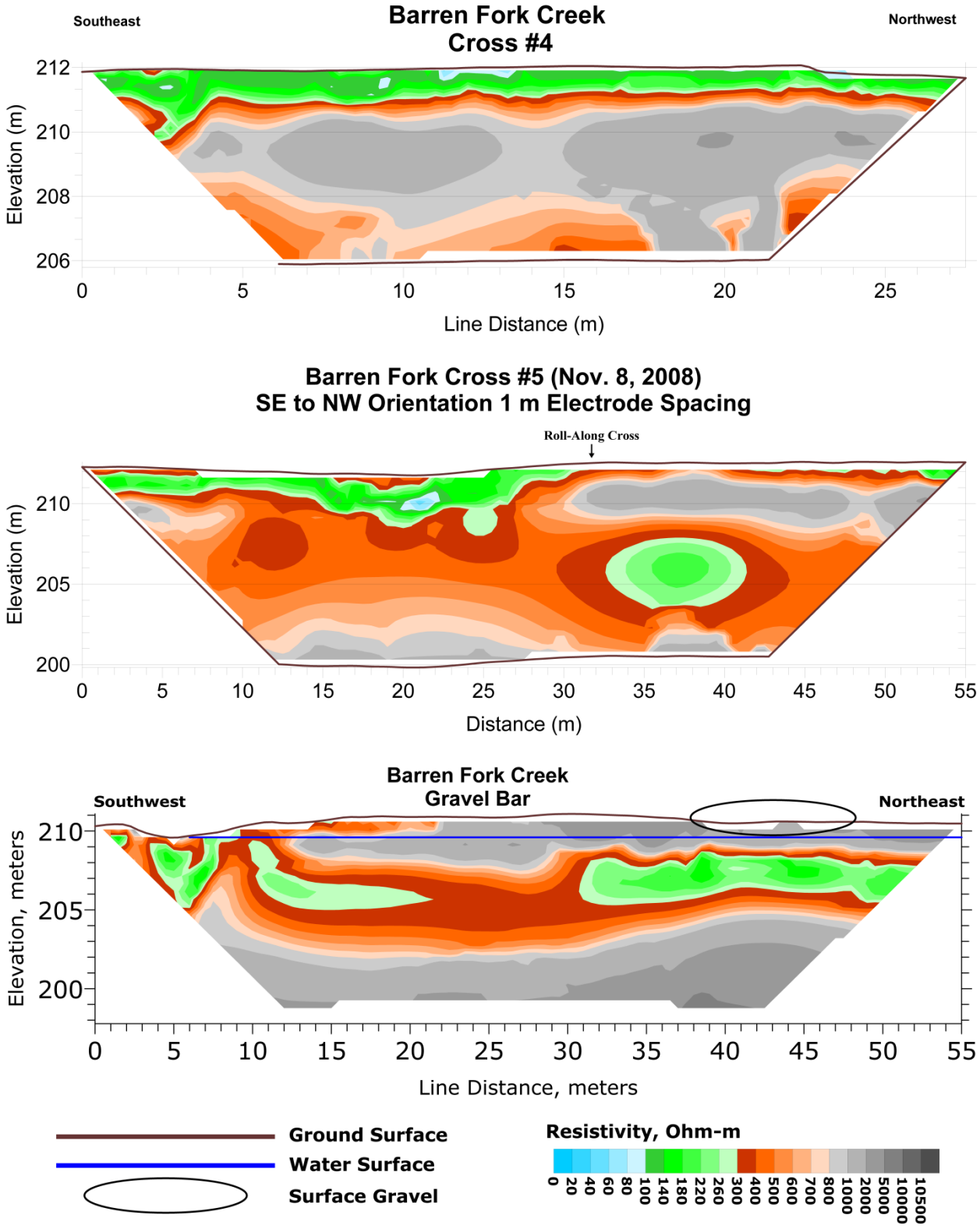
Barren Fork Creek
Cross #4
Southeast
Northwest
Elevation (m)
212
210
208
206
0
5
10
15
20
25
Line Distance (m)
Barren Fork Cross #5 (Nov. 8, 2008)
SE to NW Orientation 1 m Electrode Spacing
Roll-Along Cross
Elevation (m)
210
205
200
0
5
10
15
20
25
30
35
40
45
50
55
Distance (m)
Barren Fork Creek
Gravel Bar
Southwest
Northeast
Elevation, meters
210
205
200
0
5
10
15
20
25
30
35
40
45
50
55
Line Distance, meters
Ground Surface
Water Surface
Surface Gravel
Resistivity, Ohm-m
0
20
40
60
80
100
140
180
220
260
300
400
500
600
700
800
1000
2000
5000
10000
10500

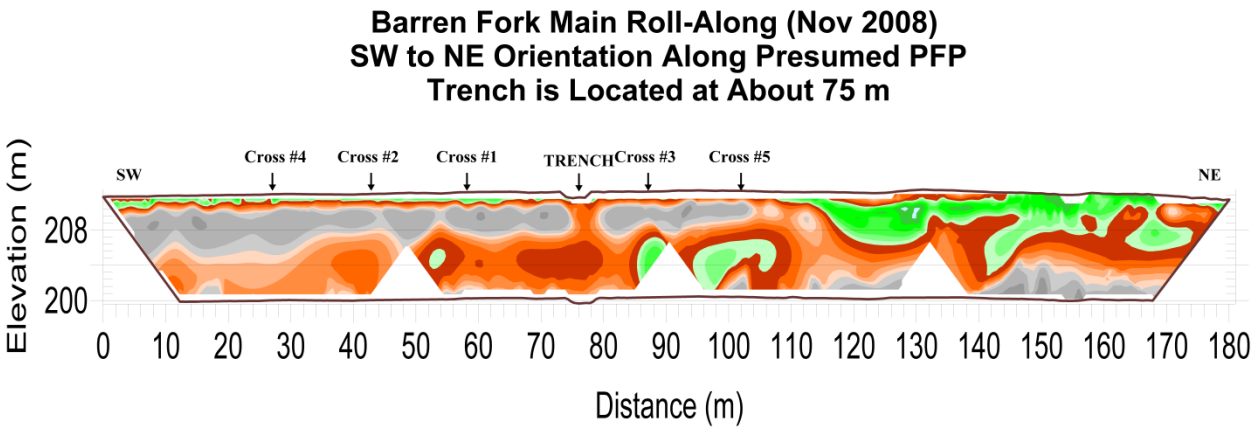
Barren Fork Main Roll-Along (Nov 2008)
SW to NE Orientation Along Presumed PFP
Trench is Located at About 75 m
SW
Cross #4
Cross #2
Cross #1
TRENCH
Cross #3
Cross #5
NE
Elevation (m)
208
200
0 10 20 30 40 50 60 70 80 90 100 110 120 130 140 150 160 170 180
Distance (m)

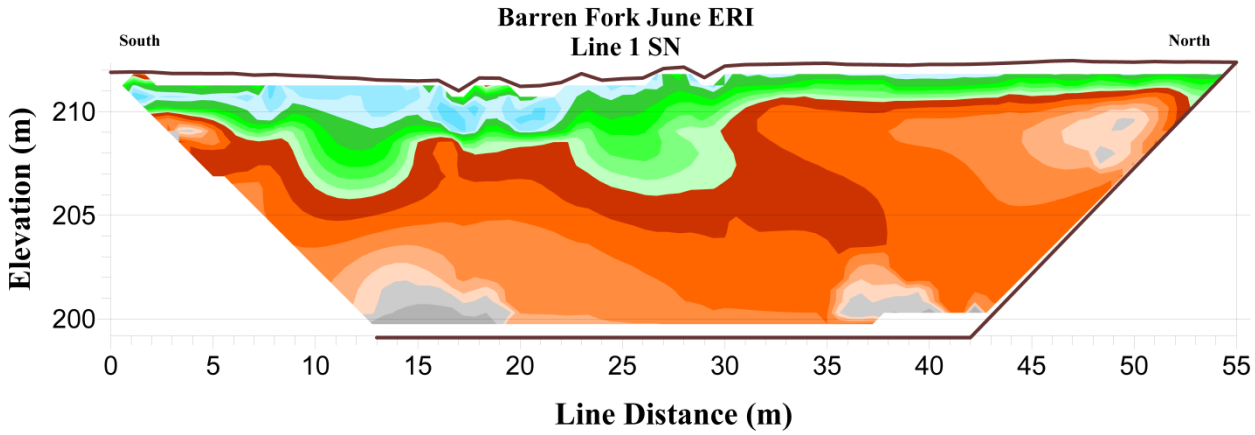
Barren Fork June ERI
Line 1 SN
South
North
Elevation (m)
210
205
200
0 5 10 15 20 25 30 35 40 45 50 55
Line Distance (m)

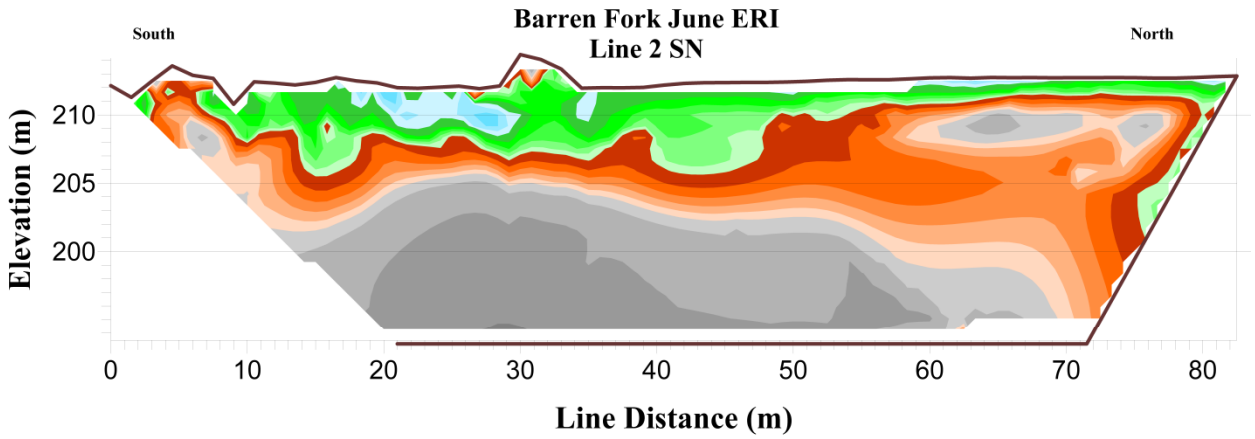
Barren Fork June ERI
Line 2 SN
South
North
Elevation (m)
210
205
200
0 10 20 30 40 50 60 70 80
Line Distance (m)

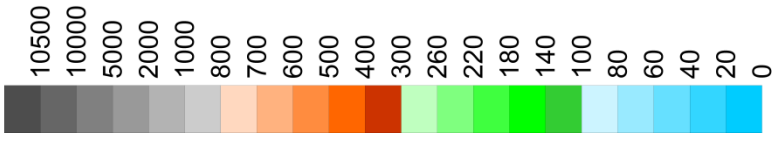
10500
10000
5000
2000
1000
800
700
600
500
400
300
260
220
180
140
100
80
60
40
20
0

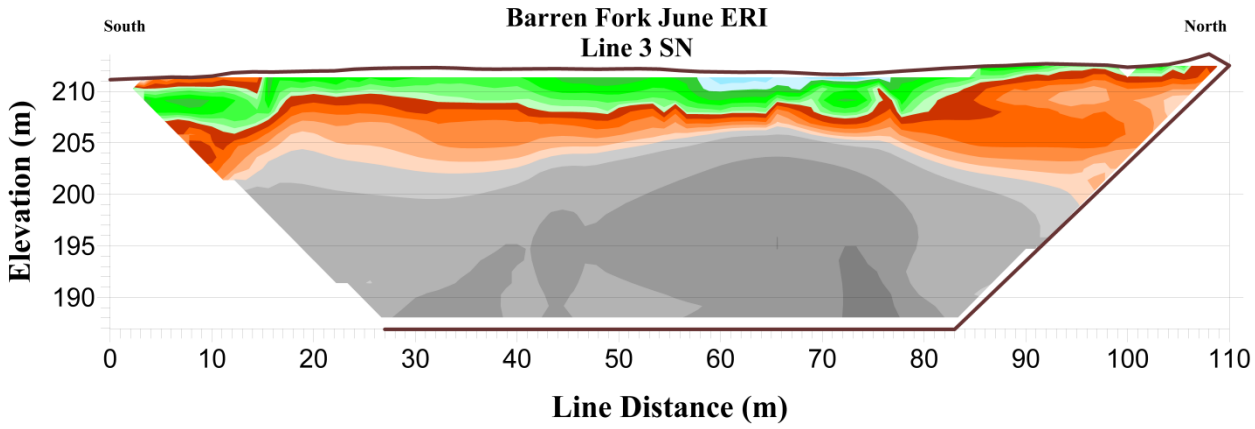
Barren Fork June ERI
Line 3 SN
South
North
Elevation (m)
210
205
200
195
190
0
10
20
30
40
50
60
70
80
90
100
110
Line Distance (m)

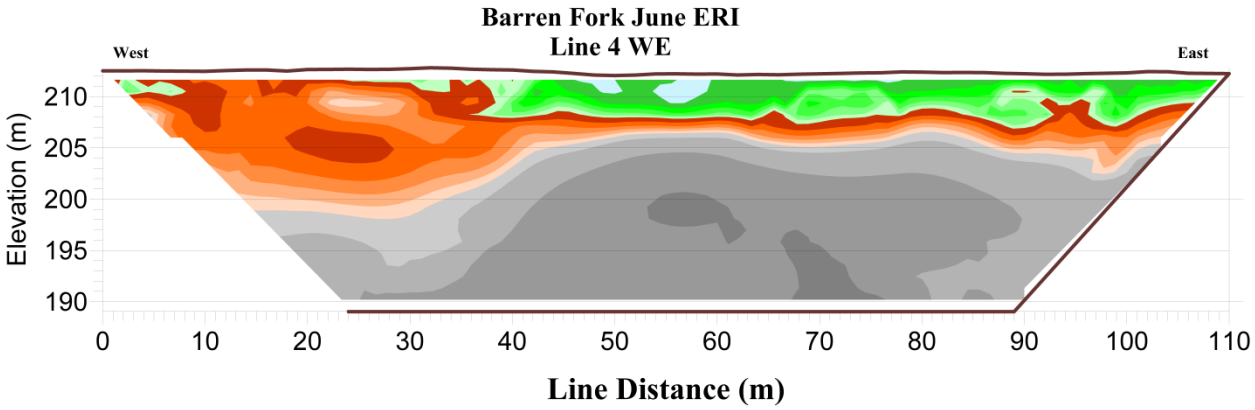
Barren Fork June ERI
Line 4 WE
West
East
Elevation (m)
210
205
200
195
190
0
10
20
30
40
50
60
70
80
90
100
110
Line Distance (m)

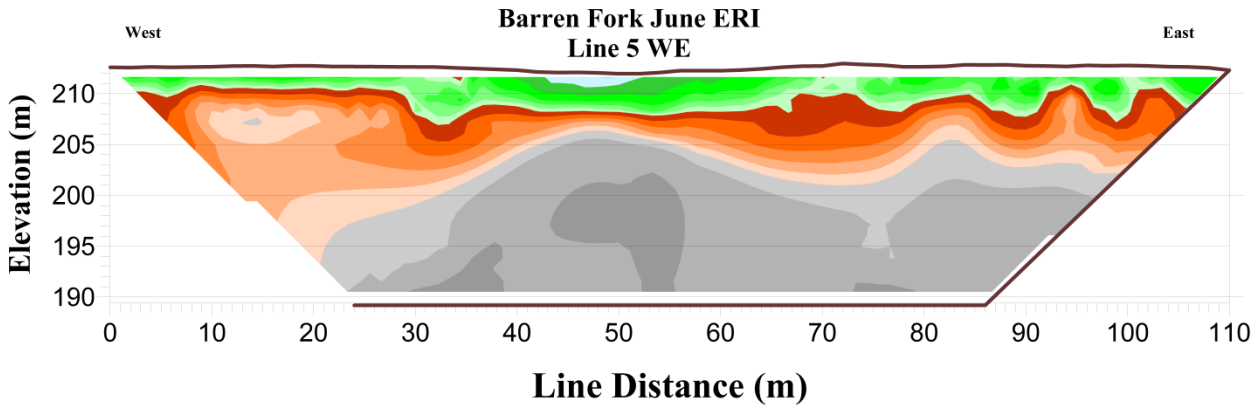
Barren Fork June ERI
Line 5 WE
West
East
Elevation (m)
210
205
200
195
190
0
10
20
30
40
50
60
70
80
90
100
110
Line Distance (m)

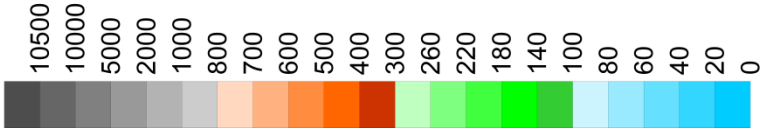
10500
10000
5000
2000
1000
800
700
600
500
400
300
260
220
180
140
100
80
60
40
20
0

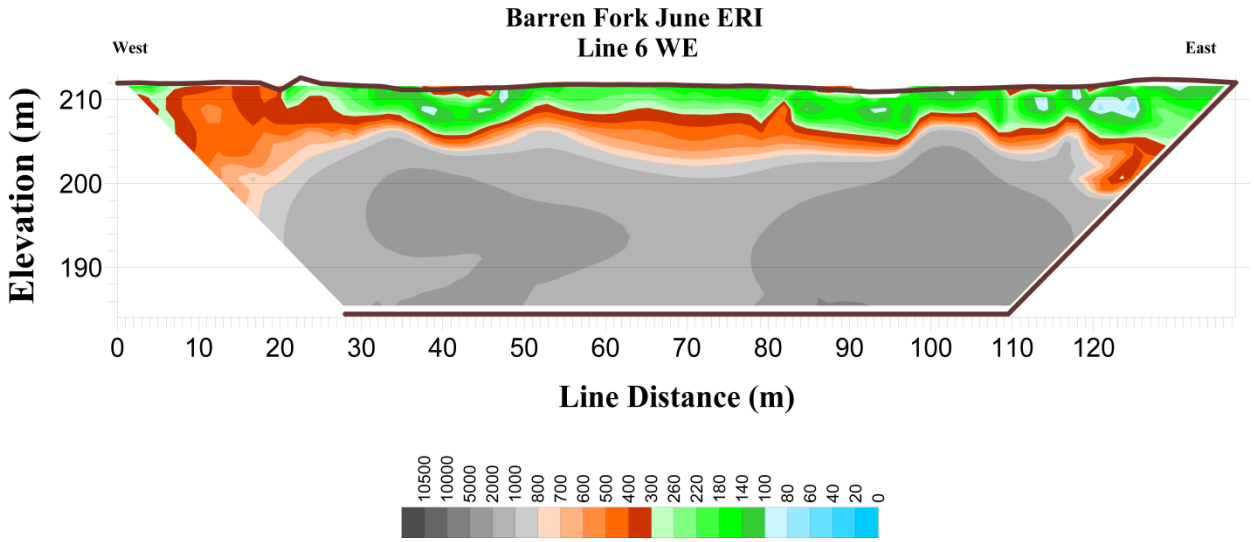
Barren Fork June ERI
Line 6 WE
West
East
Elevation (m)
210
200
190
0
10
20
30
40
50
60
70
80
90
100
110
120
Line Distance (m)
10500
10000
5000
2000
1000
800
700
600
500
400
300
260
220
180
140
100
80
60
40
20
0

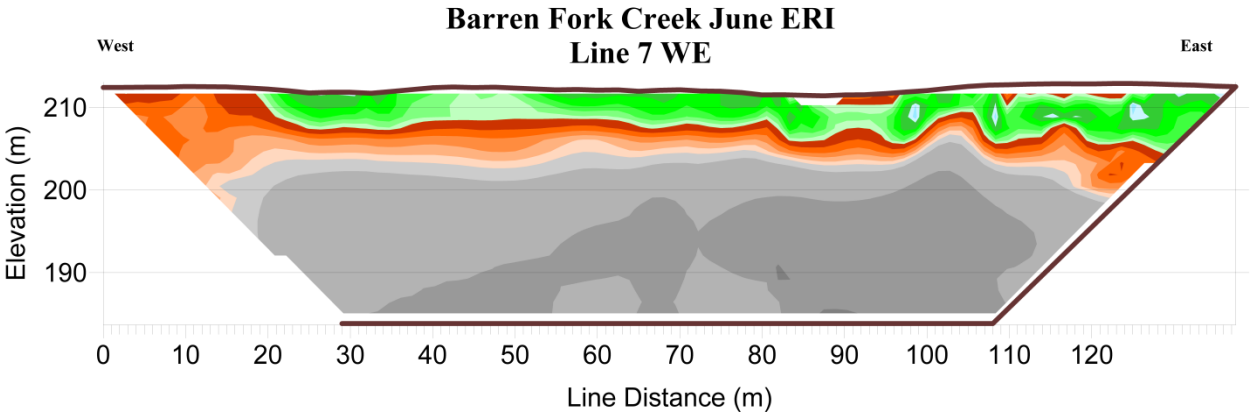
Barren Fork Creek June ERI
Line 7 WE
West
East
Elevation (m)
210
200
190
0
10
20
30
40
50
60
70
80
90
100
110
120
Line Distance (m)

APPENDIX B

Locator Map and ERI Profiles for the Honey Creek Study Site in Eastern Oklahoma

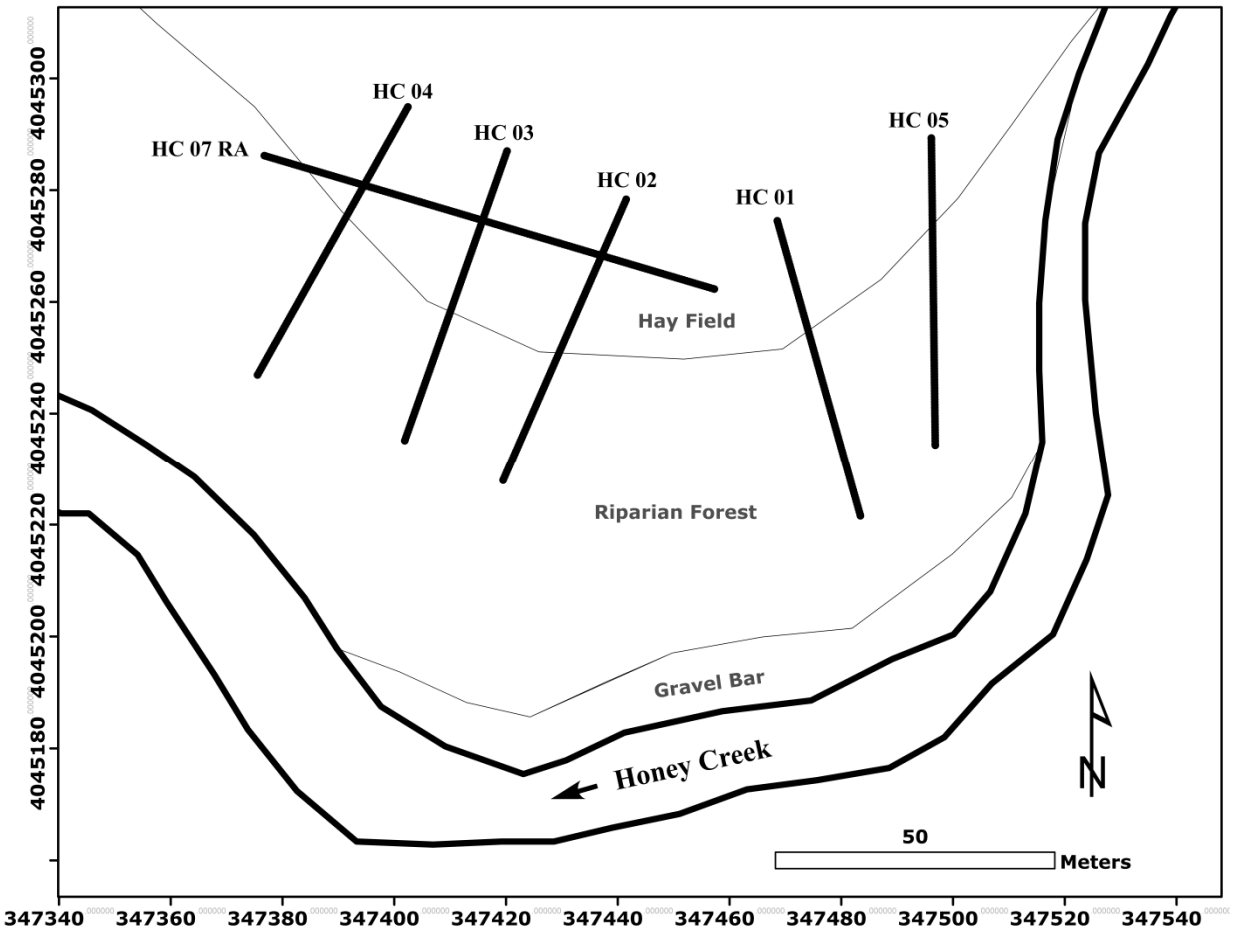

The Honey Creek study site is located near Grove, Oklahoma (latitude 36.54°, longitude -94.70°). Map units are meters (UTM Zone 15 N, WGS 84). Labeled straight black lines indicate locations of ERI profiles.

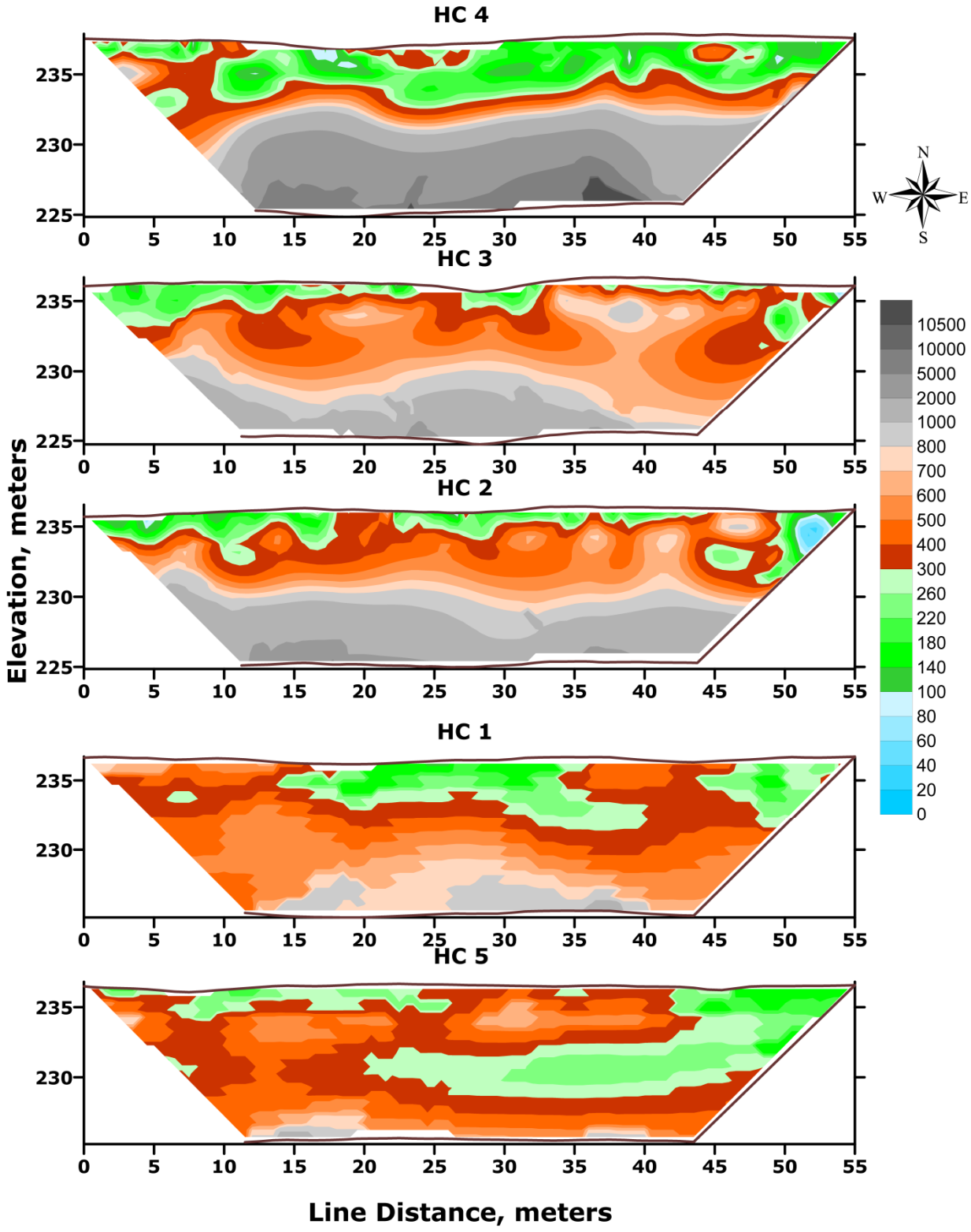
HC 4
HC 3
HC 2
HC 1
HC 5
Elevation, meters
Line Distance, meters
235
230
225
0
5
10
15
20
25
30
35
40
45
50
55
N
W
E
S
10500
10000
5000
2000
1000
800
700
600
500
400
300
260
220
180
140
100
80
60
40
20
0

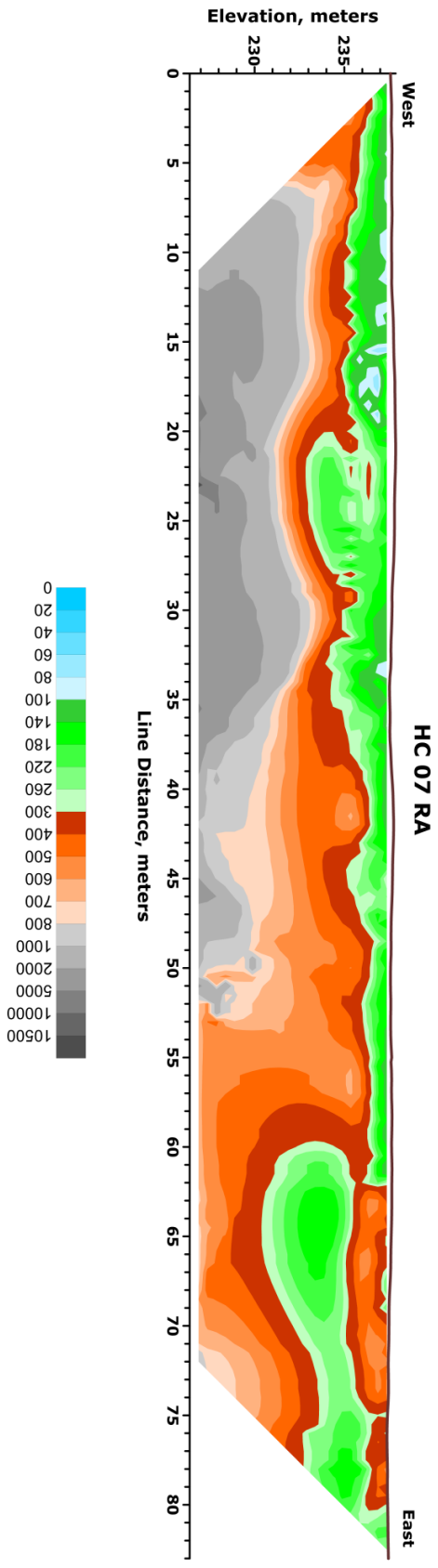
Elevation, meters
230
235
West
East
HC 07 RA
Line Distance, meters
0
5
10
15
20
25
30
35
40
45
50
55
60
65
70
75
80
0
20
40
60
80
100
140
180
220
260
300
400
500
600
700
800
1000
2000
5000
10000
10500

APPENDIX C

Locator Map and ERI Profiles for the Flint Creek Study Site in Eastern Oklahoma

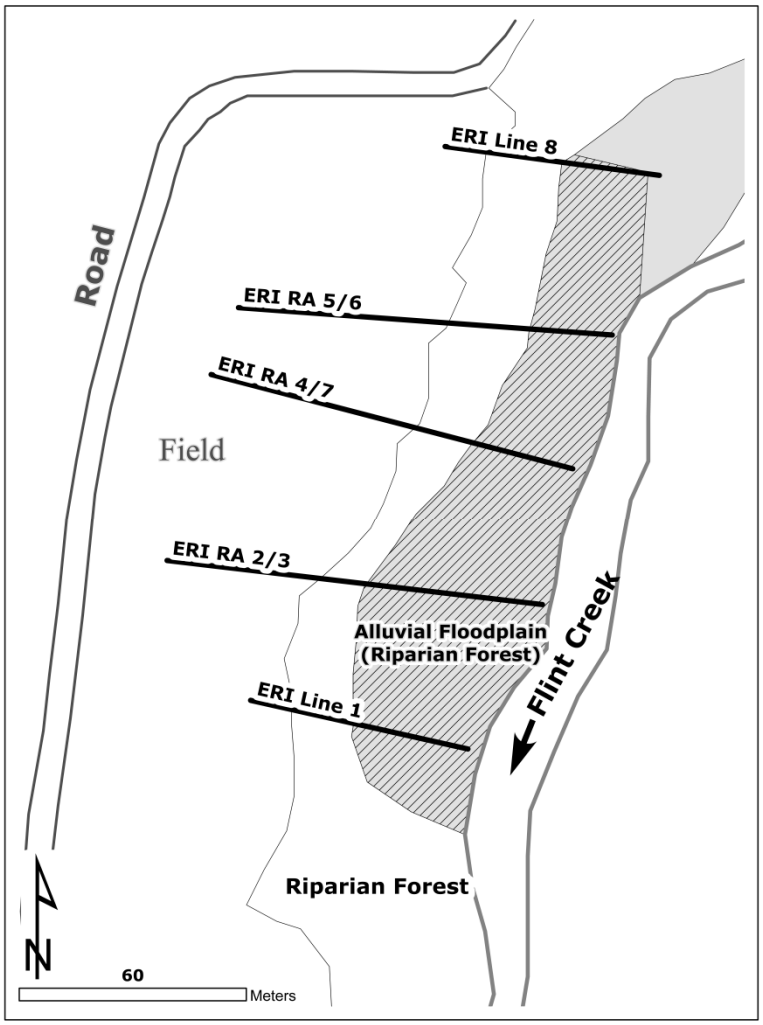

The Flint Creek floodplain site is located near Kansas, Oklahoma (latitude 36.20°, longitude -94.71°). Labeled black lines indicated locations of ERI profiles.

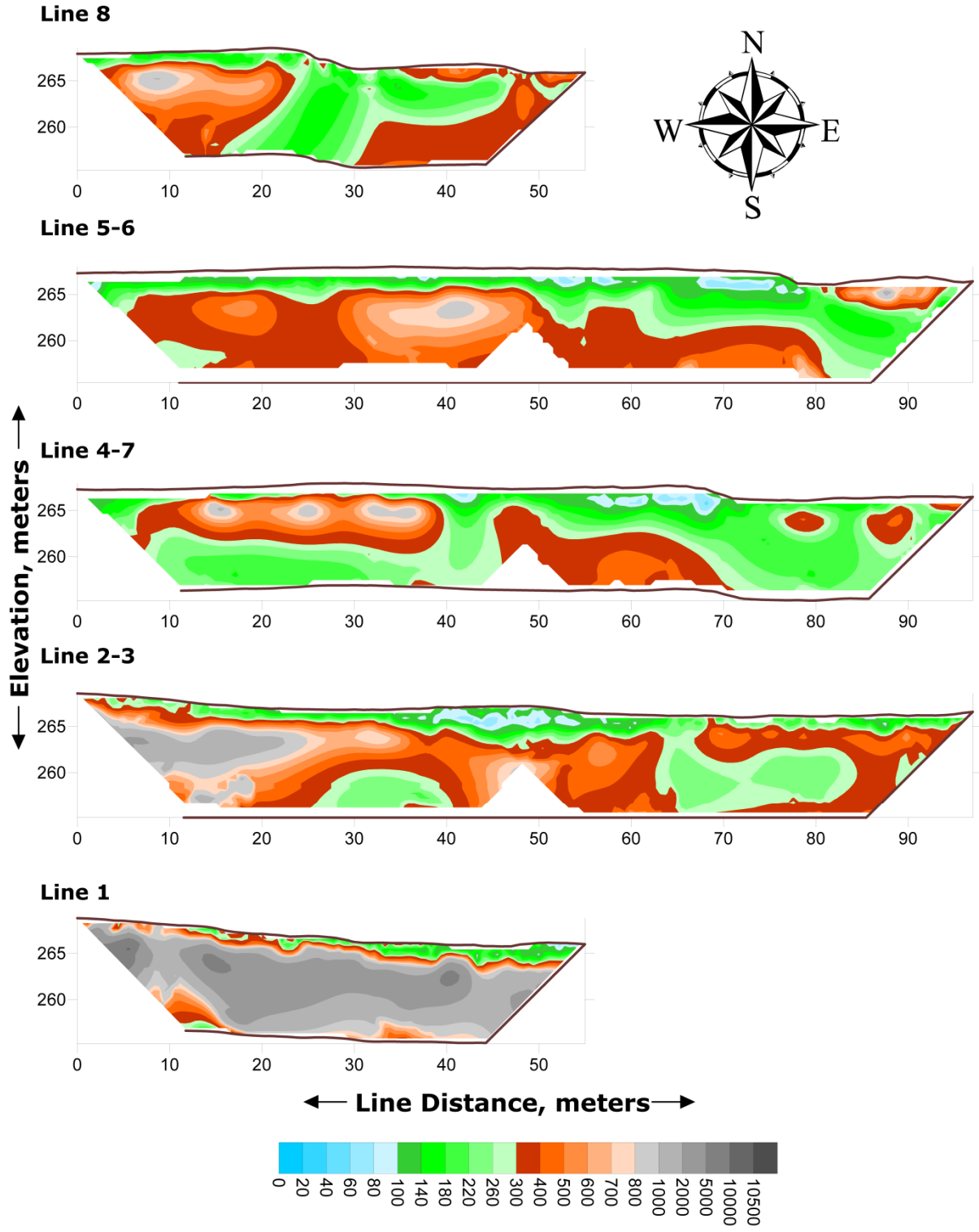
Line 8
Line 5-6
Line 4-7
Line 2-3
Line 1
N
W
E
S
265
260
0
10
20
30
40
50
60
70
80
90
Elevation, meters
Line Distance, meters
0
20
40
60
80
100
140
180
220
260
300
400
500
600
700
800
1000
2000
5000
10000
10500

APPENDIX D

Locator Map and ERI Profiles for the Pumpkin Hollow Creek

Study Site in Eastern Oklahoma

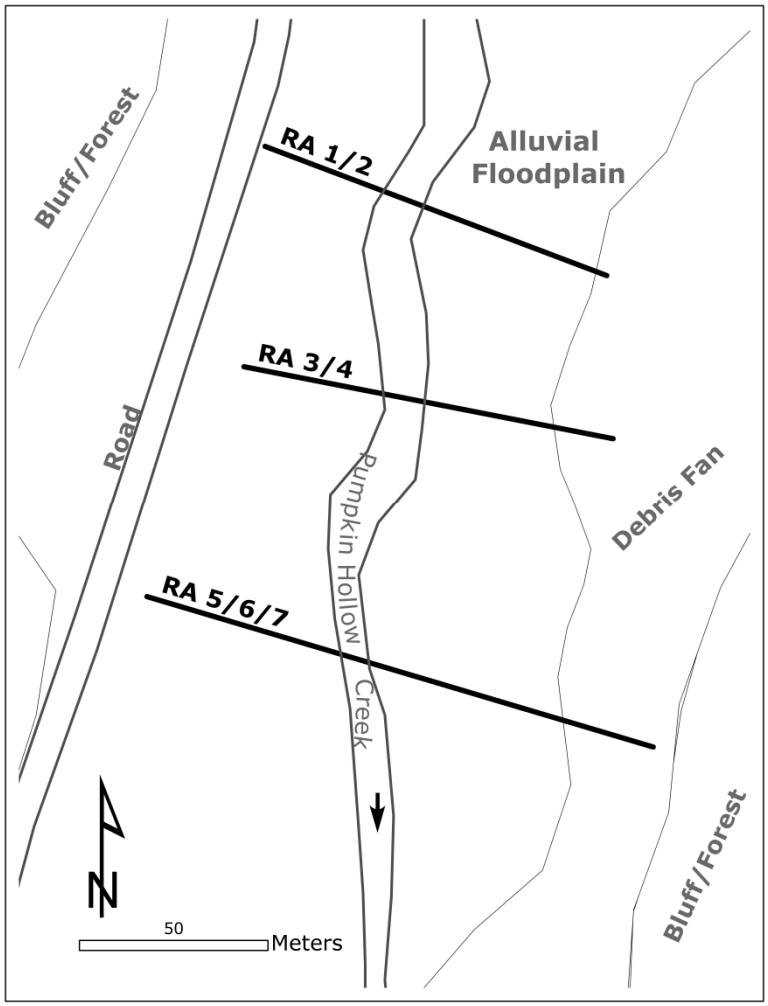

The Pumpkin Hollow Creek floodplain study site is near Tahlequah, Oklahoma (latitude 36.02°, longitude -94.81°). Labeled black lines indicate positions of ERI profiles.

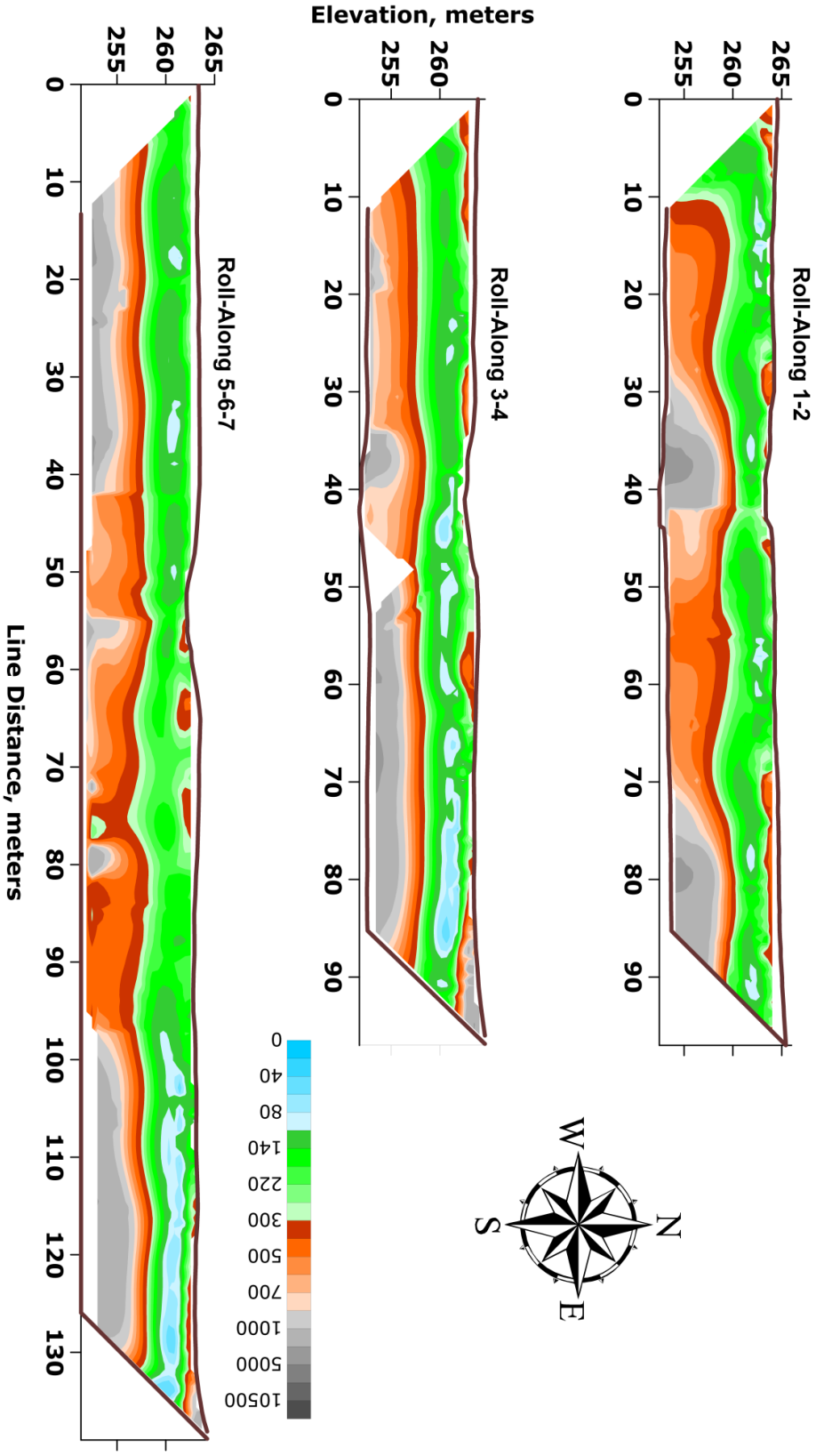
Elevation, meters
Roll-Along 1-2
Roll-Along 3-4
Roll-Along 5-6-7
Line Distance, meters
265
260
255
0
10
20
30
40
50
60
70
80
90
100
110
120
130
W
N
S
E
0
40
80
140
220
300
500
700
1000
5000
10500

APPENDIX E

Hydraulic Testing Results at Barren Fork Creek, Honey Creek, and Flint Creek Alluvial Floodplain Study Sites

Permeameter Dimensions	inches	meters
Well (inside) radius	1.50	0.038
Borehole (outside) radius	1.75	0.044
Screen length	8.00	0.203

USBR Method 3: Values that are constant…

a	0.12	ft^2	surface area of test section (ft^2)
a_{fs}	0.57	ft^2	area of perforated section (ft^2)
l	0.67	ft	Length of screen (ft)
r_1	0.14	ft	Outside radius of the casing (ft)
r_e	0.03	ft	effective radius of well (ft)
l/r_e	24	DIM	ratio of screen length to effective radius

NOTE: The following table includes values recorded in the field, and calculations for hydraulic tests. "Zone 1" is far above water table (K_{fs} calculated with Equation (1.1)), "Zone 2" is close to water table (K_{fs} calculated with Equation (1.2)), and "Zone 3" is below the water table (K_{fs} calculated with Hvorslev slug test solution. "Zone 3" results were not used in the study. *Q/a* is the ratio of discharge to screen area. *Q/a* values above 0.1 are assumed to indicate turbulent (non-Darcian) flow conditions and were not utilized in the study. A detailed description of the Gravel Permeameter can be found in Chapter 1.

Test Name	Notes	Zone	Start Time	End Time	Start ET (min)	End ET (min)	Elapsed time (min)	Average head (meters)
FLCR65_1	Assume 0.0001m^3 in 1 min;	1	14:28:40	14:40:00	0:11:20		1.0	0.39
FLCR65_2	Duplicate close to WT	2	3:06:00	3:37:00	0:31:00		31.0	1.18
FLCR65_3	Duplicate close to WT	2	3:40:00	3:58:00	0:18:00		18.0	0.54
FLCR65_4	below WT	3	4:21:00	4:51:00	0:30:00		30.0	2.45
FLCR68_1		1	5:43:00	6:17:00	0:34:00		34.0	0.43
FLCR68_2	close to WT	2	6:40:00	7:10:00	0:30:00		30.0	1.17
FLCR68_3	below WT	3	8:10:45	8:22:00	0:11:15		11.3	2.38
FLCR75_1		1					1.5	0.42
FLCR75_2	Duplicate close to WT	2	9:38:30	9:48:30	0:10:00		10.0	1.04
FLCR75_3	Duplicate close to WT	2	10:03:30	10:18:30	0:15:00		15.0	0.72
FLCR87_1		1	13:09:13	13:29:39	0:20:26		0.2	0.42
FLCR87_2	close to WT	2	1:15:00	1:29:39	0:14:39		14.7	1.09
FLCR87_3	below WT	3	14:02:55	14:31:52	0:28:57		29.0	2.47
HCKsat4_T1		1	15:00:52	15:28:26	7.1	34.6667	27.6	1.77
HCKsat4_T2		1	15:56:39	16:14:05	17.867	35.3	17.4	1.68
HCKsat6_T1		1	12:15:47	12:44:39	3	31.8667	28.9	1.79
HCKsat1_T1		1	14:06:20	14:19:11	8.2667	21.1167	12.9	0.51
HCKsat1_T2		1	14:45:34	14:57:00	10.05	21.4833	11.4	0.89
HCKsat1_T3	close to WT	2	15:19:30	15:43:41	0.45	24.6333	24.2	2.18
HCKsat3_T1	close to WT	2	10:41:26	11:05:22	0	23.9333	23.9	0.52
HCKsat3_T2	below WT	3	11:26:45	11:38:41	7.85	19.7833	11.9	1.88
HCKsat6_T2		1	13:22:00	13:29:00	0.5569	0.56181	7.0	2.05
HCKsat2_T1		1	8:59:14	9:03:13	0	0	0.0	1.21
HCKsat2_T2		1	9:19:29	9:22:03	0	0	0.0	1.25
HCKsat5_T1			11:48:48	12:04:53	12.567	28.65	16.1	1.16
HCKsat7_T1		1	12:39:00	12:50:21	9.0667	20.4167	11.4	1.28
HCKsat7_T2	close to WT	2	13:25:21	13:46:40	15.5	36.8167	21.3	2.30
HCKsat7_T3	close to WT	2	14:11:45	14:24:54	1.3333	14.4833	13.2	1.06
BFKsat1_T1_1204		1	16:21:00	16:51:10	12.67	42.83	30.2	1.53
BFKsat1_T2_1205	close to WT	2	10:38:42	10:57:56	6.80	26.03	19.2	1.93
BFKsat1_T3_1205	close to WT	2	11:42:24	11:58:32	13.40	29.53	16.1	1.72
BFKsat1_T3_1205_Redo	close to WT	2	11:46:00	11:58:00	13.40	29.53	12.0	1.70
BFKsat3_T1_1205	below WT	3	9:28:31	10:09:25	32.37	73.27	40.9	1.82
BFKsat4_T1_1203		1	14:42:30	14:58:10	27.00	42.67	15.7	1.45
BFKsat4_T2_1204	close to WT	2	10:05:29	10:43:59	11.43	49.93	38.5	1.70
BFKsat5_T1_1204	close to WT	2	11:50:49	12:03:13	16.47	28.87	12.4	1.10
BFKsat8_Test1		1	11:05:31	11:26:34	5.45	26.5	21.1	0.21
BFKsat8_Test2a		1	12:28:00	12:52:40	3.1333	27.8	24.7	0.28
BFKsat8_Test 2b		1	13:12:30	13:24:19	47.633	59.45	11.8	0.42
BFKsat8_Test3		1	15:21:54	15:43:29	3.5667	25.15	21.6	0.28
BFKsat9_Test1		1	10:04:54	10:25:45	5.45	26.95	21.5	1.56
BFKsat9_Test2	close to WT	2	11:07:37	11:29:46	1.15	23.3	22.2	1.53
BFKsat10_Test1		1	12:53:36	13:26:46	8.85	42.0167	33.2	1.54
BFKsat10_Test2	close to WT	2	14:40:42	15:04:45	3.85	27.9	24.1	1.53
BFKsat11_Test1		1	16:11:50	16:37:47	1.15	27.1	26.0	1.48
BFKsat12_Test1		1	16:30:02	16:45:09	0.55	15.6667	15.1	1.18
BFKsat12_Test2	close to WT	2	16:54:20	17:01:14	0.55	7.45	6.9	1.53

Test Name	Standard Deviation	Start Tank Depth (meters)	End Tank Depth (meters)	Volume (m^3)	Discharge Q (m^3/min)	Q (ft^3/s)	Tip Type	Number of pipes	Length exposed (m)	Stilling Tip
FLCR65_1		0.350	0.349	1.00E-04	1.00E-04	5.88E-05	Solid	1	0.737	
FLCR65_2		1.090	0.910	0.550	0.018	0.0104	Solid	2	1.219	
FLCR65_3		0.910	0.890	0.073	0.004	0.0024	Solid	2	1.219	
FLCR65_4		0.870	0.830	0.154	0.005	0.0030	Solid	2	0.559	
FLCR68_1		0.760	0.740	0.082	0.002	0.0014	Solid	1	0.737	
FLCR68_2		0.710	0.510	0.829	0.028	0.0163	Solid	1	0.000	
FLCR68_3		0.988	0.474	2.024	0.180	0.1058	Solid	2	0.559	
FLCR75_1		bottle test		0.001	0.0004	0.0002	Solid	1	0.711	
FLCR75_2		0.853	0.603	1.026	0.103	0.0603	Solid	1	0.000	
FLCR75_3		0.548	0.441	0.421	0.028	0.0165	Solid	1	0.000	
FLCR87_1		bottle test		0.001	0.002	0.0015	Solid	1	0.711	
FLCR87_2		1.099	0.743	1.223	0.084	0.0491	Solid	1	0.051	
FLCR87_3		1.175	0.972	0.513	0.018	0.0104	Solid	2	0.356	
HCKsat4_T1	0.06	1.175	0.725	1.451	0.053	0.0310	Solid	2	1.260	
HCKsat4_T2	0.07	1.072	0.090	3.315	0.190	0.1118	Solid	2	0.740	
HCKsat6_T1	0.05	0.882	0.474	1.658	0.057	0.0338	CORE	2	1.310	
HCKsat1_T1	0.01	0.828	0.688	0.572	0.045	0.0262	CORE	1	0.680	
HCKsat1_T2	0.08	0.987	0.254	2.755	0.241	0.1417	CORE	1	0.115	
HCKsat1_T3	0.04	1.021	0.627	1.502	0.062	0.0365	CORE	2	0.690	
HCKsat3_T1	0.01	0.844	0.722	0.493	0.021	0.0121	Solid	2	0.820	
HCKsat3_T2	0.03	1.237	0.420	2.771	0.232	0.1366	Solid	2	0.490	
HCKsat6_T2	0.01	1.174	1.167	0.012	0.002	0.0010	CORE	2	0.830	
HCKsat2_T1	0.05	1.112	1.112	0.00E+00	0.000	0.0001	CORE	1	0.530	
HCKsat2_T2	0.01	1.105	1.104	0.002	0.000	0.0001	CORE	1	0.150	
HCKsat5_T1	0.06	0.992	0.091	3.085	0.192	0.1128	CORE	1	0.450	
HCKsat7_T1	0.05	1.109	1.076	0.079	0.007	0.0041	CORE	1	0.330	
HCKsat7_T2	0.07	1.109	0.055	3.437	0.161	0.0948	CORE	2	0.780	
HCKsat7_T3	0.07	1.289	0.089	3.654	0.278	0.1634	CORE	2	0.150	
BFKsat1_T1_1204	0.04	0.946	0.723	0.861	0.029	0.0168	Solid	2	84.500	
BFKsat1_T2_1205	0.04	0.482	0.376	0.391	0.020	0.0120	Solid	2	39.000	
BFKsat1_T3_1205	0.12	1.033	0.270	2.851	0.177	0.1039	Solid	3	143.000	
BFKsat1_T3_1205_Redo	0.12	1.275	0.320	3.141	0.262	0.1539	Solid	3	143.000	
BFKsat3_T1_1205	0.02	1.165	0.798	1.136	0.028	0.0163	Solid	3	143.000	
BFKsat4_T1_1203	0.04	0.687	0.338	1.361	0.087	0.0511	CORE	2	86.000	
BFKsat4_T2_1204	0.05	1.069	0.377	2.615	0.068	0.0399	CORE	2	41.000	
BFKsat5_T1_1204	0.10	1.210	0.372	2.910	0.235	0.1380	Solid	2	38.000	
BFKsat8_Test1	0.00	1.038	0.890	0.487	0.023	0.014	Solid	1	0.190	N
BFKsat8_Test2a	0.00	0.981	0.935	0.154	0.006	0.004	Solid	2	0.920	N
BFKsat8_Test 2b	0.01	0.889	0.841	0.182	0.015	0.009	Solid	2	0.920	N
BFKsat8_Test3	0.01	0.787	0.687	0.413	0.019	0.011	Solid	2	0.470	N
BFKsat9_Test1	0.03	1.088	0.891	0.615	0.029	0.017	Solid	2	0.150	Y
BFKsat9_Test2	0.01	1.091	0.925	0.499	0.023	0.013	Solid	3	0.855	Y
BFKsat10_Test1	0.01	1.072	0.906	0.520	0.016	0.009	Solid	2	0.180	Y
BFKsat10_Test2	0.00	1.171	1.064	0.233	0.010	0.006	Solid	3	0.955	Y
BFKsat11_Test1	0.01	1.005	0.846	0.556	0.021	0.013	Solid	2	0.670	Y
BFKsat12_Test1	0.00	0.678	0.677	0.004	2.78E-04	1.63E-04	Solid	1	0.435	N
BFKsat12_Test2	0.02	0.673	0.672	0.004	0.001	3.58E-04	Solid	2	1.150	N

Test Name	Effective head (m)	H (ft)	D Depth to bottom of screen (m)	D (ft)	Depth to top of screen (m)	Depth to WT (m)	U (ft)	Depth to bedrock (m)	Bot Screen Ht above WT (m)	Tu (ft)	Tu/l	X
FLCR65_1	0.346	1.13	0.44	1.44	0.24	1.35	4.43	n/a	0.91	4.13	6.19	27.5
FLCR65_2	1.136	3.73	1.18	3.86	0.97	1.35	4.43	n/a	0.18	4.30	6.45	86.6
FLCR65_3	0.496	1.63	1.18	3.86	0.97	1.35	4.43	n/a	0.18	2.20	3.30	73.9
FLCR65_4	2.406	7.89	1.84	6.03	1.63	1.35	4.43	n/a	-0.49	6.30	9.45	125.3
FLCR68_1	0.386	1.26	0.44	1.44	0.24	1.53	5.03	n/a	1.09	4.85	7.27	26.1
FLCR68_2	1.126	3.69	1.18	3.86	0.97	1.53	5.03	n/a	0.36	4.86	7.29	76.0
FLCR68_3	2.336	7.66	1.84	6.03	1.63	1.53	5.03	n/a	-0.31	6.66	9.99	115.0
FLCR75_1	0.376	1.23	0.46	1.52	0.26	1.66	5.45	n/a	1.20	5.16	7.74	23.9
FLCR75_2	0.999	3.28	1.18	3.86	0.97	1.66	5.45	n/a	0.49	4.87	7.30	67.3
FLCR75_3	0.676	2.22	1.18	3.86	0.97	1.66	5.45	n/a	0.49	3.81	5.71	58.2
FLCR87_1	0.376	1.23	0.46	1.52	0.26	1.52	5.00	n/a	1.06	4.70	7.06	26.2
FLCR87_2	1.041	3.41	1.12	3.69	0.92	1.52	5.00	n/a	0.40	4.72	7.08	72.3
FLCR87_3	2.426	7.96	2.04	6.69	1.84	1.52	5.00	n/a	-0.52	6.26	9.39	127.1
HCKsat4_T1	1.747	5.73	1.14	3.73	0.93	2.80	9.18	3.69	1.66	11.18	16.78	51.3
HCKsat4_T2	1.655	5.43	1.66	5.43	1.45	2.80	9.18	3.69	1.14	9.17	13.76	59.2
HCKsat6_T1	1.723	5.65	1.09	3.56	0.88	2.89	9.49	3.43	1.81	11.59	17.38	48.8
HCKsat1_T1	0.448	1.47	0.50	1.63	0.29	2.21	7.25	2.93	1.71	7.10	10.64	20.7
HCKsat1_T2	0.825	2.71	1.06	3.48	0.86	2.21	7.25	2.93	1.15	6.48	9.72	41.8
HCKsat1_T3	2.110	6.92	1.71	5.60	1.50	2.21	7.25	2.93	0.50	8.58	12.86	80.7
HCKsat3_T1	0.498	1.63	1.58	5.17	1.37	1.86	6.12	2.76	0.29	2.58	3.87	63.3
HCKsat3_T2	1.861	6.11	1.91	6.25	1.70	1.86	6.12	2.76	-0.04	5.97	8.96	102.3
HCKsat6_T2	1.988	6.52	1.57	5.14	1.36	2.89	9.49	3.43	1.33	10.88	16.32	59.9
HCKsat2_T1	1.146	3.76	0.65	2.12	0.44	2.11	6.93	2.73	1.47	8.57	12.85	43.9
HCKsat2_T2	1.180	3.87	1.03	3.36	0.82	2.11	6.93	2.73	1.09	7.43	11.15	52.1
HCKsat5_T1	1.092	3.58	0.73	2.38	0.52	no data		no data				
HCKsat7_T1	1.210	3.97	0.85	2.77	0.64	2.33	7.63	3.21	1.48	8.82	13.24	45.0
HCKsat7_T2	2.232	7.32	1.62	5.30	1.41	2.33	7.63	3.21	0.71	9.65	14.48	75.9
HCKsat7_T3	0.990	3.25	2.25	7.37	2.04	2.33	7.63	3.21	0.08	3.51	5.26	92.6
BFKsat1_T1_1204	1.513	4.96	1.55	5.09	1.35	2.81	9.22	n/a	1.26	9.09	13.64	54.6
BFKsat1_T2_1205	1.908	6.26	2.01	6.58	1.80	2.81	9.22	n/a	0.80	8.90	13.35	70.3
BFKsat1_T3_1205	1.696	5.56	2.19	7.17	1.98	2.81	9.22	n/a	0.62	7.61	11.42	73.1
BFKsat1_T3_1205_Redo	1.678	5.51	2.19	7.17	1.98	2.81	9.22	n/a	0.62	7.56	11.33	72.9
BFKsat3_T1_1205	1.799	5.90	2.19	7.17	1.98	2.13	6.99	n/a	-0.06	5.72	8.58	103.2
BFKsat4_T1_1203	1.384	4.54	1.54	5.04	1.33	2.59	8.50	n/a	1.05	8.00	12.00	56.8
BFKsat4_T2_1204	1.633	5.36	1.99	6.51	1.78	2.59	8.50	n/a	0.60	7.34	11.01	73.0
BFKsat5_T1_1204	1.083	3.55	2.02	6.61	1.81	2.57	8.43	n/a	0.55	5.37	8.06	66.1
BFKsat8_Test1	0.19	0.62	0.78	2.57	0.58	2.76	9.06	n/a	1.98	7.11	10.66	8.7
BFKsat8_Test2a	0.26	0.85	1.27	4.17	1.07	2.76	9.06	n/a	1.49	5.73	8.60	14.8
BFKsat8_Test 2b	0.40	1.31	1.27	4.17	1.07	2.76	9.06	n/a	1.49	6.19	9.28	21.1
BFKsat8_Test3	0.26	0.86	1.72	5.65	1.52	2.76	9.06	n/a	1.04	4.26	6.39	20.1
BFKsat9_Test1	0.32	1.04	2.04	6.70	1.84	2.84	9.32	n/a	0.80	3.66	5.48	28.4
BFKsat9_Test2	0.29	0.95	2.56	8.39	2.36	2.84	9.32	n/a	0.28	1.88	2.81	50.5
BFKsat10_Test1	0.30	0.98	2.01	6.60	1.81	2.8	9.19	n/a	0.79	3.57	5.35	27.5
BFKsat10_Test2	0.29	0.94	2.46	8.06	2.26	2.8	9.19	n/a	0.34	2.06	3.09	45.4
BFKsat11_Test1	0.23	0.76	1.52	4.99	1.32	2.62	8.60	n/a	1.10	4.36	6.54	17.4
BFKsat12_Test1	1.16	3.81	0.54	1.76	0.34	2.89	9.48	n/a	2.35	11.53	17.29	33.0
BFKsat12_Test2	1.51	4.95	1.04	3.42	0.84	2.89	9.48	n/a	1.85	11.01	16.51	44.9

Test Name	H/re	l/H	Zone 1			Zone 2			Zone 3		Resistivity	K (m/d)	Q/a
			Cu	K (ft/s)	K (m/d)	Cs	K (ft/s)	K (m/d)	K (ft/s)	K (m/d)			
FLCR65_1	40	0.6	60	3.07E-05	0.8	*	*	*	*	*	222.2	0.8	0.00
FLCR65_2	132	0.2	*	*	*	47.5	0.002	55.9	*	*	224.9	55.9	0.09
FLCR65_3	58	0.4	*	*	*	47.5	0.001	29.6	*	*	224.9	29.6	0.02
FLCR65_4	280	0.1				47.5			3E-04	7.5	237.6	7.5	0.03
FLCR68_1	45	0.5	65	6.15E-04	16.2	*	*	*	*	*	253.3	16.2	0.01
FLCR68_2	131	0.2	*	*	*	47.5	0.003	81.1	*	*	254.4	81.1	0.14
FLCR68_3	272	0.1				47.5			0.01	271.8	254.4	271.8	0.90
FLCR75_1	44	0.5	65	9.71E-05	2.6	*	*	*	*	*			0.00
FLCR75_2	116	0.2	*	*	*	47.5	0.012	317.5	*	*	293.7	317.5	0.51
FLCR75_3	79	0.3	*	*	*	47.5	0.005	121.3	*	*	293.7	121.3	0.14
FLCR87_1	44	0.5	65	6.50E-04	17.1	*	*	*	*	*	165.0	17.1	0.01
FLCR87_2	121	0.2	*	*	*	47.5	0.01	258.9	*	*	68.8	258.9	0.42
FLCR87_3	282	0.1				47.5			1E-03	25.8	68.8	25.8	0.09
HCKsat4_T1	204	0.1	70	2.74E-03	72.1	*	*	*	*	*	461.495	72.1	0.26
HCKsat4_T2	193	0.1	68	1.08E-02	283.2	*	*	*	*	*	721.91	283.2	0.95
HCKsat6_T1	201	0.1	70	3.03E-03	79.8	*	*	*	*	*	457.045	79.8	0.29
HCKsat1_T1	52	0.5	70	9.03E-03	237.8	*	*	*	*	*	468.76	237.8	0.22
HCKsat1_T2	96	0.2	58	3.21E-02	844.2	*	*	*	*	*	544.9	844.2	1.20
HCKsat1_T3	246	0.1	*	*	*	47.5	0.004	97.0	*	*	500.63	97.0	0.31
HCKsat3_T1	58	0.4	*	*	*	47.5	0.005	134.4	*	*	280.64	134.4	0.10
HCKsat3_T2	217	0.1				47.5			0.017	440.1	302.8075	440.1	1.16
HCKsat6_T2	231	0.1	75	7.23E-05	1.9	*	*	*	*	*	701.365	1.9	0.01
HCKsat2_T1	133	0.2	72.5	7.66E-06	0.2	*	*	*	*	*	105.281	0.2	0.00
HCKsat2_T2	137	0.2	72.5	7.44E-06	0.2	*	*	*	*	*	71.112	0.2	0.00
HCKsat5_T1	127	0.2	*	*	*	*	*	*	*	*	439.18		
HCKsat7_T1	141	0.2	75	4.89E-04	12.9	*	*	*	*	*	484.5325	12.9	0.03
HCKsat7_T2	260	0.1	*	*	*	47.5	0.009	228.8	*	*	415.95	228.8	0.80
HCKsat7_T3	115	0.2	*	*	*	47.5	0.04	1056.1	*	*	256.6675	1056.1	1.38
BFKsat1_T1_1204	176	0.1	51	2.36E-03	62.0	*	*	*	*	*	753.3	62.0	0.14
BFKsat1_T2_1205	222	0.1	*	*	*	47.5	0.001	32.5	*	*	1117.4	32.5	0.10
BFKsat1_T3_1205	198	0.1	*	*	*	47.5	0.012	327.0	*	*	1117.4	327.0	0.88
BFKsat1_T3_1205_Redo	195	0.1	*	*	*	47.5	0.019	488.8	*	*	1117.4	488.8	1.30
BFKsat3_T1_1205	210	0.1				47.5			0.002	54.4	123.6	54.4	0.14
BFKsat4_T1_1203	161	0.1	50	7.99E-03	210.5	*	*	*	*	*	216.3	210.5	0.43
BFKsat4_T2_1204	190	0.1	*	*	*	47.5	0.005	130.7	*	*	180.5	130.7	0.34
BFKsat5_T1_1204	126	0.2	*	*	*	47.5	0.025	657.7	*	*	209.6	657.7	1.17
BFKsat8_Test1	22	1.1	50	1.55E-02	409.1	*	*	*	*	*	666	409.1	0.12
BFKsat8_Test2a	30	0.8	55	2.78E-03	73.2	*	*	*	*	*	1115	73.2	0.03
BFKsat8_Test 2b	46	0.5	65	3.78E-03	99.5	*	*	*	*	*	1115	99.5	0.08
BFKsat8_Test3	30	0.8	67	6.96E-03	183.4	*	*	*	*	*	1504	183.4	0.10
BFKsat9_Test1	37	0.6	56	1.03E-02	270.4	*	*	*	*	*	1020	270.4	0.14
BFKsat9_Test2	34	0.7	60	***	***	47.5	0.009	242.0	*	*	1460	242.0	0.11
BFKsat10_Test1	35	0.7	60	5.56E-03	146.3	*	*	*	*	*	665.61	146.3	0.08
BFKsat10_Test2	33	0.7	59	***	***	47.5	0.004	96.2	*	*	657.62	96.2	0.05
BFKsat11_Test1	27	0.9	59	9.98E-03	262.7	*	*	*	*	*	228.82	262.7	0.11
BFKsat12_Test1	135	0.2	59	2.58E-05	0.68	*	*	*	*	*	89	#####	0.00
BFKsat12_Test2	176	0.1	*	*	*	47.5	3E-05	0.9	*	*	113.3	0.9	0.00

VITA

Ronald B. Miller

Candidate for the Degree of

Doctor of Philosophy

Thesis: HYDROGEOPHYSICS OF GRAVEL-DOMINATED ALLUVIAL FLOODPLAINS IN EASTERN OKLAHOMA

Major Field: Environmental Science

Biographical:

Education:

Completed the requirements for the Doctor of Philosophy/Education in Environmental Science at Oklahoma State University, Stillwater, Oklahoma in December, 2011.

Completed the requirements for the Master of Science/Arts in Geospatial Science at Missouri State University, Springfield, Missouri in 2005.

Completed the requirements for the Bachelor of Arts in Cultural Anthropology at University of California, Davis, in 1981.

Name: Ronald B. Miller Date of Degree: May, 2012

Institution: Oklahoma State University Location: Stillwater, Oklahoma

Title of Study: HYDROGEOPHYSICS OF GRAVEL-DOMINATED ALLUVIAL FLOODPLAINS IN EASTERN OKLAHOMA

Pages in Study: 97 Candidate for the Degree of Doctor of Philosophy

Major Field: Environmental Science

Scope and Method of Study: Geophysical and hydraulic surveys of three floodplains in eastern Oklahoma with the purpose of estimating floodplain heterogeneity and identifying high-flow domains or preferential flow paths.

Findings and Conclusions: Multi-electrode surface electrical resistivity (ERI) profiles of the floodplains show lenticular features with high resistivity within a domain of lower resistivity. Floodplain subsoil is composed of mixture of coarse and fine fractions (less than 0.25 mm). The proportion of the fine fraction from cores at the sites shows a negative power relationship with both resistivity ($R^2 = 0.85$) and hydraulic conductivity ($R^2 = 0.72$), suggesting that the fine content is the major factor in the hydraulic and electrical behavior of the gravel subsoil. A linear relationship between hydraulic conductivity and resistivity is significant and the resulting equation $K_{sat} = 0.11\rho$ allows resistivity (ρ) to be interpreted as saturated hydraulic conductivity (K_{sat}). The median hydraulic conductivity on all profiles from all sites was at least 20 m d^{-1}, which is within the range for gravel soils. This high hydraulic conductivity suggests that at least half of the subsurface at each floodplain is likely to behave as a "high-flow domain" with the ability to conduct water at rates of 20 m d^{-1} or greater. Several ERI profiles at Barren Fork Creek (BFC) had high resistivity values that were significantly higher than the remaining ERI profiles at BFC and the other sites measured at the 84^{th} percentile. Those ERI profiles were obtained from an area within the BFC study site where a trench injection test found a tracer (Rhodamine WT) to move in a manner that suggests preferential flow. A storm runoff pulse passed the BFC site over May 1-5, 2009 featuring 2.2 m of stage increase, which caused the water table to rise into the gravel-dominated vadose zone at the site. Water table maps, corresponding to the times when stream elevation matched the selected hydraulic conductivity elevations, were prepared from pressure transducers placed in monitoring wells at the site. It appeared that there was little attenuation of the energy of the storm pulse even at the furthest point in the study site: at 180 m from the stream the flood peak had only dropped 0.25 m and was delayed by 1.5 hours, suggesting that the floodplain was a "high-flow domain". Comparisons between depth slices of hydraulic conductivity, created by interpolating the ERI profiles, and the water table maps showed that areas of highest resistivity coincided with areas of relatively low water table slope and vice versa. Since high hydraulic conductivity implies less resistance to flow (and less loss of energy over distance), this is the response one would expect to see. Therefore, despite the floodplain as a whole constituting a high-flow domain, areas of preferential flow exist within the floodplain, characterized by highs in both hydraulic conductivity and resistivity.

ADVISOR'S APPROVAL: Garey A. Fox